CONJUGATED POLYELECTROLYTES AGGREGATION AND SENSOR APPLICATIONS

By

JIE YANG

A DISSERTATION PRESENTED TO THE GRADUATE SCHOOL
OF THE UNIVERSITY OF FLORIDA IN PARTIAL FULFILLMENT
OF THE REQUIREMENTS FOR THE DEGREE OF
DOCTOR OF PHILOSOPHY

UNIVERSITY OF FLORIDA

2013

To my family

ACKNOWLEDGEMENTS

First of all, I would like to acknowledge my research advisor, Dr. Kirk Schanze, for his support, advice and encouragement. He guided me into the amazing area of optical sensors based on conjugated polyelectrolytes and encouraged me to think independently and creatively. He is such a great supervisor with enthusiasm for science and kindness to help people and I sincerely appreciated all his advice and help for the past five years.

My deepest gratitude also goes to all the former and current members from Dr. Schanze's group. Many of my projects couldn't have been completed without the guidance and help of Dr. Fude Feng, who has broad knowledge and extensive experience about Polymer Chemistry and most importantly, he shared a lot with me and helped me to overcome several difficulties in my projects. Dr. Abby Shelton and Dr. Eunkyung Ji kindly taught me how to use the almost all the instruments in my lab and helped me out whenever I had a technical problem. I'd like to thanks to Dr. Liao Chen for his patience and kindness to answering all kinds of my questions when we shared the same office. Dr. Jonathan Sommer gave me a lot of good advice on my first project and I still remembered his humor and his passion for surfing. I am also thankful to Dr. Aand Parthasarathy, Dr. Dongping Xie, Dr. Seoung Ho Lee, Dr. Julia Keller, Zhuo Chen all the nice suggestion and discussion about my research. It is also dedicated to Xuzh Zhu for his help and advice on principal component analysis and matlab. Of course, I'd like to

thank other group members, Dr. Galyna Dubinina, Dr. Jan-Moritz Koene, Dr. Danlu Wu, Randi Price, Zhengxing Pan, Subhadip Goswami for their group work to make my research easier.

I would like to extend my appreciation to all my committee members: Dr. Ronald Castellano, Dr. Charles Cao, Dr. David Powell and Dr. Elliot Douglas for their time, encouragement, insightful comment and suggestion. I'd also like to thank Dr. Erkan Kose from North Dakota State University for his nice advice on my last project.

Finally, I'd like to express my gratitude to my family and my boyfriend Dou for their love and understanding for my work. Without their support and love, I will not make my dream come true.

TABLE OF CONTENTS

page

APPENDIX

LIST OF TABLES

LIST OF FIGURES

LIST OF ABBREVIATIONS

3D	Three dimension
ACK	Acetate kinase
ADP	Adenosine diphosphate
ALP	Alkaline phosphate
AMP	Adenosine monophosphate
AP	Acetyl phosphate
APD	Avalanche photodiode
ATP	Adenosine triphosphate
BSA	Bovine serum albumin
BT	Benzothiadiazole
C2N2	Ethylenediamine
C5N2	Cavaderine
CO_2^-	Carboxylate
CPE	Conjugated polyelectrolyte
D	Diffusion coefficient
D-A	Donor-acceptor
DNA	Deoxyribonucleic acid
DTA	Dodecyltrimethylammonium bromide
FCS	Fluorescence correlation spectroscopy
FET	Field-effect transistor
FRET	Fluorescence resonance energy transfer
G (τ)	Autocorrelation function

GOX	Glucose oxidase from *Aspergillus niger*
HEPES	4-(2-Hydroxyethyl)-1-piperazineethanesulfonic acid
HOK	Hexokinase from saccharomyces cerevisiae, type III
HTS	High-throughput screening
I	Fluorescence intensity
LED	Light emitting device
MED	Microemulsion droplet
MES	2-(N-morpholino) ethanesulfonic acid
MIP	Molecularly imprinted polymer
MPS-PPV	Sulfonated poly(phenylene vinylene)
MV^{2+}	Methyl viologen
MW	Molecular weight
N4	Tris(2-aminoethyl)amine
NADH	Nicotine adenine dinucleotide, reduced
NR_3^+	Quarternary ammonium
P1	Meta-linked sulfonated poly(phenylene ethynylene)
P2	Sulfonated poly(phenylene-co-bisthienylbenzothiadiazole)
P3	Poly(phenylene ethynylene) with bis-carboxylate methylene side groups
Pi	Phosphate
PCA	Principal component analysis
PFB	Poly(fluorene-co-benzothiadiazole) with alkyl ammonium side groups
PFP	Sulfonated poly(fluoeine-co-phenylene)

PLD	Phospholipase D from peanut, type II
PO_3^{2-}	Phosphonate
POD	Peroxidase from horseradish, type I
PPi	Pyrophosphate
PPE	Poly(phenylene ethynylene)
PPE-CO_2	Carboxylated poly(phenylene ethynylene)
PPE-$^dCO_2$	Anionic poly(phenylene ethynylene) with dendric carboxylate side chains
PPE-$^dNH_3$	Cationic poly(phenylene ethynylene) with dendric ammonium side chains
PPE-SO_3	Sulfonated poly(phenylene ethynylene)
PPP	Poly(phenylene phenylene)
PPV	Poly(phenylene vinylene)
PT	Polythiophene
PTD	Peptidase from porcine intestinal mucosa
R_H	Hydrodynamic radius
RNA	Ribonucleic acid
SS-DNA	Single strand DNA
SV	Stern-Volmer
TBT	Bisthienylbenzothiadiazole
THF	Tetrahydrofuran
TNT	Trinitrotoluene
TMR	Tetramethylrhodamine
TR	Texas red

V_{eff}	Effective detection volume
Φ_F	Fluorescence quantum yield
λ_{max}	Wavelength of maximum emission peak
η	Viscosity of the solvent
τ	Diffusion time
k	Boltzmann's constant
ω	Structure parameter
ω_r	Transversal or waist radius of confocal volume
ω_z	Longitudinal radius of confocal volume

Abstract of Dissertation Presented to the Graduate School of
University of Florida in Partial Fulfillment of the Requirements
for the Degree of Doctor of Philosophy

CONJUGATED POLYELECTROLYTES AGGREGATION AND SENSOR APPLICATIONS

By

Jie Yang

May 2013

Chair: Kirk S. Schanze
Major: Chemistry

Over the past several years, significant effort has been devoted to explore the application of conjugated polyelectrolytes (CPEs) as chemical and biosensors for the detection and analysis of a variety of molecules of environmental and biological interests. Well established sensing mechanisms have been reported to provide guidelines for underlying concepts of CPE-based sensors. In this dissertation, we focus on the design and development of fluorescent biosensors based on functionalized poly(phenylene ethynylene)s (PPEs) by taking advantage of the aggregation-induced quenching mechanism.

The aggregation behavior of an anionic poly(phenylene-ethynylene) (PPE-$^{d}CO_2$) upon the addition of different metal ions was first investigated by fluorescence correlation

spectroscopy (FCS). FCS results show the diffusion time increases in the order $K^+ \approx Na^+ < Ca^{2+} < Cu^{2+} < Fe^{2+} < Fe^{3+}$, and large diffusion time usually indicates the formation of large aggregates. Comparison of the diffusion time ratio plot to Stern-Volmer plot shows that most efficient Stern-Volmer quenching is seen for ions that give rise to a large increase in FCS diffusion time, and it underscores the importance of aggregation on the amplified quenching effect.

Then, a fluorescent “turn-on” sensor for PPi based on a carboxylate-substituted CPE was developed. The “on-off-on” fluorescence change is based on the “deaggregate-aggregate-deaggregate” conformational change of PPE in the process of adding a tetraamine and PPi, respectively. Then principle component analysis (PCA) method was utilized to convert a large set of complicated fluorescence spectra into two linearly uncorrelated eigenvectors. Regression analysis was performed to predict the concentration of unknown PPi with ~ 95% accuracy.

Last, a cationic polyamine-substituted PPE (PPE-$^{d}NH_3$) was used to develop a real-time fluorescent assay for acetate kinase (ACK) based on the fluorescence quenching of PPE-$^{d}NH_3$ by PPi. The introduction of ACK is able to catalyze the phosphate transfer from acetyl-Pi to Pi and produce PPi, leading to significant spectroscopic changes. Therefore, it allows a direct detection of PPi and measurement of ACK activity.

CHAPTER 1
INTRODUCTION

Conjugated Polyelectrolytes

In the past 40 years, π-conjugated polymers such as poly(phenylene ethynylene) (PPE), poly(phenylene vinylene) (PPV), polythiophene (PT) and poly(para-phenylene) (PPP) (structures shown in Figure 1-1A) have attracted considerable attention for their important roles in a variety of applications, including solar cells,[1] light emitting diodes (LEDs),[2,3] field-effect transistors (FETs),[4,5] and chemo- and biosensors.[6,7] The delocalized electronic structures, variations in extent of conjugation and rapid excition transport along the backbone enable conjugated polymers to show strong optical absorption and emission, reversible electrochemical switching and increased sensitivity to target molecules. [7-9]

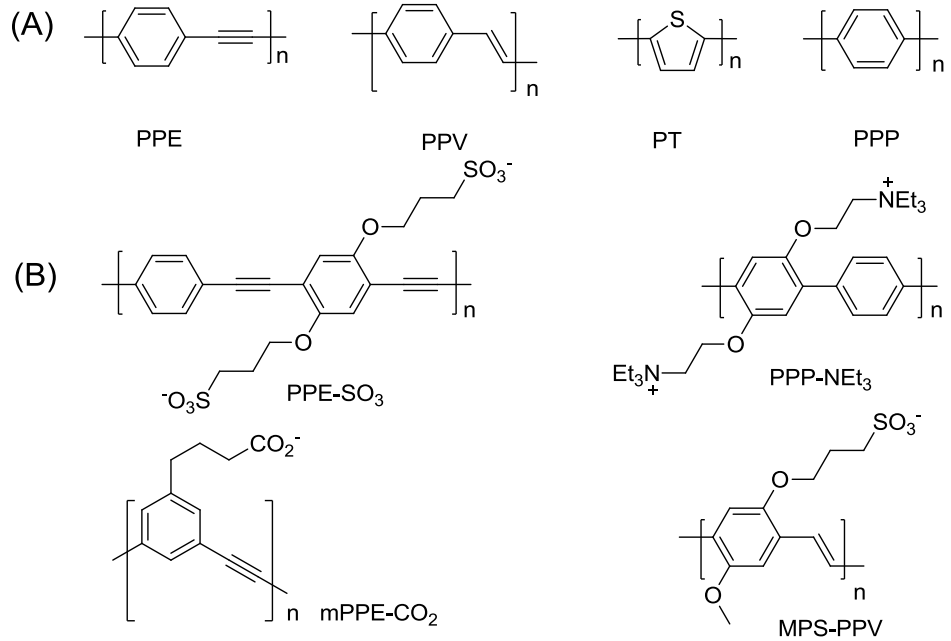

Figure 1-1. Molecular structures of commonly used: (A) conjugated polymers; (B) conjugated polyelectrolytes.

Conjugated polyelectrolytes (CPEs) are water-soluble conjugated polymers having ionic functional side groups. Commonly used charged side groups include sulfonate (SO_3^-), carboxylate (CO_2^-), phosphonate (PO_3^{2-}) and quarternary ammonium (NR_3^+) and some examples are presented in Figure 1-1B.[10] CPEs combine the intrinsic electronic and optical properties which arise from the organic conjugated backbone[11] and good solubility in water or polar organic solvents.[12,13] The unique structures provide CPEs with additional advantages. For example, CPEs are able to bind strongly with other ionic species via electrostatic interactions with their charged side groups. Many CPE-based sensors have been established and investigated by taking advantage of this property to detect target ions of environmental and biological interest, such as toxic metal ions, proteins and oligo and polynucleic acids.[7,14] The ionic and amphiphilic nature of CPEs also makes them capable of self-assembly into films, colloids or other supermolecular structures.[15]

Poly(phenylene ethynylene)s (PPEs) comprise one of the most important classes of CPEs, where the backbones are composed of conjugated ethynylene linked with phenylene rings. Traditionally, PPEs have been used as electroluminescent devices, since they are insulators in the neutral state and become conductive when the polymer's π-electron system is either oxidized or reduced.[16,17] More recently, PPEs have been of increasing interest in areas like chemo- and biosensors. Many sensory systems, including TNT sensors,[12,13] metal ion sensors,[18] glucose sensors[14] and avidin sensors,[19]

have been built based on PPEs. Based on the main chain conformation, PPEs can exist as three isomers: *para*-, *meta*- and *ortho*- poly(phenylene ethynylene)s (structures shown in Figure 1-2). Compared to other CPEs, PPEs have several superior properties. First, because of their versatile chemistry, small modifications to the structure can lead to very different electronic and photophysical properties. Second, they can adopt various conformations in different solvents. For example, in polar solvents *meta*-linked PPEs can self-assemble into a helical conformation, which is stabilized by π-π stacking interactions between the phenyl rings.[20,21] Third, they usually feature high photostability. All of these properties enable them to be good candidates for use in sensors.

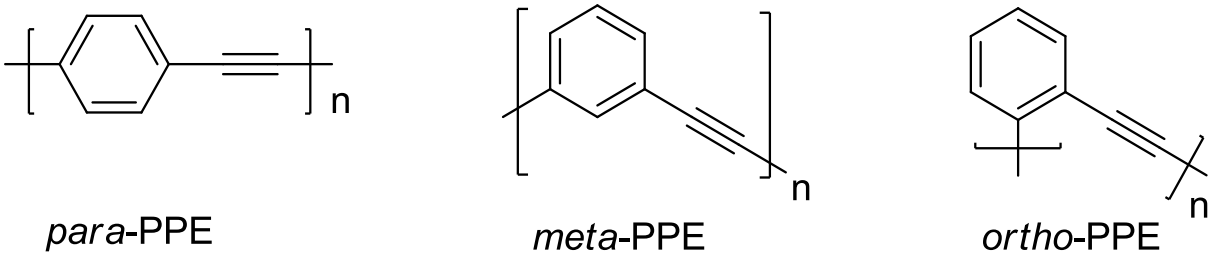

Figure 1-2. Molecular structures of PPEs with different backbone configurations.

Aggregation of Conjugated Polyelectrolytes

In general, CPEs exhibit photophysical properties similar to these conjugated polymers having the same backbones, because the optical properties are primarily determined by their π-conjugated backbone. However, because of the inherent amphiphilic structures of the CPEs (hydrophobic backbones and hydrophilic side chains), they tend to self-assemble into supramolecular aggregates in aqueous solutions or polar

organic solvents, and the aggregation process induces significant changes in both absorption and fluorescence spectra.[22]

Factors that Influence the Aggregation of Conjugated Polyelectrolytes

Solvent dependence

The existence of CPEs in different conformational and aggregation states in different solvents was explored in 2002 by Tan and Schanze,[22,23] who investigated the absorption and fluorescence properties of an anionic CPE, PPE-SO_3 (Figure 1-1B) in water, methanol and a 1:1 water:methanol mixture. As shown in Figure 1-3, the absorption and fluorescence spectra both undergo red-shifts with an increase in the water:methanol ratio, with the effect most pronounced in the fluorescence spectrum. In methanol, the fluorescence appears as a narrow band with a sharp peak at 450 nm corresponding to a small Stokes shift relative to the absorption maximum at 430 nm. Upon the introduction of water, the fluorescence decreases significant in intensity at 450 nm and a weaker and broader band appears at longer wavelength ~550 nm.

Schanze et al. suggested that in an organic solvent like methanol, PPE-SO_3 is "molecularly dissolved", existing as isolated polymer chains with photophysical properties similar to those of neutral structurally-related conjugated polymers dissolved in good solvents like $CHCl_3$ or THF.[24] As a result, the emission is dominated by excitions that are restricted to single chains. In comparison, in aqueous solution, it is believed the PPE-SO_3 chains form supramolecular aggregates through π-π stacking between

adjacent polymer chains.[25-27] The decreased fluorescence intensity and the shift to longer emission wavelength are due to emission from inter-chain excimer-like states, which have lower energies and longer radiative lifetimes than the intra-chain exciton state. It is also important to note that the quantum yield of CPEs decreases with increasing water concentration, providing additional evidence of formation of low-emissive interchain excited states that arise from π-π stacking between two or more polymer chains.[28]

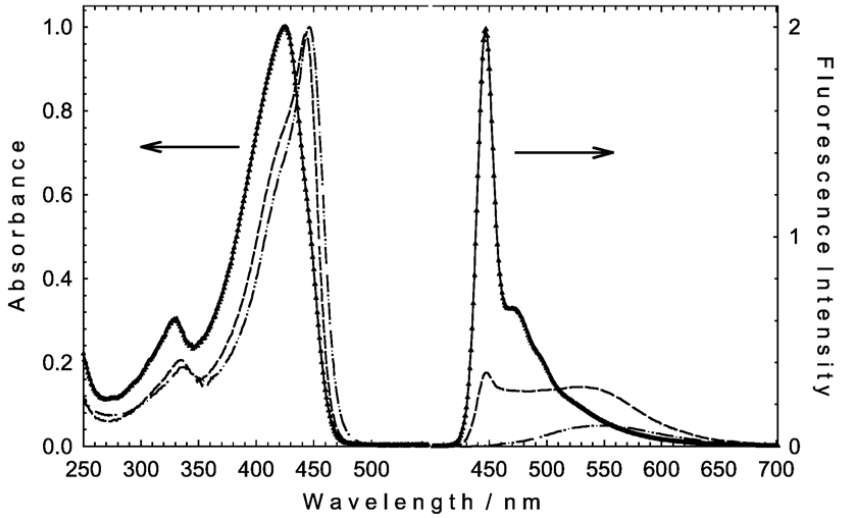

Figure 1-3. Absorption (left) and fluorescence (right) spectra of PPE-SO_3 in MeOH (solid line), H_2O (dashed line), (1:1) H_2O/MeOH (dash dot line). Fluorescence spectra are area normalized to reflect relative quantum yields. Reprinted with permission from Tan *et al*.[29]

Branched side groups and pH effects

Considerable effort has been devoted to decreasing the degree of aggregation in aqueous solution by incorporating with different functional groups. Zhao and Lee[30,31] introduced a series of conjugated polyelectrolytes modified with two branched polyionic

side chains (Figure 1-4A). These bulky and highly charged functional groups are capable of increasing the electrostatic repulsion between adjacent polymer chains, effectively decreasing the hydrophobic π-π stacking interaction. The presence of these large ionic groups also significantly enhances the solubility of CPEs in aqueous solution.

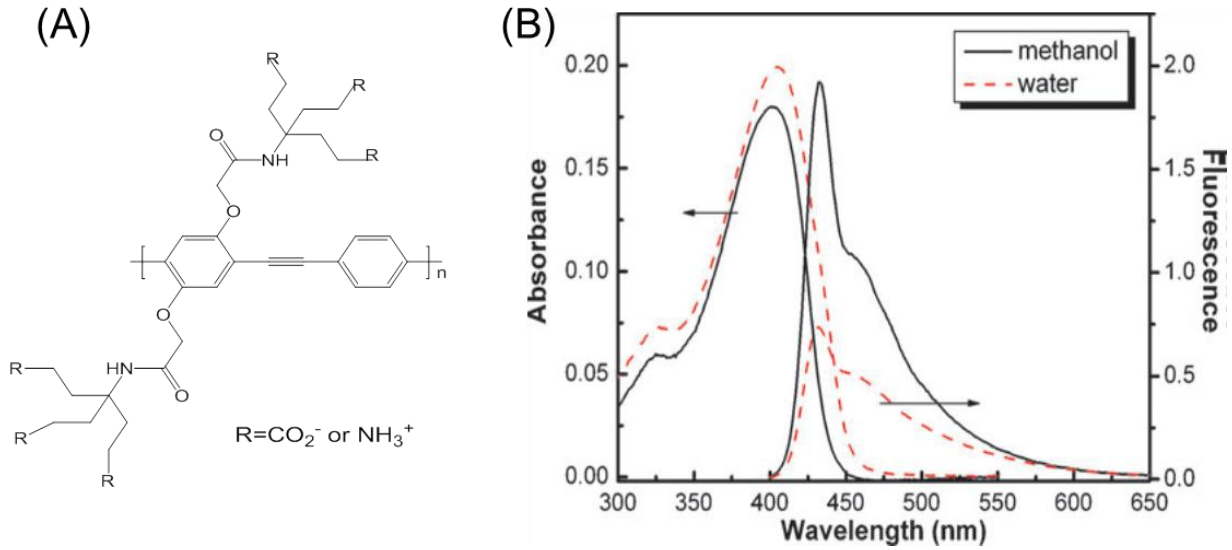

Figure 1-4. (A) Structure of PPEs with branched side chains; (B) Absorption and emission spectra of PPE-$^{d}NH_3$ in methanol and water. [PPE-$^{d}NH_3$] = 4 μM. Reprinted with permission from Lee *et al*.[30]

Figure 1-4B shows the absorption and emission spectra for one of these CPEs (PPE-$^{d}NH_3$) in both methanol and water. As described above, PPE-SO_3 exhibits structured emission in methanol with a small Stokes shift, while in aqueous solution it appears as a broad and red-shifted band.[22] In contrast, PPE-NH_3 shows negligible change in its absorption spectrum with a subtle red shift of about 3 nm in water. In water, the emission spectrum is similar to that in methanol with λ_{em} at the same peak wavelength (~440 nm), although the fluorescence intensity is slightly reduced in water.

This comparison indicates that PPE-$^{d}NH_3$ is much less aggregated in water and compared to PPE-SO_3, most likely due to the high ionic charge density and the large size of the branched side groups, which are assumed to interrupt the coplanarity of the adjacent conjugated backbones. The quantum yield is moderately retained in water (Φ=0.23) compared to methanol (Φ=0.45).

The strong electrostatic repulsion among the multiple NH_3^+ groups effectively reduces CPE aggregation in water. Therefore it is believed the modification to the pH conditions can significantly change the optical properties. Lee studied the pH dependence of their branched polymers in the range of 4.5 to 10.5, and the results are presented in Figure 1-5. The PPE-$^{d}CO_2$ absorption spectrum exhibits a strong peak with a λ_{max} of 404 nm in the pH range of 8.5 to 10.5. As pH decreases, the absorption red-shifts and a shoulder at 435 nm increases. The change in its fluorescence is more significant. At high pH, there is a strong peak for structured emission at 444 nm. As the pH is lowered, another wide band appears at ~515 nm, indicating that PPE-$^{d}CO_2$ has a tendency to aggregate at lower pH, where the anionic carboxylate groups are gradually protonated. The charge neutralization process leads to reduction of the electrostatic repulsion, and the more hydrophobic environment induces aggregation of the polymer chains through hydrophobic and π–π stacking interactions. The conformational change of the PPE backbones finally contributes to the spectral change. Similar to PPE-$^{d}CO_2$, the optical properties of cationic PPE-$^{d}NH_3$ are also pH-dependent. At higher pH, the

weakly basic groups are deprotonated, resulting in a decrease of the high energy fluorescence, a low quantum yield emission and a red-shift in both the absorption and emission spectra.

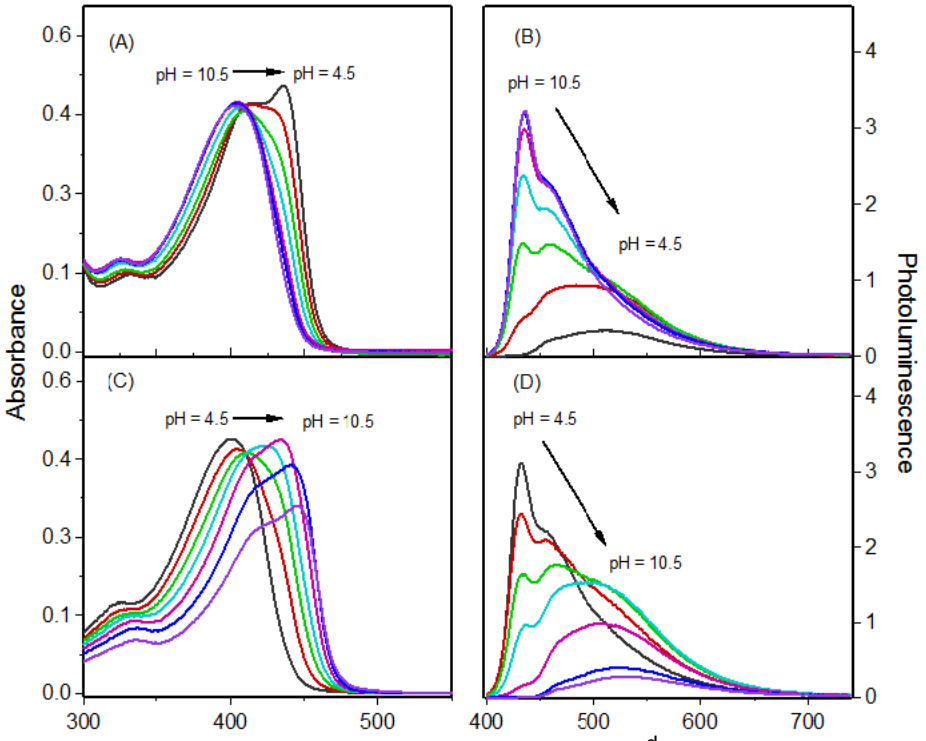

Figure 1-5. Absorption and fluorescence spectra of PPE-$^{d}CO_2$ (A, B) and PPE-$^{d}NH_3$ (C, D) as a functional of pH in water. [PPE] = 5 μM. In each case the pH increment is 1.0 unit. Reprinted with permission from Lee *et al*.[30]

Addition of oppositely charged ions

The addition of oppositely charged ions can also induce the inter-chain aggregation of CPEs.[22,32] In 2006, Jiang and Schanze found that the spectral changes observed when calcium (II) ions are added to anionic PPE-CO_2 (Figure 1-6A) in methanol,[33] are similar to those seen when PPE-SO_3 is aggregated in water. A broad band appears at longer wavelength with low fluorescence intensity. In a good solvent like methanol,

PPE-CO_2 shows structured emission with a strong and narrow band. However, the addition of Ca^{2+} results in a pronounced decrease in fluorescence intensity, emission red-shift and band broadening (Figure 1-6B). Since Ca^{2+} has a closed-shell structure and is therefore unable to act as an electron or energy acceptor, so the observed spectral changes are probably due to the formation of CPE aggregates. Since PPE-CO_2 has two negatively charged side groups on each repeat unit, the positively charged Ca^{2+} is assumed to induce the aggregation of PPE–CO_2 in methanol by acting as an ionic bridge between the polymer chains through electrostatic interactions and complexation with the carboxyl functional groups. The aggregation behavior of other CPEs systems have also been investigated by adding different additives ligands, such as oxalic acid and diamines.[34,35]

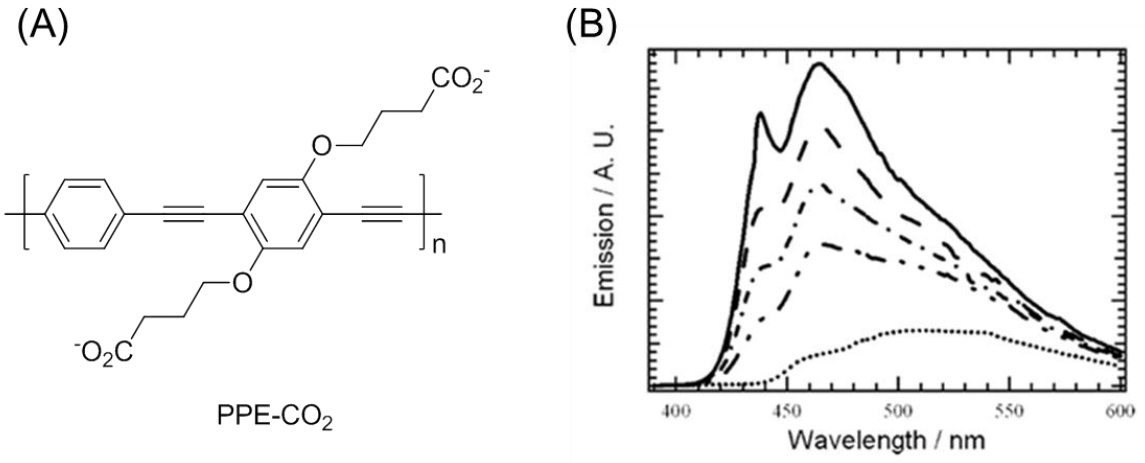

Figure 1-6. (A) Structure of PPE-CO_2; (B) Fluorescence emission of 10 μM PPE-CO_2 in the presence of 0 μM (dotted line), 2.5 μM (dot-dot-dash line), 5 μM (dot-dash line), 7.5 μM (dashed line) and 10 μM (solid line) Ca^{2+} in methanol. Reprinted with permission from Jiang *et al*.[33]

Interaction of surfactants with CPEs

Due to the amphiphilic nature of CPEs, it is suggested they can form stable complexes with oppositely charged molecules, such as surfactants.[36,37] In 2000, Whitten and co-workers first reported that the geometric conformation of CPEs can be adjusted by adding appropriate surfactants, leading to dramatic changes in their photophysical properties.[38] In their work, Whitten et al. synthesized an anionic poly(phenylene vinylene) CPE (MPS-PPV, Figure 1-7) whose optical properties are strongly dependent on solvent. Upon adding the cationic surfactants dodecyltrimethylammonium bromide (DTA, Figure 1-7) to the aqueous solution of MPS-PPV, the emission spectrum of the CPE/surfactant complex changed dramatically. As shown in Figure 1-8, the fluorescence spectrum after addition of DTA has well-defined vibrational structure with a noticeable blue-shift and dramatic intensity enhancement; while the absorption spectrum is red-shifted and narrowed. MPS-PPV tends to aggregate in poor solvents like water, and its fluorescence spectrum shows a broad emission. However, the enhancement of the fluorescence intensity and the shape of the emission spectrum for the CPE/surfactant complex are very similar to the properties of the structured emission exhibited by single polymer chains in good solvents. Whitten et al. proposed that CPE and DTA form a polymer-surfactant complex due to a Columbic interaction between the anionic polymer side chains and the cationic surfactant headgroups, as well as hydrophobic interactions between the surfactant tail and the conjugated polymer backbone, successfully

disrupting polymer-polymer interaction (aggregation). Additionally, they suggested that this is an entropically favored process due to the release of interfacial water molecules (hydrophobic effect). Both factors reduce polymer interchains interactions and reduce the conformational disorder. Therefore, the polymer backbone becomes more extended and ordered, and the fluorescence quantum efficiency is increased.

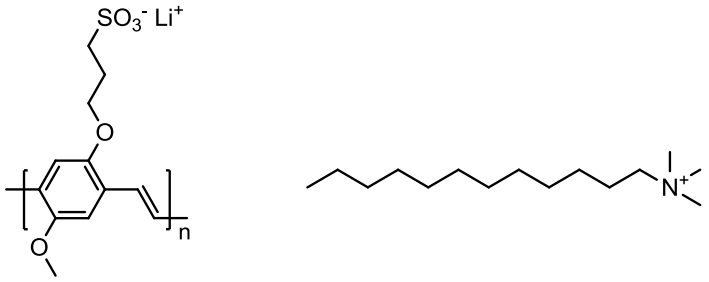

MPS-PPV DTA

Figure 1-7. Structures of MPS-PPV and DTA.

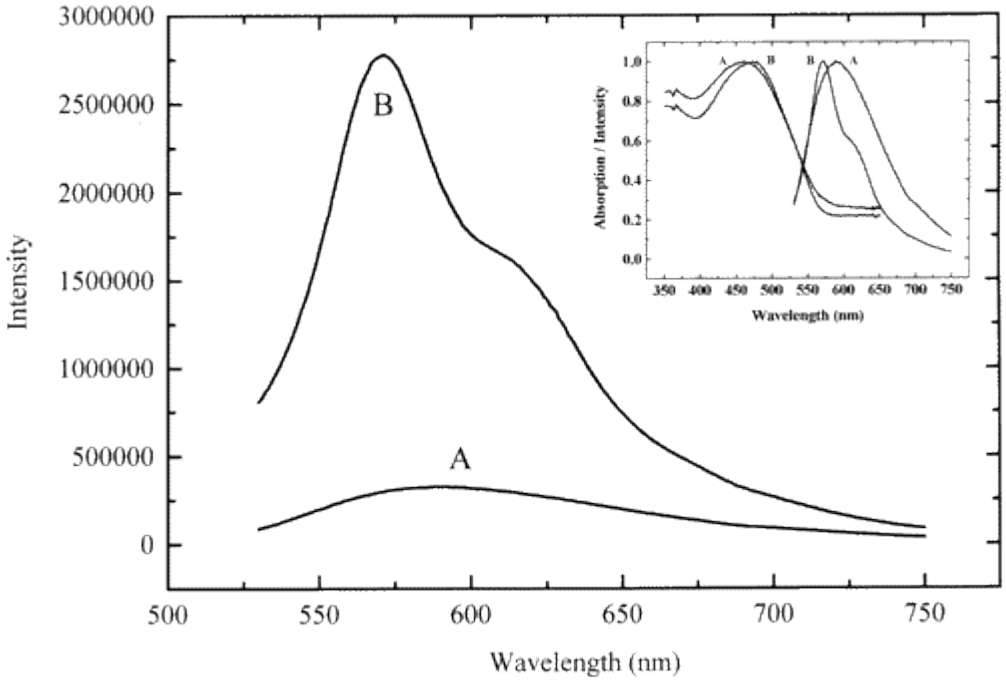

Figure 1-8. The emission spectra of 20 μM MPS-PPV in water: (A) MPS-PPV alone and (B) in the presence of 1 μM DTA. Inset: Normalized absorption and emission spectra of MPS-PPV in water. Reprinted with permission from Chen *et al*.[38]

Effect of Aggregation on Amplified Quenching

Amplified quenching in conjugated polymers was first reported by Swager and co-workers,[39] who showed that the quenching response of a fluorescent PPE functionalized on each repeat unit with a cyclophane receptor to methyl viologen (MV^{2+}, structure in Figure 1-10) is enhanced 50- to 100-fold compared to that of a small fluorophore. As illustrated in Figure 1-9, they attributed the amplified quenching of PPE to a “molecular wire effect”, which is due to the ability of the polymer side chains to complex with the quenchers, leading to extended exciton transport along the conjugated polymer chains.

Several studies found that multiple factors, including molecular weight,[40] polymer aggregation,[22,41] chain length[42] and quencher binding affinity[43,44] can influence the amplified quenching effect. The effect of aggregation on amplified quenching has been widely discussed. The comparison shown in Figure 1-10 indicates that the quenching efficiency has increased from ~10^3 M^{-1} to ~10^6 M^{-1} using a negatively charged conjugated polymer compared to its oligomer with the same MV^{2+} quencher. This behavior was used to design a CPE-based sensor with significant quenching amplification and a detection limit for MV^{2+} is in the submicromolar concentration range. Most importantly, even higher Stern-Volmer constants in excess of 10^7 M^{-1} have been reported for the aggregated CPE systems, further improving the sensing response to the low nanomolar concentration range. It is believed that formation of aggregates provides

the opportunity for excitions to diffuse in a three-dimensional pathway, leading to a significant increase in their chance to encounter the quenchers.

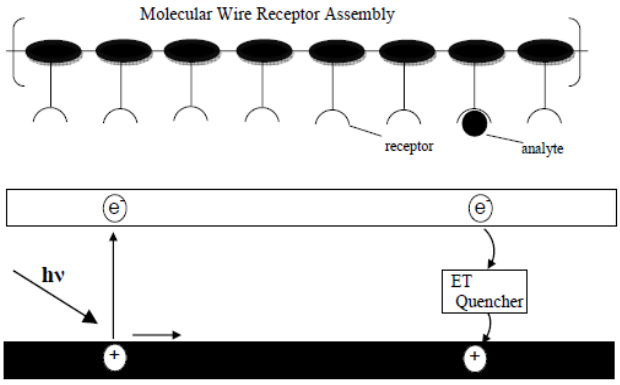

Figure 1-9. Illustration of the molecular wire effect. Reprinted with permission from Zhou *et al*.[39]

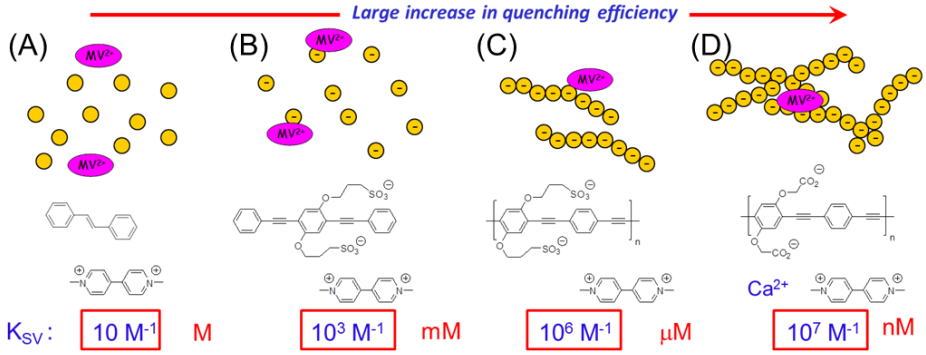

Figure 1-10. Comparison of Stern-Volmer response for various polymer/quencher (MV^{2+}) systems. The numbers in boxes are the Stern-Volmer quenching constants and the concentration units to the right give quencher ion detection limit. (A) Uncharged small molecule chromophores; (B) anionic small molecular ion chromophores; (C) unaggregated anionic CPEs; (D) aggregated anionic CPEs.

Fluorescence Correlation Spectroscopy (FCS)

Fluorescence correlation spectroscopy (FCS) is a spectroscopic technique based on the statistical analysis of spontaneous fluorescence fluctuations. It was first

introduced by Madge, Elson and Webb in 1972,[45] who used the technique to study the kinetics of DNA-drug intercalation. This method is a very sensitive tool for high resolution spatial and temporal analysis of fluorophores in the nanomolar concentration range, as well as for single molecule detection.[46] In addition, FCS provides parameters about dynamic events such as diffusion constants, hydrodynamic radii, chemical reaction rates and conformational changes, and it is an ideal approach to investigate the thermodynamics and kinetics of molecular interactions.[47-49]

Principles of FCS

FCS analysis calculates a correlation function from the time dependent intensity fluctuations of fluorescent particles observed by confocal microscopy. As shown in Figure 1-11, FCS records the emission fluctuations from fluorescent particles moving in and out of a femtoliter confocal volume formed by a focused laser beam. These fluctuations are due to Brownian motion, which can be affected by a number of factors, including enzymatic activity, protein folding, phase fluctuations and conformational dynamics.[50,51] The number of fluorescent particles in the observation volume is measured as a function of time. After an auto correlation function $G(\tau)$ is applied, the data are transformed into a correlation curve. Two major results can be obtained from this correlation curve: the temporal autocorrelation defines the time scale of the diffusion time; and the variance of the intensity provides the average number of fluorescent particles in the detection volume. As illustrated in Figure 1-11, large molecules usually

feature a longer diffusion time as they diffuse slowly, and the correlation curve shifts to the right when the particle size increases, and the value of $G(\tau)$ is inversely proportional to the number of particles in the volume. In addition, changes in particle fluorescence intensity can be recorded during observation. Hence, FCS can be used to determine sample concentrations, dynamic information, diffusion coefficients and rate constants related to rotation and translation, all important parameters in biochemical research, biophysics and chemistry.[52]

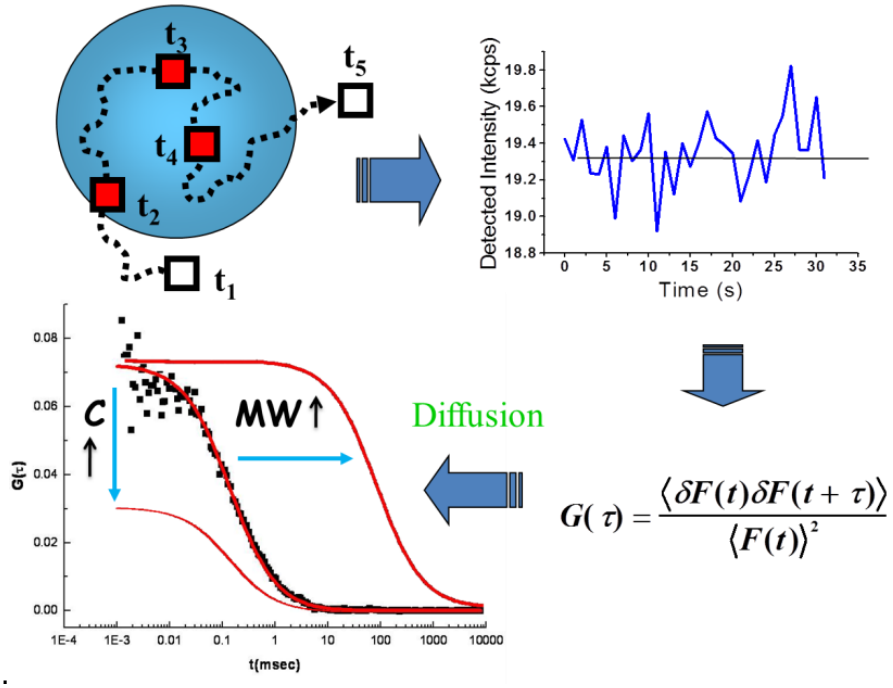

Figure 1-11. Working principles of FCS.

Typical FCS Setup

A block diagram of a confocal microscope as the foundation for an FCS system is schematically depicted in Figure 1-12. A laser beam at the desired wavelength passes

through a microscope objective via a dichroic mirror after being optimized with several optical elements. Then the laser is focused on a small volume and excites the fluorescent particles in the sample. The emitted fluorescence is collected and it passes through the same dichroic mirror and an emission filter. There is a pinhole right below the emission filter to block any background fluorescent light that is not from the sample volume. By properly adjusting the pinhole, the resolution and signal in the desired plane is greatly enhanced and optimized. The pinhole is followed by a detector, preferably an avalanche photodiode (APD) with single photon sensitivity, to convert all the photon signals to electric signals and to amplify the signals, which are passed to the correlator and software for calculation of the auto correlation function, and display of the decay curve.

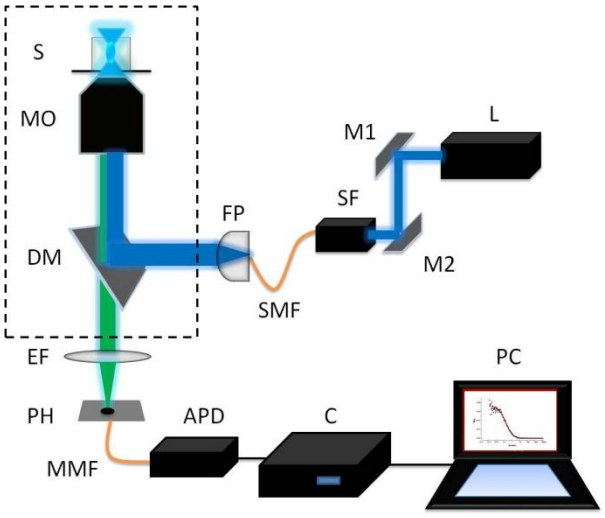

Figure 1-12. A typical FCS setup. L, laser; M1, M2, mirrors; SF, spatial filter; SMF, single mode filter; FP, fiberport; DM, dichroic mirror; MO, microscope objective lens; S, sample; EF, emission filter; PH, pinhole; MMF, multi-mode fiber; APD, Avalanche Photo Diode; C, correlator; PC, personal computer. Black dash line represents the outline of fluorescence microscope.

Applications of FCS

Recently, FCS has been employed in various areas to study molecular concentrations and diffusion times,[49] sizes and conformational changes[53] and molecular interactions.[54] Most importantly, FCS is also capable of obtaining kinetic parameters for bimolecular interactions if they cause fluorescence fluctuations on a shorter time scale than the diffusion time.[54,55] These include unimolecular reactions, intersystem crossing, triplet state dynamics, and reversible photobleaching. The following section describes the use of FCS to address problems with size changes of the fluorescent particles.

Aggregation behavior

In a recent paper, Schanze and co-workers applied FCS to explain the intercalative binding between a *meta*-linked CPE (**P1**) that adopts a helical conformation in water and a biotin-tetramethylrhodamine (TMR) conjugate (**2**, Figure 1-13A).[19] The biotin can bind to **P1** via intercalation between the π-stacked phenylene units in the helical assembly. Addition of avidin, which is a protein well-known to bind strongly to biotin, led to supramolecular polymer aggregates formation by non-covalent cross-linking between the biotin unit of intercalated **2** and avidin (See Figure 1-13). Since the fluorescence change was not significant when avidin was added, FCS was used to detect the size change, leading to a detection limit for avidin of less than 100 pM.

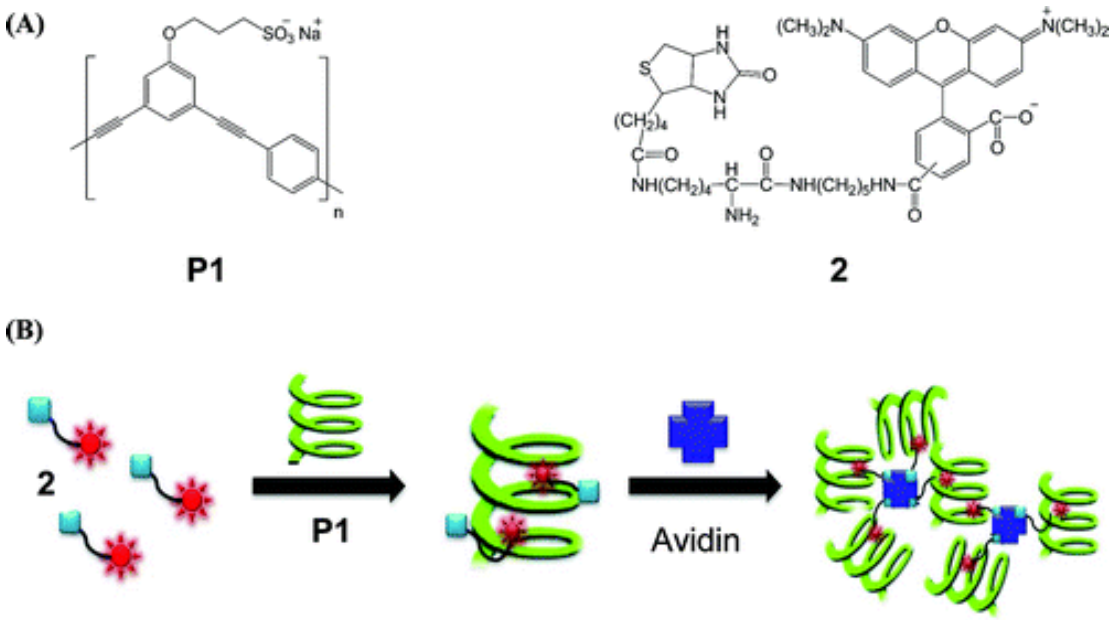

Figure 1-13. (A) Structures of **P1** and **2**, (B) Mechanism of protein-induced aggregation. Reprinted with permission from Wu *et al*.[19]

The FCS results are displayed in Figure 1-14. The small dye molecule **2**, has the lowest diffusion time of ~0.29 ms. After the introduction of **P1**, the **P1**/**2** complex exhibited a longer diffusion time ~0.79 ms, due to the intercalative binding of **2** with **P1**. The most significant increase of the diffusion time was observed when avidin was added to the **P1**/**2** mixture at a stoichiometric concentration, and the correlation curve revealed the highest diffusion time of 11.50 ms. The dramatic shift of the correlation curve suggests the presence of very large polymer−protein aggregates. The avidin/**2** complex (control experiment) has a diffusion time of 1.21 ms slightly larger than that of the **P1**/**2** complex, but considerably smaller than the time for the supramolecular **P1**/**2**-avidin assembly.

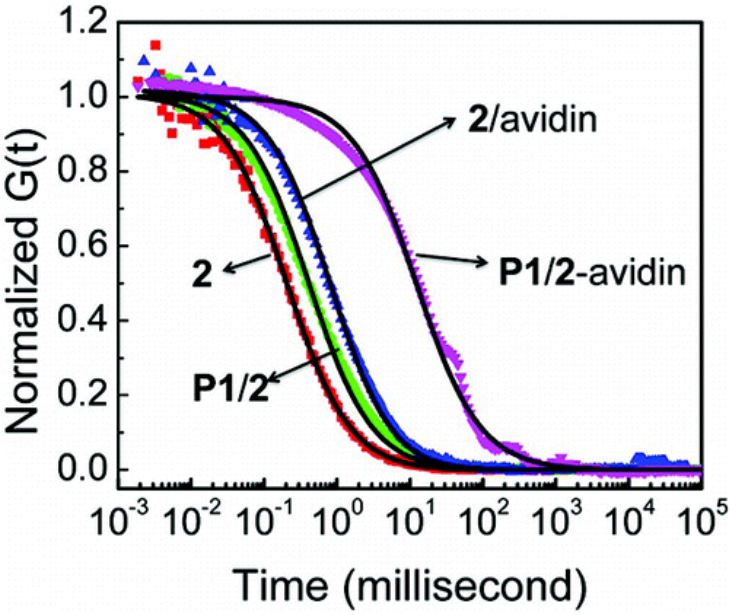

Figure 1-14. Normalized correlation functions of **2**, **P1**/**2**, **2**/avidin, and **P1**/**2**-avidin with [avidin]/[**2**] = 0.25 in phosphate buffer solution (10 mM, pH 7.4). The black solid lines are single species fitting curves. Reprinted with permission from Wu *et al*.[19]

Size measurement

FCS is also an ideal tool to measure diffusion and size distribution for single molecule detection. In 2011, Pal and co-workers demonstrated the use of FCS to measure the size, size distribution and polydispersity of a supramolecular nanostructure (microemulsion droplets, MEDs).[56] A group of MEDs with 13 different core sizes (W_0) ranging from 2 to 50 nm were prepared with sulforhodamine-B as a fluorescent marker. A maximum-entropy-based FCS data fitting model was used to analyze the correlation curves for these MEDs in solution. As shown in Figure 1-15, as the size of the droplet increased, the correlation curve shifted to a longer diffusion time. It is clear that FCS is an ultra-sensitive analytical tool that it can detect very smaller size differences. From the

relationship between the diffusion time and the hydrodynamic radius of their nanoparticles, the authors could predict the size of an unknown nanoparticle.

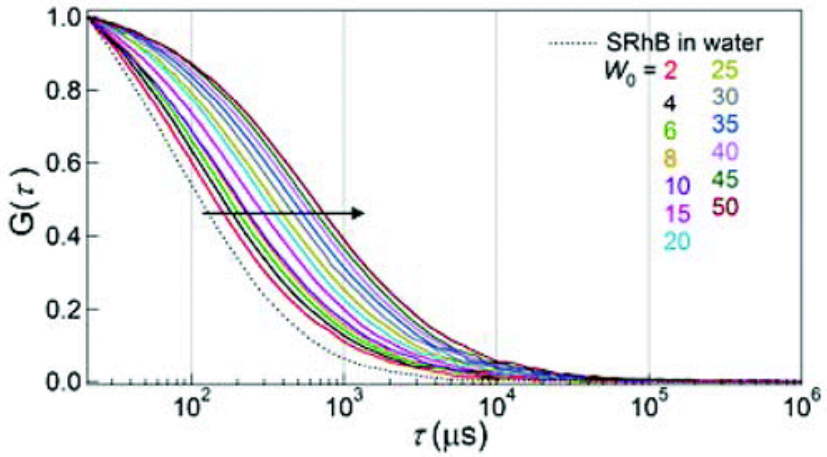

Figure 1-15. Normalized fluorescence correlation curves for MEDs of different W_0. As W_0 increases, the curves shift to the longer lag times, indicating the increase in size of the droplets. The correlation curve for SRhB (control) in water (dotted line) is also included for comparison. Reprinted with permission from Pal *et al*.[56]

Sensor Applications

During the past few decades, CPE systems have been broadly investigated as optical chemical and bio-sensors, and researchers have designed different CPEs systems for application to various analytes, including small ions, biomolecules, proteins and nucleic acids. In contrast to conventional sensing methods, fluorescence-based CPE systems provide several advantages. First and most essentially, CPEs are water-soluble and are more adaptable and compatible to biological systems. Second, these CPE-based sensors usually utilize fluorescence detection, which is rapid and easy, and it affords great sensitivity and real-time measurements. Third, CPE-based sensor

systems can be easily adapted to high-throughput screening (HTS) formats. As a consequence, many sensory systems based on CPEs have been studied and reported.

In general, most CPE-based sensors utilize one of the following mechanisms: amplified quenching, fluorescence resonance energy transfer (FRET), and conformational change (including aggregation-induced quenching). In most cases, sensors utilize more than one mechanism in a given assay, since these three mechanisms are not independent. In the following, we will introduce some examples primarily based on the aggregation-induced quenching mechanism.

Small Ion Sensing

Many fluorescence-based sensing systems have been developed for small species, such as heavy metal ions and small organic ions, which can be toxic hazards or threats. In 2007, Swager and co-workers demonstrated the detection of nonquenching, multicationic small molecules, including spermine, spermidine and neomycin, by using a blue-emitting polyanionic PPE doped with green-emitting exciton traps sites (anthryl units, Figure 1-16).[57] In their investigation, they found that these multicationic amines were able to effectively induce the formation of strongly associated aggregates between the polymer chains in solution. As illustrated in Figure 1-17, anionic-PPE*y* was dissolved as isolated single chains, because of the presence of bulky side groups. Therefore, most of the fluorescence observed from the polymer arises from the inherent blue emission band at around 430 nm. Spermidine, which predominantly has four positive charges

under acidic pH conditions, was then introduced to the polymer solution. The small and multicationic spermidine effectively attracts and complexes with the polyanionic PPE to form large aggregates, bringing the polymer chains into close proximity. This leads to expansion of excitions migration to a three-dimensional space, greatly enhancing exciton transport. As long as these excitions were trapped by the lower energy anthryl sites, a visually noticeable blue-to-green fluorescence emission was observed. As little as ~1.6 μM, spermidine was sufficient to produce a fluorescence color change from blue to green. Among all the analytes they have tested, only those with more than two positive charges were capable of inducing efficient inter-chain aggregation of PPE, thus giving this system selectivity towards different small-molecule amines. This color-change sensor method is expected to be useful for detecting and monitoring of biologically relevant and nonquenching multicationic species.

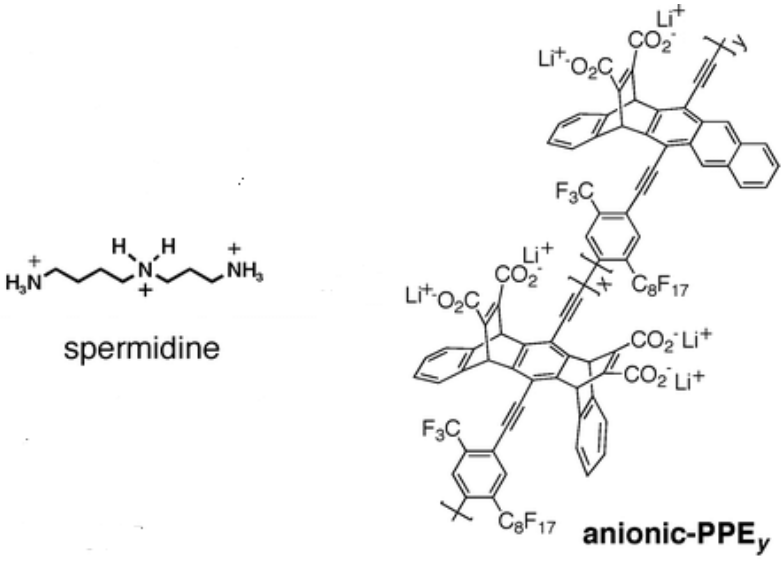

Figure 1-16. Structures of PPE$_y$ and spermidine.

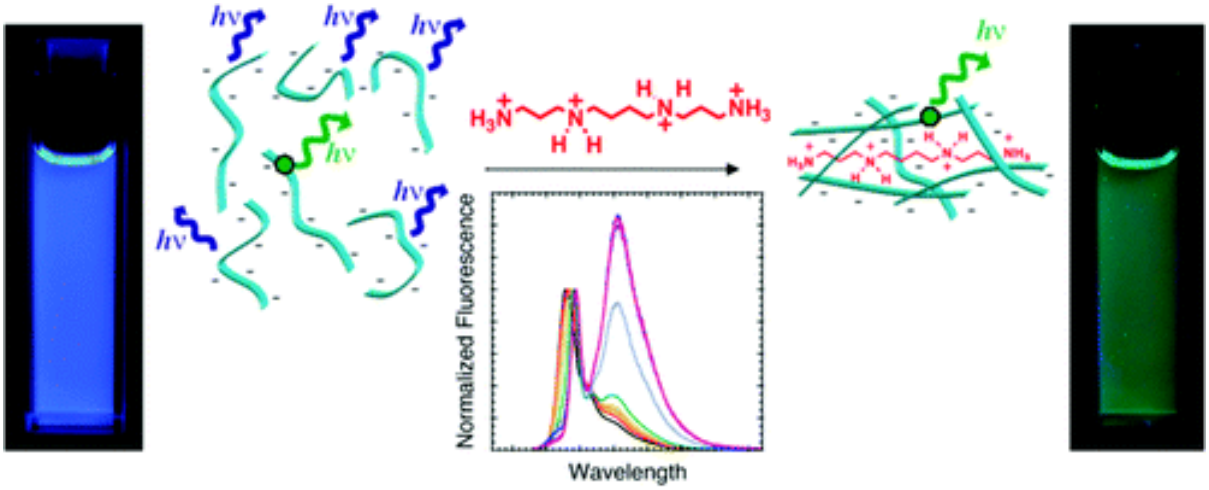

Figure 1-17. Schematic illustration of spermine-induced aggregation of the anionic conjugated polyelectrolyte and the accompanying blue-to-green fluorescence color change. Reprinted with permission from Swager *et al*.[57]

Protein Sensing

Proteins play an essential role in facilitating physiological and biochemical functions, catalysis of tens of thousands of reactions as enzymes, cell signaling, molecular recognition, cellular communication, and gene expression.[58,59] Many methods and strategies have been developed for protein detection and analysis for medical diagnostics and clinical research. In 2011, Lee et al. synthesized an anionic conjugated polyelectrolyte which can exhibit blue-to-green or blue-to-red change in fluorescence upon exposure to different charged proteins.[60] The conjugated polyelectrolyte (**P2**, Figure 1-18) was functionalized with sulfonate groups and a certain percentage of bisthienylbenzothiadiazole groups (TBT), which served as energy acceptors. The aggregation-induced intermolecular excition can migrate from the energy donor (phenylene groups) to these TBT units to exhibit different emissions. The authors

conducted a screening assay array for different biologically relevant proteins, and the results are presented in Figure 1-19. The proteins examined in their project and their isoelectric points were lysozyme (pI = 11.0), Bovine serum albumin (BSA, pI = 4.9), Lecin (pI = 5.47) and cytochrome C (pI = 10.7). The sensing mechanism was mainly attributed to electrostatic and hydrophobic interactions between the polymers and proteins. As a result of these factors, different degrees of aggregation occurred, leading to development of different emission color changes. Over the entire pH range, proteins may carry one positive/negative charge or remain neutral in aqueous solution depending on their pI value. Therefore, the pI for each specific protein is very important in this sensing strategy. This rapid and visually noticeable (blue-to-red emission) CPE-based method will be useful in sensory arrays for detecting various cationic proteins under pH control.

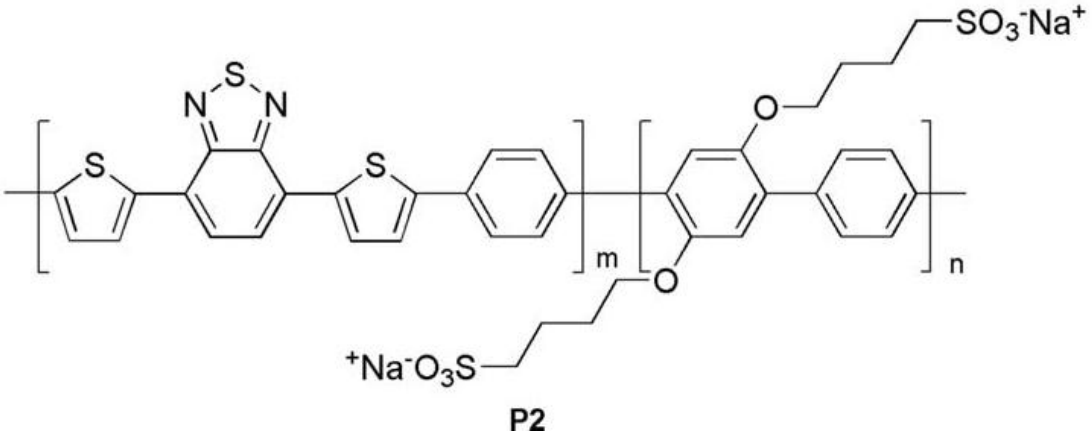

P2

Figure 1-18. Structure of **P2**.

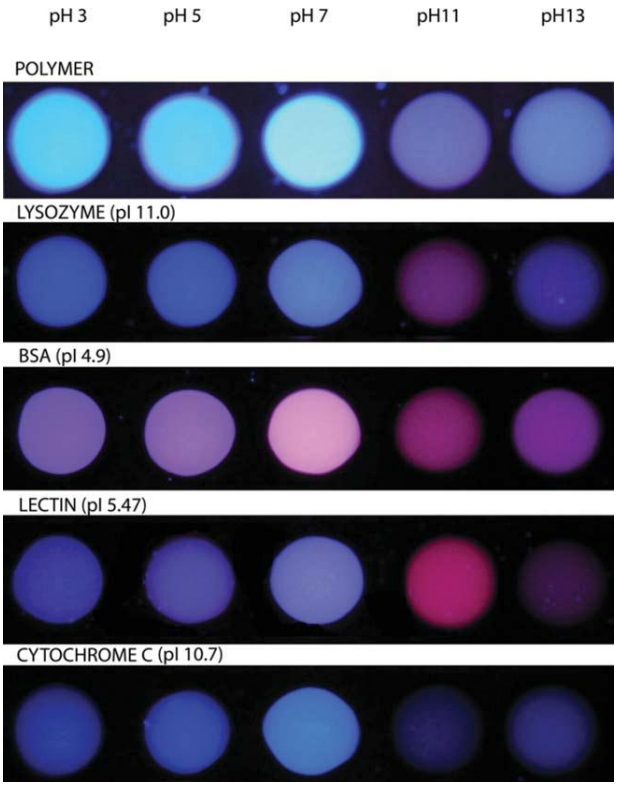

Figure 1-19. Photographs of fluorescence array of **P2** (10 μM) at various pHs in the presence of proteins (100 nM). From top to bottom: polymer; Lysozyme (pI = 11.0); BSA (pI = 4.9); Lecin (pI = 5.47) and Cytochrome C (pI = 10.7). Reprinted with permission from Lee *et al*.[60]

DNA Sensing

DNA has been recognized as a key target for cancer diagnosis and detection of bacteria and viruses,[61,62] and significant developments have been achieved to make DNA sensing more accessible.[63,64] In 2011, Woo and co-workers reported a FRET-based DNA biosensor, which can be mediated by the aggregation of a complex between an anionic CPE (a-PFP, Figure 1-20) and a cationic CPE (c-PFB15, Figure 1-20).[65] In their approach (see Figure 1-21), electrostatic complexation induced by the oppositely charged polyelectrolytes a-PFP and c-PFB15 led to the aggregation of

polymer chains with a concomitant decrease in intersegment distances. Thus, the excited energy state was transferred to the BT (benzothiadiazole, 15% in c-PFB15) segments and a green emission was observed. When a single-stranded DNA labeled with Texas Red (ssDNA-TR, Figure 1-20) was introduced, the negatively charged DNA bound to the polymer complex to give rise to further energy transfer from the BT segment to TR, and the red emission was used to signal the presence of target DNA. Overall, this method involves a two-step FRET process: the energy of the excited fluorine-phenylene on a-PFP (initially blue fluorescence) is delivered to the BT segment on c-PFB15 due to the formation of the CPE complex, leading to green fluorescence. Then, the green emission disappears with a red emission appearing via a subsequent FRET after complexation with ssDNA-TR. The optical signal is also significantly amplified, resulting in increased sensitivity in CPE-based FRET DNA detection assays. It should be pointed out that several parameters are important in this sensory system, including the D-A distance, spectra overlap, DNA:CPE concentration ratio, and dipole orientation.

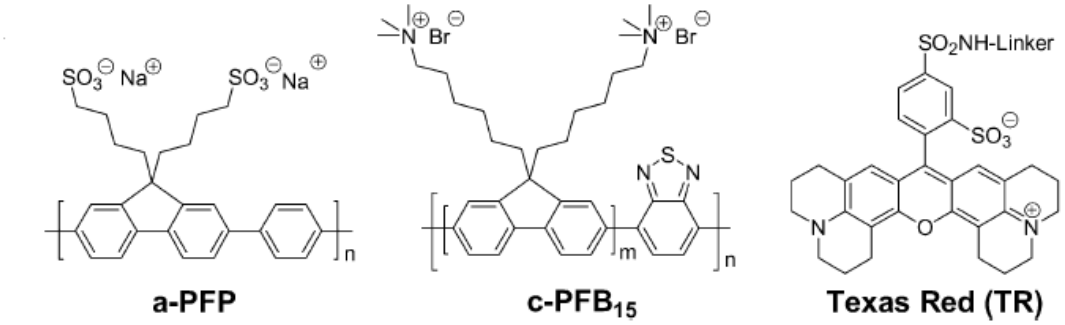

Figure 1-20. Molecular structure of a-PFP, c-PFB15, and TR.

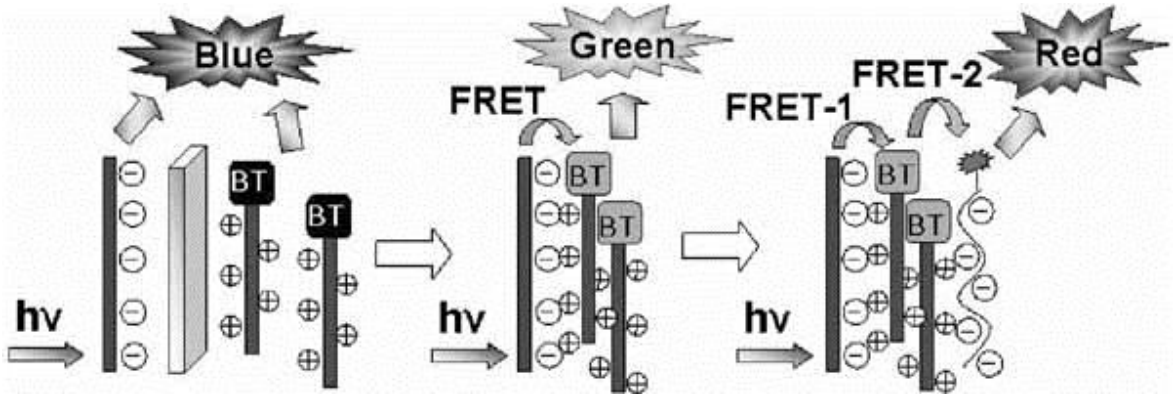

Figure 1-21. Illustration of aggregation-mediated fluorescence energy transfer to dye-labeled DNA. Reprinted with permission from Jin *et al*.[65]

Challenges of CPE-based Optical Sensors

Most CPE-based sensory systems provide several advantages, including superior sensitivity, a high degree of selectivity, and simplicity. While highly useful, there are some shortcomings associated with the methods. First, photobleaching, which is inherent to most CPEs, can lead to false signals and cause errors in analytical studies where quantitative analysis is required.[7,66] Second, the selectivity of the sensors to the specific target molecules remains a problem, as most of the sensing mechanisms involve relatively weak electrostatic and/or hydrophobic interactions. Thus, interference from unwanted nonspecific interactions between CPEs and non-target species must be carefully examined.[67,68] Third, subtle changes in the experimental conditions (ionic strength, temperature, pH, and additives) may induce significant changes in the sensor systems. As a result, all experimental conditions must be controlled and optimized to achieve reproducibility.

Overview of This Dissertation

The primary goal of the present study is to investigate the aggregation behavior of functionalized poly(phenylene ethynylene) (PPE) upon the addition of different analytes and to explore their optical sensor applications towards various targets, including metal ions and pyrophosphate (PPi).

Chapter 2 reports a study of the ion-induced quenching of an anionic PPE (PPE-$^{d}CO_2$) using FCS. The interaction of the CPE with a variety of metal ions including Na^+, K^+, Ca^{2+}, Cu^{2+}, Fe^{2+} and Fe^{3+}, was investigated. FCS results showed that the diffusion time increases in the order $K^+ \approx Na^+ < Ca^{2+} < Cu^{2+} < Fe^{2+} < Fe^{3+}$. As discussed above, long diffusion times usually indicate large CPE aggregates. Comparison of the diffusion time ratio plot from FCS to the Stern-Volmer plot from fluorescence spectroscopy showed different responses of the two techniques, most likely due to an amplified quenching effect.

Chapters 3 and 4 illustrate the aggregation-based detection of structurally similar diamines and tetraamines using a carboxylate-functionalized poly (phenylene ethynylene). Upon the addition of amines, the PPE can cross-linked via electrostatic interactions between the polymer carboxylic acid binding sites and the amino groups of the multiamines to form interpolymer aggregates, leading to fluorescence self-quenching of the polymer. FCS was also utilized to study the size change of the polymer with different amines. Only tetraamines was able to bind strongly to PPE to form tight

aggregates. In addition, a “turn-on” sensor for pyrophosphate (PPi) was designed based on the strong association of PPi with tetraamine. Application of principal component analysis (PCA) to this system yielded two principal components. The PCA method was able to determine the concentration of PPi with an approximately 95% accuracy when PPi is within concentration range from 100 μM to 3 mM.

Chapter 5 describes a real-time fluorescence assay for acetate kinase (ACK) using a PPE with branched ammonium side chains (PPE-$^{d}NH_3$). The cationic PPE can be quenched very efficiently by PPi due to the formation of large aggregates, while other substrates, including Pi, acetyl-phosphate and acetate, fail to induce any significant fluorescence change. Therefore, a real-time fluorescence turn-off assay for the enzyme acetate kinase (ACK) using PPE-$^{d}NH_3$ as the signal transducer was developed. The assay operates with substrates in the micromolar range, and it offers a straightforward and rapid detection of ACK activity for enzyme present in the nanomolar concentration range.

CHAPTER 2
ION-INDUCED AGGREGATION OF CONJUGATED POLYELECTROLYTES STUDIED BY FLUORESCENCE CORRELATION SPECTROSCOPY

Background

As discussed in Chapter 1, the addition of oppositely charged small ions into a CPE solution leads to significant changes in the photophysical properties.[39,69] Early studies found that some metal ions, such as Pd^{2+} and Ca^{2+}, exhibit a superquenching ability towards carboxylated poly(phenylene ethynylene)s (PPE) in aqueous solution.[18,22,32,33] The sensitive photophysical response of conjugated polymer has been ascribed to either the electron transfer properties of the conjugated polymers, the so called “molecular wire effect”, or a multivalency effect. In the latter case, the cations may be simultaneously bound by more than one carboxylate belonging either to a single polymer chain or to adjacent polymer chains to form aggregates. Several ion sensors have been developed based on cation-induced CPE fluorescence change.[18,70]

Although fluorescence spectroscopic studies on CPE aggregation have been fully elucidated in the literature,[18,22,33] direct evidence of polymer aggregation upon addition of various types and concentration of ions is still insufficient. In order to better interpret the spectral change of CPE and to clarify potential ambiguities, this work made use of fluorescence correlation spectroscopy (FCS). FCS has been primarily employed for the analysis of biological systems,[46,52] but application to polymers, in particular CPEs, has gained increasing interest throughout the past decade due to the high sensitivity and the

capability of single molecular analysis. Because of their inherent fluorescence, CPEs can be observed directly, avoiding the tedious dye-labeling process and simplifying studies of conformational or diffusional changes. In the current work, we introduce an FCS system coupled with a 405 nm diode laser and it was applied to investigate the aggregation behavior of two CPEs induced by small molecules.

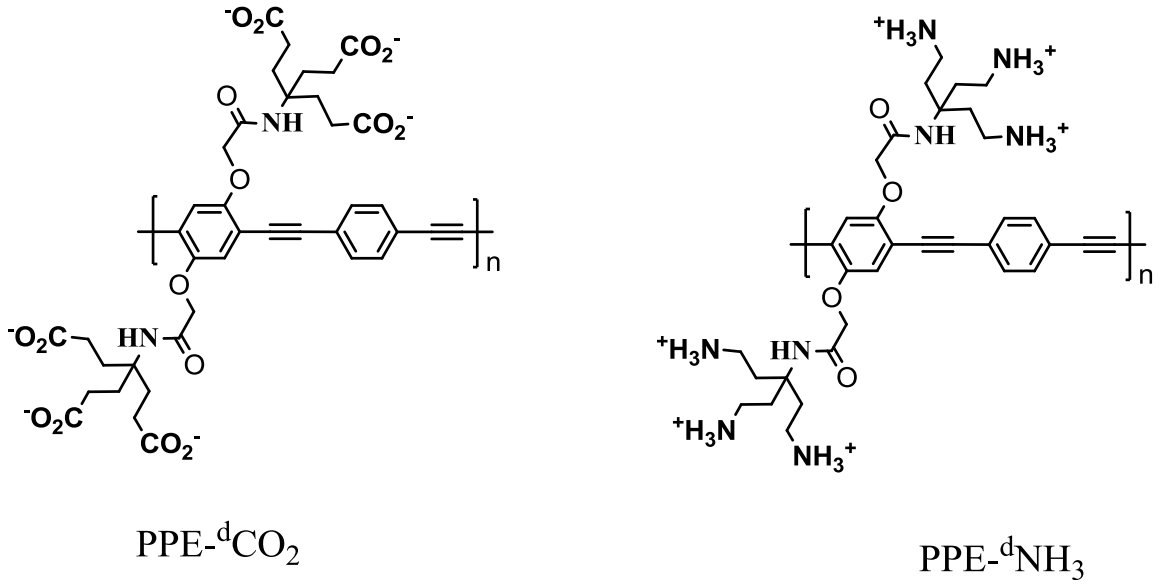

Figure 2-1.Structures of dentritic polymers.

The two CPEs (PPE-$^{d}CO_2$ and PPE-$^{d}NH_3$, Figure 2-1) studied here have poly(phenylene ethynylene) backbones substituted with bulky, highly charged ionic side chains.[30,31] Anionic PPE-$^{d}CO_2$ contains carboxylate groups as the side chain while PPE-$^{d}NH_3$ is cationic with a branched polyamine as the functional group. As discussed previously, both polymers exhibit similar optical properties in methanol and water, since they exist as free single polymer chain in these solvents.[71] In this chapter, the interactions of the CPEs with six metal cations (PPE-$^{d}CO_2$) or pyrophosphate anions

(PPE-$^{d}NH_3$) were investigated by FCS to observe the relationship between the chain aggregation and fluorescence quenching. The FCS results indicate that addition of Fe^{2+}, Fe^{3+} and Cu^{2+}, all transition metal ions with high charge density, can readily induce aggregation of PPE-$^{d}CO_2$ chains. Similarly, the addition of negatively charged PPi to the cationic PPE-$^{d}NH_3$ system also induces aggregate formation. These findings agree well with the results obtained by fluorescence titration experiments. We explain the fluorescence change by different quenching mechanisms and also explore the amplified quenching mechanism in terms of aggregation/physical interactions of CPE. The results demonstrate that FCS with 405 nm excitation has great potential for studies of the molecular conformational and diffusional behavior of CPEs.

Results and Discussion

Investigation of Interaction of Anionic PPE-$^{d}CO_2$ with Metal Cations

Fluorescence quenching of PPE-$^{d}CO_2$ induced by metal cations

The objective for developing the FCS system was to utilize it to probe the interactions of CPE chains with ions in aqueous solution. We also have the goal to correlate the metal ion induced changes in CPE solutions with the changes in fluorescence. Six different metal cations (Na^+, K^+, Ca^{2+}, Cu^{2+}, Fe^{2+} and Fe^{3+}) with a concentration range of 0 - 25 μM were added to 780 nM aqueous PPE-$^{d}CO_2$ and the fluorescence spectra were recorded. Figure 2-2 illustrates the Stern-Volmer plots of I_0/I as a function of the concentration for different metal ions at the maximum emission

wavelength of 436 nm for PPE-$^{d}CO_2$, where I_0 and I are the emission intensities of polymer before and after the addition of metal ions. Little quenching is observed for PPE-$^{d}CO_2$ for $[M^{n+}] < 2$ μM. However, when the concentration increases above 3 μM, a dramatic increase in the slope of the plots is observed for Fe^{2+}, Fe^{3+} and Cu^{2+}, signaling the onset of a highly efficient quenching process. The fluorescence intensity for PPE-$^{d}CO_2$ begins to decrease very sharply from this point for Fe^{2+} and Fe^{3+} until the SV plot levels off. At the highest concentration level, 25 μM, the fluorescence intensity is quenched 97%, 96% and 95% relative to fluorescence of the unquenched PPE-$^{d}CO_2$ for Fe^{2+}, Fe^{3+}, Cu^{2+}, respectively. In comparison, all the other ions Na^{+}, K^{+} and Ca^{2+} were unable to induce any significant quenching.

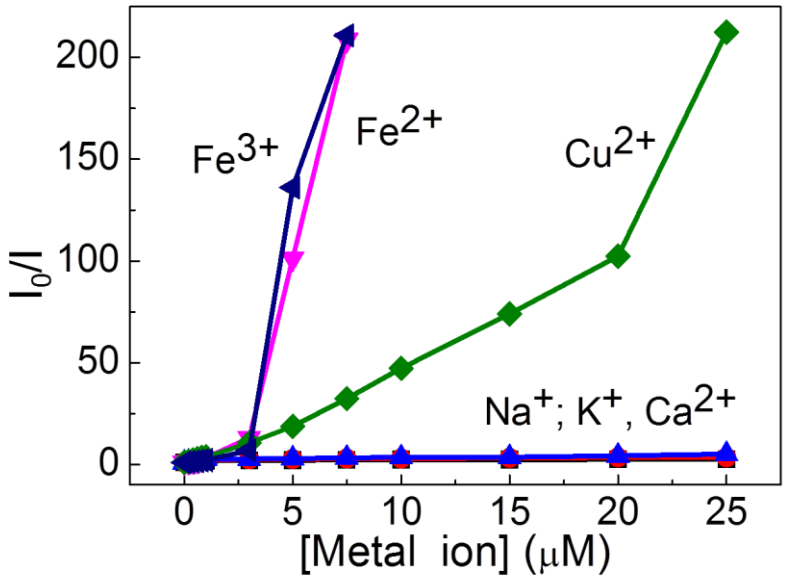

Figure 2-2. Stern-Volmer Plot for PPE-$^{d}CO_2$ (780 nM) in water with different metal ions, I_0 and I are the fluorescence intensities of PPE-$^{d}CO_2$ before and after the addition of metal ions.

FCS measurements

The diffusion behavior of 780 nM aqueous PPE-$^{d}CO_2$ with the same six metal ions was investigated via FCS. The normalized FCS correlation curves for PPE-$^{d}CO_2$ with six metal ions at 15 μM are shown in Figure 2-3A. Although the sizes of the polymer and the polymer/metal complexes are not absolutely uniform, the single species fitting equation (see Equation 2-2 in experimental section) was nonetheless used to fit the FCS curves, so that the average diffusion time for each CPE sample could be obtained. As can be seen, the polymer alone has the shortest diffusion time at 60.2 ± 1.8 μs. The addition of Na^+, K^+ and Ca^{2+} ions induces very little change in the correlation curves, and the diffusion time increases only slightly to 69.2 ± 3.1 μs for Na^+, 66.8 ± 2.7 μs for K^+, and 90.9 ± 5.2 μs for Ca^{2+}, indicating that the size of the polymer increases very little in the presence of these metal ions. However, when the same concentration of Cu^{2+} is added to the polymer solution, the curve shifts to a much longer diffusion time of 0.406 ms, which is almost 7 times that of the pure polymer. The curve shifts even further with a diffusion time of 1.06 ms upon the addition of Fe^{2+}, suggesting the formation of large aggregates in the presence of these metal ions. The largest change is observed after addition of Fe^{3+}, which features the longest diffusion time of 4.38 ms. From the comparison, we can conclude that the ability of metal ions to induce aggregation increases in the order of $K^+ \approx Na^+ < Ca^{2+} < Cu^{2+} < Fe^{2+} < Fe^{3+}$, which is consistent with the increase of the positive charge density on the metal ions as well as their binding

affinities to the carboxylate groups on the polymer side chains. In addition, Fe^{2+} and Fe^{3+} and Cu^{2+} tend to bind to multiple donor atoms, and thus can bridge two of the tri-acid units on two adjacent PPE-$^{d}CO_2$ chains. Note there are some unusual spikes showing up in the diffusion curve with Fe^{3+} and this is due to the formation of very large aggregates.[53]

The count rates (corresponding to the fluorescence intensity) versus observation time for polymer/metal ion mixtures at [metal ion] = 15 μM are shown in Figure 2-3B. Most of the fluctuation profiles have a narrow distribution of fluorescence events, and therefore the fluctuation profiles often have a stable baseline.[62] However, in some cases,[51,53] a few peaks are observed in the fluctuation profiles of some polymer-metal mixtures (such as PPE-$^{d}CO_2$ with Fe^{2+}). Such peaks have usually been attributed to the existence of some relatively large particles passing through the excitation volume,[72,73] indicating the formation of aggregates. Note that the count rate, which reflects the corresponding to the fluorescence intensity, decreases in the order of $Na^{+} > K^{+} > Ca^{2+} > Fe^{2+} > Cu^{2+} > Fe^{3+}$. According to previous reports[29] and the results described above, the formation of aggregates can efficiently quench the CPE fluorescence, because the emission is dominated by excitons, which are trapped in the aggregated state. Thus, the above intensity order is consistent with the observed quenching ability of these metal ions.

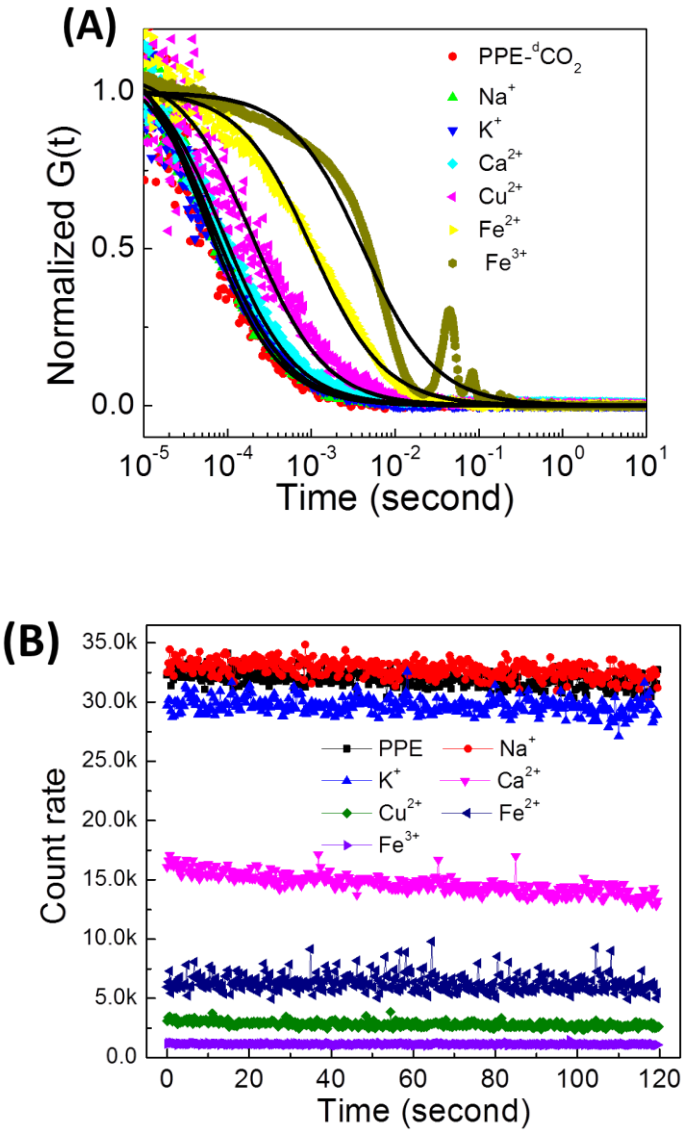

Figure 2-3. (A) Normalized correlation curve for PPE-$^{d}CO_2$ (780 nM) in water with different ions (15 μM). (B) Count rates for PPE-$^{d}CO_2$ (780 nM) in water with different ions (15 μM). The black solid lines are single specific fitting curves.

The effect of metal ion concentration on the size of the PPE aggregates was also investigated. The correlation curves for PPE-$^{d}CO_2$/Fe^{2+} mixtures at [Fe^{2+}] = 5 - 25 μM are specifically selected and presented in Figure 2-4. In general, the diffusion time increases gradually with increasing [Fe^{2+}], reflecting an increase in aggregate size. In particular,

this is a considerable increase in size from 5 μM to 7.5 μM, indicating that the formation of very large aggregates is triggered at this point, with [Fe^{2+}] ≈ 7.5 μM as the onset concentration for formation of large CPE aggregates. A small spike is observed near the end of the curve when [Fe^{2+}] = 25 μM. This is presumably due to the formation of larger particles.[53]

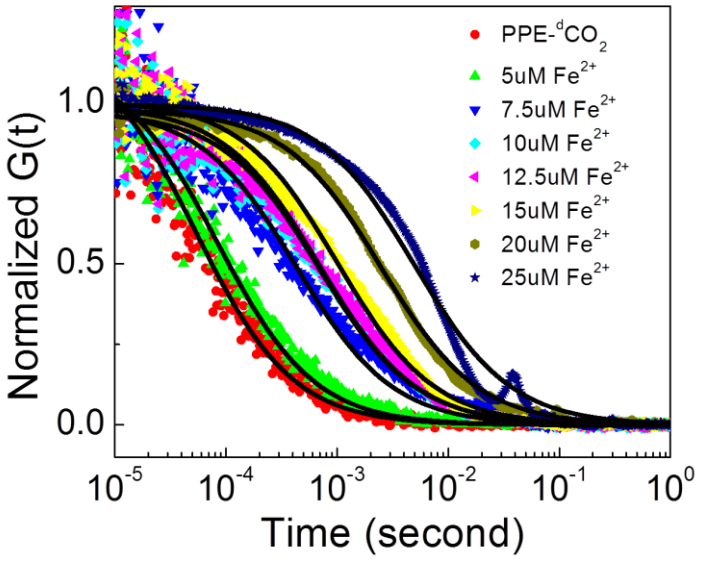

Figure 2-4**.** Normalized correlation curves of PPE-$^{d}CO_2$ (780 nM) in water with different [Fe^{2+}] (5 - 25 μM). The black solid lines are single specific fitting curves.

In order to gain a complete picture of the effect of metal ions on the diffusion behavior of PPE-$^{d}CO_2$, the diffusion time ratios τ_d/τ_{d0} for PPE-$^{d}CO_2$ in water before and after the addition of metal ions with varying concentrations from 5 μM to 25 μM were calculated and are plotted in Figure 2-5. Detailed diffusion time ratio data for each ion is summarized in Table 2-1.

Table 2-1. Diffusion time ratio (τ_d/τ_{d0}) of PPE-$^{d}CO_2$ ([PPE-$^{d}CO_2$] = 780 nM) with different metal ions at different concentrations.

Concentration of ions (μM)	Na^+	K^+	Ca^{2+}	Fe^{2+}	Fe^{3+}	Cu^{2+}
5	1.04	1.07	1.05	1.38	2.97	1.3
7.5				7.52	11.84	2.4
10				8.97	18.18	3.5
12.5				12.10	41.61	4.5
15	1.15	1.11	1.51	17.66	72.72	6.75
20				43.53	>100	7.24
25	1.16	1.21	1.90	77.34	>100	8.59

Based on Equations 2-3 and 2-5 (see experimental section), the diffusion time τ_d is proportional to *R*, the hydrodynamic radius of the particle. Therefore, any changes in the hydrodynamic radius will affect the mobility of the molecules; a large particle would usually have a longer diffusion time than small particles in a certain fixed volume.[74,75] As a result, each of the plots provides insight as to how the size of the polymer changes in the presence of different metal ions at varying concentrations. As illustrated in Figure 2-5, the τ_d/τ_{d0} is very close to 1 for Na^+ and K^+ at all concentrations, suggesting that monovalent metal ions fail to induce the aggregation of PPE-$^{d}CO_2$. The ratio increases to 2 for Ca^{2+} at 25 μM, and for Cu^{2+} the ratio is about 8 at this concentration, indicating that divalent metal ions intend to bind with polymers and induce the formation of small aggregates. However, for Fe^{2+} and Fe^{3+}, τ_d/τ_{d0} increases greatly with the increasing of

concentration and reaches 70 when [Fe^{2+}] = 25 μM and [Fe^{3+}] = 15 μM. Very large CPE aggregates are believed to be formed in these systems.

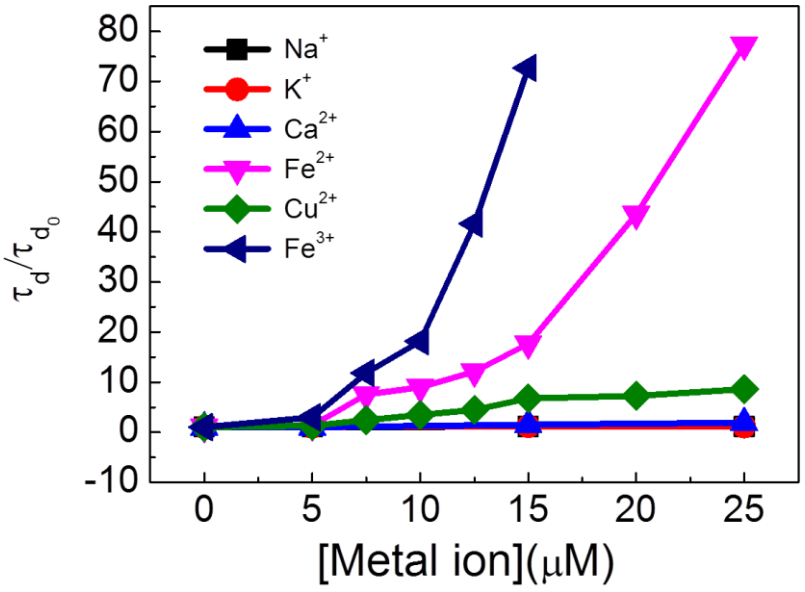

Figure 2-5. Diffusion time ratio for PPE-$^d CO_2$ (780 nM) in water with different metal ions measured by FCS, τ_{d0} and τ_d are the diffusion time of PPE-$^d CO_2$ before and after the addition of metal ions.

By comparing Figures 2-2 and 2-5, a direct relationship between fluorescence quenching and polymer aggregation is observed. It is evident that metal ions display similar trends in polymer fluorescence quenching and aggregation. The most efficient Stern-Volmer quenching is observed for the metal ions that give rise to the longest diffusion times, i.e., largest polymer aggregates, verifying previous reports that polymer aggregation plays an important role in the amplified quenching effect.[18,22,23,33] Moreover, these results also shed light on the origin of the super-linear Stern-Volmer correlations that are frequently observed for CPE-quencher systems. From the FCS results, it is

evident that there is a minimum concentration of metal ions needed to induce aggregation (7.5 μM for Fe^{2+} in this study).

Size calculation and AFM studies

Although it is difficult to know the exact shapes of the particles in different systems, we assume that they are approximately spherical particles to calculate approximate hydrodynamic radius, R_H. By using Equation 2-3 and 2-5 (see experimental section), the R_H of PPE-$^dCO_2$ is calculated to be ~1.9 nm. After the addition of 15 μM metal ions, the values of R_H are 2.2, 2.1 and 2.9 nm for PPE-$^dCO_2$ with Na^+, K^+ and Ca^{2+}, respectively, while for Fe^{2+}, Fe^{3+} and Cu^{2+}, the calculated R_H values are 34, 140 and 13 nm, respectively. Additional information about the size of the mixture is summarized in Table 2-2.

Table 2-2. Hydrodynamic radius (R_H/nm) of PPE-$^dCO_2$ ([PPE-$^dCO_2$] = 780 nM) with different metal ions at different concentrations.

Concentration of ions (μM)	Na^+	K^+	Ca^{2+}	Fe^{2+}	Fe^{3+}	Cu^{2+}
5	2.02	2.08	2.04	2.68	5.76	2.52
7.5				14.6	23.0	4.66
10				17.4	35.3	6.79
12.5				23.5	80.7	8.55
15	2.23	2.15	2.93	34.3	141	13.1
20				84.4	>194	14.0
25	2.25	2.35	3.69	150	>194	16.7

AFM was also used to study the size change of the polymer in the presence of Fe^{3+} at different concentrations. The solutions were deposited on the surfaces of mica substrates and dried overnight before undergoing AFM measurement. As shown in Figure 2-6, pure PPE-$^{d}CO_2$ without any metal ions is well dispersed and no large particles are observed. After adding 5 μM of Fe^{3+} to the polymer solution, several clusters of the polymer are observed with fairly large sizes. As [Fe^{3+}] increases to 30 μM, a much larger aggregate is observed with a significant height of 200 nm. It was not easy to find this aggregate during sample scanning, indicating that the aggregates formed in dilute solution are few in number with many polymer strands per particle. The AFM image supports the FCS results that Fe^{3+} can successfully induce strong inter-chain aggregation of PPE-$^{d}CO_2$.

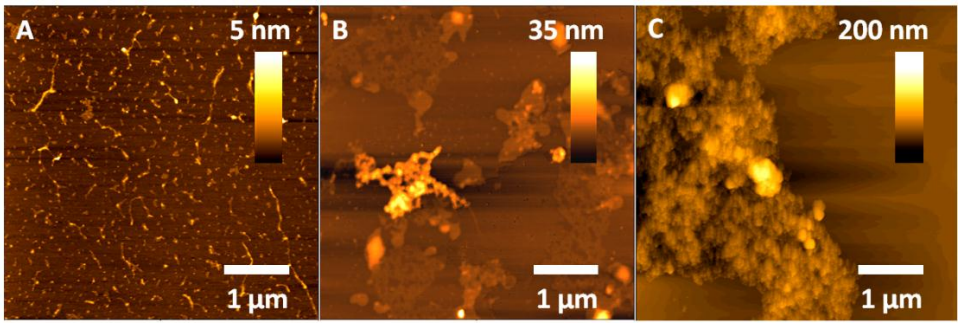

Figure 2-6. AFM images of PPE-$^{d}CO_2$ (1 μM) with different [Fe^{3+}] (0 - 30 μM). (A) PPE is well dispersed when no Fe^{3+} is added. (B) Small aggregates formed when [Fe^{3+}] = 5 μM. (C) Large aggregated formed when [Fe^{3+}] = 30 μM.

PPi Induced Aggregation of Cationic PPE-$^{d}NH_3$

In an earlier study,[30,31] we reported that PPi (structures in Figure 2-7) can efficiently quench the fluorescence of cationic PPE-$^{d}NH_3$ (structure in Figure 2-1). Due to the fact

that PPi cannot directly participate in any electron or energy transfer process with the polymer, the most likely reason for this quenching capability is aggregation of the polymer through electrostatic or hydrophobic interactions. In our previous work, direct evidence for aggregation-induced quenching was insufficient, and in the present report we utilize FCS to prove the hypothesis. Initially, fluorescence spectra of 1 μM PPE-$^{d}NH_3$ in MES buffer in the presence of PPi from 0.5 to 10 μM were recorded (Figure 2-7). When the PPi concentration increases, the strong blue emission at λ = 430 nm decreases, accompanied by appearance of a broad and structureless green band at around λ = 520 nm. The large red shift (~90 nm) of the fluorescence spectrum suggests that the photoluminescence emanates from a lower energy state,[29] and that strong inter-chain interactions (e.g., π-π stacking) between phenylene rings in adjacent chains may enhance the conjugation effect and lower the overall energy level.

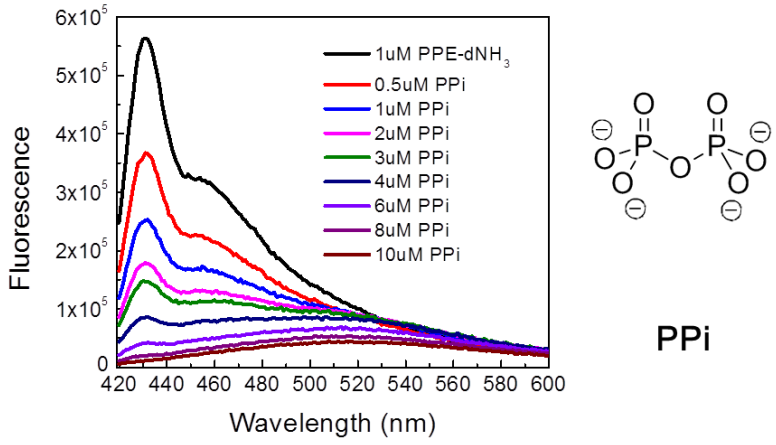

Figure 2-7. Fluorescence spectra of PPE-$^{d}NH_3$ solution (1 μM) titrated with PPi in MES buffer (10 mM, pH 6.5).

To further investigate the reason for the PPi-induced fluorescence quenching of PPE-$^{d}NH_3$, FCS measurements are carried out on 1 μM PPE-$^{d}NH_3$ solutions with varying PPi concentrations of 1, 10 and 25 μM in MES buffer solution. The normalized correlation functions obtained for each mixture are displayed in Figure 2-8A. The initiate diffusion time of PPE-$^{d}NH_3$ is 58.0 μs, however, after the addition of 1 μM PPi, the correlation curve does not change much (τ_D= 58.5 μs). When [PPi] increases to 10 μM, a shift in the FCS curve is observed, indicating the formation of large aggregates with an estimated diffusion time of 2.03 ms. After 25 μM PPi is added to the polymer solution, a more pronounced shift is observed and the diffusion time is ~11.8 ms. The result demonstrates that even larger aggregates are formed with increasing [PPi]. The calculated R_H are 1.88 nm for PPE-$^{d}NH_3$ itself; and 65.7 nm and 382 nm when [PPi] = 10 μM and 25 μM, respectively.

Figure 2-8B illustrates the count rate of PPE-$^{d}NH_3$ (1 μM)/PPi mixtures with different [PPi] in MES buffer. In the control experiment of PPE-$^{d}NH_3$ without PPi, the baseline is quite stable with no obvious peaks and it has relatively high fluorescence intensity. A large peak appears after the addition of 10 μM PPi to the polymer solution, indicating that large aggregates are passing through the illumination volume. The fluorescence intensity largely decreases when PPi is added. When the [PPi] increases to 25 μM, a higher peak appears, attributed to the formation of even larger aggregates in

the solution. The fluorescence intensity of this system is the lowest, and the intensity trend is consistent with the spectra shown in the Figure 2-7.

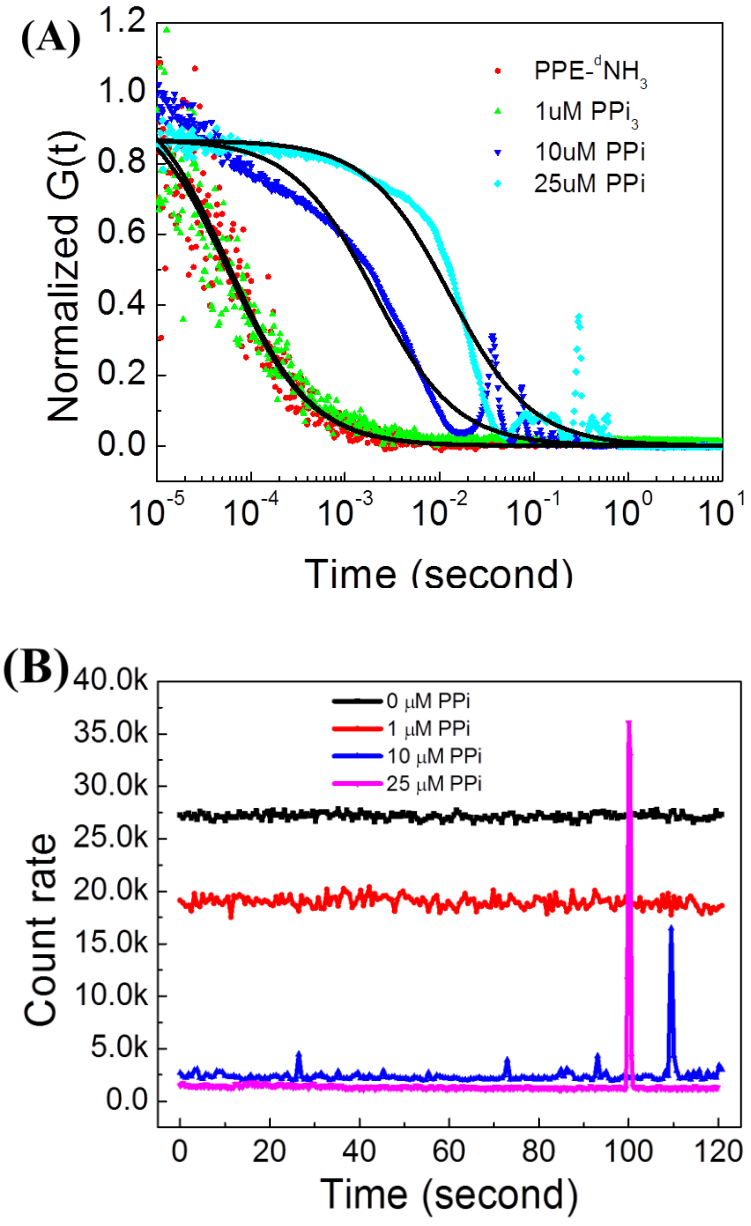

Figure 2-8. (A) Normalized correlation curve for PPE-$^{d}NH_3$ (1 μM) with different [PPi] in MES buffer (10 mM, pH 6.5). The black solid lines are single specific fitting. curves. (B) Count Rates for PPE-$^{d}NH_3$ (1 μM) with different [PPi] in MES buffer (10 mM, pH 6.5).

Mechanisms

In the first system with PPE-$^{d}CO_2$, the cationic ions supposedly form ion-pair complexes with the anionic polymer. A photon-induced electron transfer mechanism is responsible for the significant quenching of PPE by electron-deficient ions Cu^{2+}, Fe^{2+} and Fe^{3+}, where the excitons will be trapped and deactivated.[76-78] Other ions, like Ca^{2+}, have close-shell structures and are incapable of attracting electrons from the polymer chains.

It has been reported that the quenching efficiency of oppositely charged quenchers on CPEs is more efficient when the polymer chains are highly aggregated, due to the interchain exciton migration.[23,76,79,80] Larger aggregation is induced by those ions (Fe^{3+}, Fe^{2+} and Cu^{2+}) with higher positive charge density compared to Na^{+} and K^{+}. Moreover, the reason Fe^{2+} and Fe^{3+} have higher quenching efficiencies than Cu^{2+} is likely due to a higher association constant for binding of iron ion to the anionic side chains in contrast to Cu^{2+}, which primarily forms complexes containing four ligands (tetrahedral or distorted octahedral with water in axial position). Fe^{2+} and Fe^{3+} form octahedral complexes with six donor atoms, resulting in a greater tendency to crosslink two sets of tri-CO_2 pendants on different polymers and form aggregates. Iron (III) in particular, forms strong complexes with oxygen donors. Consequently, the amplified quenching is the result of the combined effects of both ion-pairing charge transfer and multivalent-related aggregation.

The mechanism is illustrated in Figure 2-9. When a small amount of Cu^{2+}, Fe^{2+} or Fe^{3+} ([metal ions] < 3 μM) is added to the PPE-$^{d}CO_2$ aqueous solution, the metal cation will bind with the anionic carboxylate groups on the polymer due to electrostatic interactions. At this point, the negative charge density of the polymer is partially decreased, but the polymer still retains the characteristics of molecularly dissolved chains, and photo-induced electron transfer is not pronounced for the electron-deficient metal ions. Thus, only slight quenching of the polymer is observed and the small size change is not detectable by FCS. When the concentration of metal ions exceeds 3 μM, inter-chain crosslinking of the polymer is induced, and small aggregates of PPE-$^{d}CO_2$ begin to appear in the solution. As a result, an exciton generated upon photo-excitation can migrate along different polymer chains until it meets a metal ion, where the exciton is quenched. Since any electron receptor, i. e., a metal ion, attached to a single polymer chain is capable of quenching a number of polymer chains in the aggregate, amplified quenching occurs, resulting in the onset of a large decrease of fluorescence in the Stern-Volmer plot in Figure 2-2. However, the molecular weight becomes only three- or four-times that of the single chain, as only small aggregates form at this point. Based on Equations 2-3 and 2-8 (see experimental section), the change of the molecular weight is roughly proportional to the third power of molecule's diffusion time. Therefore, the size of the polymer changes only slightly, and only small increase in the diffusion time is observed (Figure 2-5). After a large excess of metal ions is added, PPE-$^{d}CO_2$ is highly

crosslinked by the metal cations to form large aggregates. A significant extension of the diffusion time of polymer is observed, corresponding to the large increase of molecular weight and a large rise of the diffusion time ratio is observed (Figure 2-5). This model explains the response lag between the Stern-Volmer plot and the diffusion time ratio plot in Figures 2-2 and 2-5. The diffusion time ratio increases remarkably at 10 μM Fe^{2+} and at 7.5 μM Fe^{3+}, while in the Stern-Volmer plot, the fluorescence decreases significantly after the addition of only 3 μM Fe^{2+} or Fe^{3+}.

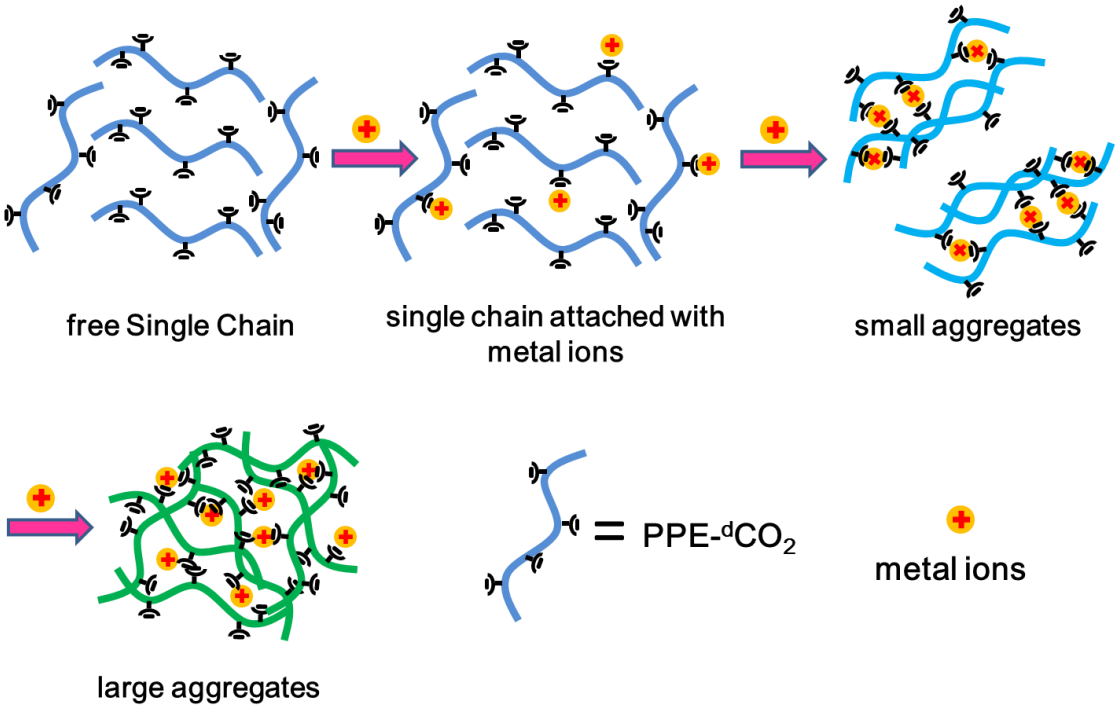

Figure 2-9. Mechanism for PPE quenched by metal ions.

A similar mechanism can be applied to the other system with PPE-$^{d}NH_3$. PPE-$^{d}NH_3$ exists as a single chain without PPi in MES buffer solution and emits high intensity blue light. After PPi is attached to the NH_3^+ groups, the intense negative charge density on

PPi neutralizes the polyamine groups and also induces inter-chain interaction of PPE-$^{d}NH_3$ to form aggregates. Fluorescence of PPE-$^{d}NH_3$ is highly quenched and shifts to longer wavelength. The FCS result gives solid proof of formation of large aggregates, especially after adding 10 μM PPi. By introducing FCS, the amplified quenching mechanism has been investigated from a new aspect. More importantly, the comparison of different responses by two techniques based on different mechanisms (fluorescence quenching and FCS), provides insight into the details of molecular interactions during the quenching process.

Summary

We have successfully constructed an FCS system with blue laser as light source and provided the details regarding the alignment, optimization, and calibration of the setup. Two examples were carefully investigated. In the study of PPE-$^{d}CO_2$ with metal ions, Fe^{3+}, Fe^{2+} and Cu^{2+}, which have much higher polymer quenching efficiencies compared to other ions, were shown to induce significant polymer aggregation based on the FCS results. The electron densities of the metal ions and their binding affinities to the carboxylate groups on the functional chains play an essential role in aggregate formation. The correlation between the Stern-Volmer and diffusion time ratio plots demonstrates that aggregation of the CPE contributes significantly to the amplified quenching phenomenon. Furthermore, the large increase in diffusion time observed by FCS clearly proved that the quenching of PPE-$^{d}NH_3$ is due to a conformational or

aggregation-induced mechanism. Both of the results are consistent with the data from fluorescence measurement.

The changes in photophysical property of CPE resulted from the combined effects of electron transfer and conformation change of polymers. It is difficult to distinguish the effects from the two mechanisms based solely on the fluorescence spectroscopy measurements. FCS is capable of measuring polymer size in solution, providing insight and direct information about physical state of the polymer. With the help of FCS, we were able to explain the fluorescence change caused by different quenching mechanisms in greater detail and also to prove the amplified quenching mechanism via a different experimental method. Ions with high charge density can induce formation of larger aggregates, consistent with their higher quenching efficiency as shown in the fluorescence spectra. Thus ion-induced aggregation significantly contributes to the fluorescence quenching of CPE.

In this work, use of a 405 nm laser has successfully expanded application of FCS to CPE area and established a platform for in depth study of conformational changes and the diffusion behavior of CPE. FCS is clearly a promising and powerful tool for investigations of the interactions between CPE and other ions or molecules, as well as resulting conformational changes.

Experimental

Materials

PPE-$^{d}CO_2$ and PPE-$^{d}NH_3$ were synthesized and prepared according to the reported procedures.[30,31] Molecular weights of the PPE-$^{d}CO_2$ and PPE-$^{d}NH_3$ were ca. 27,300 and 16,600 Da, respectively. Fluorescein was purchased from Fisher. All sample solutions were prepared using water distilled and purified by a Millipore purification system (Millipore Simplicity Ultrapure Water System). Buffer solutions were prepared with reagent-grade materials (Fisher). All polymer concentrations are reported as the polymer repeat unit concentration. Fluorescein was prepared in 10 mM phosphate buffer (pH = 8). MES buffer solution (10 mM, pH = 6.5) was prepared from 2-(N-morpholino) ethanesulfonic acid and sodium hydroxide. All metal ions were purchased from Sigma-Aldrich Company and used as received. Sodium pyrophosphate was obtained from J. T. Baker Chemical Co.

Instrumentation

FCS measurements were taken on a homemade setup using a 405 nm diode laser (Coherent, CUBE) as the excitation light (Setup in Figure 2-10). Fluorescein (30 nM in 10 mM phosphate buffer, pH = 8) was used as the calibration standard for the system. Fluorescence spectra were recorded on a Photon Technology International fluorometer and corrected by using correction factors generated with a primary standard lamp.

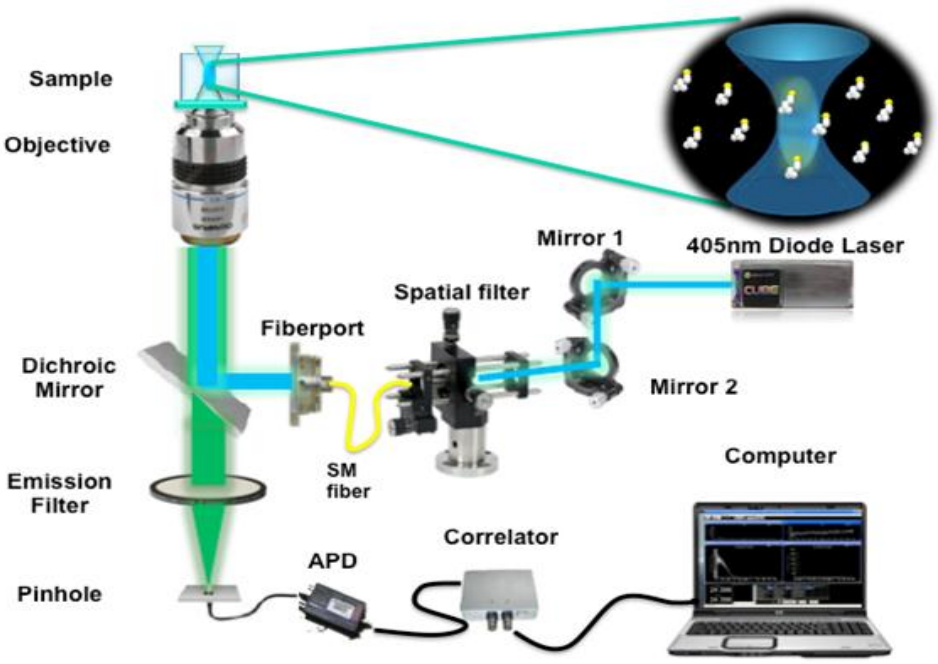

Figure 2-10. Setup of FCS system in our lab.

Theory of FCS

In principle, fluctuations in the fluorescence signal are quantified by temporally autocorrelating the recorded emission signals collected within the confocal volume. The normalized autocorrelation function,$G(\tau)$, defined as[52]

$$G(\tau) = \frac{\langle F(t)\cdot F(t+\tau)\rangle - \langle F(t)\rangle^2}{\langle F(t)\rangle^2} = \frac{\langle \delta F(t)\cdot \delta F(t+\tau)\rangle}{\langle F(t)\rangle^2} \quad (2\text{-}1)$$

is used to characterize the temporal fluctuations. In Equation 2-1, $\delta F(t) = F(t) - < F >$ describes the fluctuation of the fluorescence signal $F(t)$, as deviations from the temporal average of the signal $< F >$ at time t. A three dimensional fitting model, representing a single-component system is written as:

$$G_{3D}(\tau) = \frac{1}{N} \times \frac{1}{1+\frac{\tau}{\tau_D}} \times \frac{1}{\sqrt{1+\frac{\tau}{\omega^2 \times \tau_D}}} \quad (2\text{-}2)$$

where ω_z is the longitudinal radius and ω_r is the transversal or waist radius of the confocal volume; and ω, the structure parameter, equates to $\frac{\omega_z}{\omega_r}$. *N* is the average number of fluorescent molecules in the confocal volume; τ_D is the average time of fluorescent molecules diffusing in the detection volume, which is characteristic for a specific molecule.

The relationship of τ_D to the molecular diffusion coefficient *D* (m^2s^{-1}) is given by:

$$\tau_D = \frac{{\omega_r}^2}{4D} \tag{2-3}$$

The waist radius is obtained from its conversion equation:

$$\omega_r = \sqrt{4D_{free\ dye} \cdot \tau_D} \tag{2-4}$$

where $D_{free\ dye}$ is the diffusion coefficient of the standard calibration dye.

The translational diffusion coefficient, *D,* of a molecule is related to its size by the Stokes-Einstein equation:

$$D = \frac{kT}{6\pi\eta R} \tag{2-5}$$

where *k* is Boltzmann's constant; *T* is the temperature; η is the viscosity of the solvent; and R is the hydrodynamic radius. Equation 2-5 can be used to estimate the size of diffusing particles by assuming the particles has a spherical shape with radius *R*, which is related to the molecular weight *MW* of the molecule with a specific gravity $\bar{v}$ by

$$V = MW\bar{v} = \frac{4}{3}\pi R^3 \tag{2-6}$$

where V is the volume of molecule. Thus we have

$$R = \left(\frac{3MW\bar{v}}{4\pi}\right)^{1/3} \quad (2\text{-}7)$$

These equations show that the radius *R* and diffusion coefficient *D* are weakly dependent on the molecular weight. By combining Equation 2-5 and 2-7, we have:

$$D = \left[\frac{kT}{6\pi\eta}\left(\frac{4\pi}{3\bar{v}}\right)^{1/3}\right] MW^{-1/3} \quad (2\text{-}8)$$

This relationship is useful for estimation of the molecular weight of a spherical particle from its diffusion coefficient.

CHAPTER 3
DIFFERENT AGGREGATIVE RESPONSES FOR NONQUENCHING MULTICATIONIC AMINES USING CONJUGATED POLYELECTROLYTES

Background

Amines are a class of small organic molecules that are used extensively in industries for colorant manufacture, fertilizer production and pharmaceutical preparation.[81-85] Biogenic polyamines (e.g. cadaverine, spermine, spermidine, and putrescine) are present in living organisms and are known to be involved in regulation of gene expression, cell proliferation and differentiation.[34,86] In addition, some amines have been identified as potential indicators for various health risks, including cancer, bacterial infection and food poisoning.[87-89] The role amines play in human health and food quality is so important that it is imperative to design and develop an easy, rapid and effective method to detect the target amines. In recent decades, some methods have been developed to sense different amines, including using antibodies,[90] molecularly imprinted polymers (MIPs),[91,92] enzymes,[93] single molecule[94,95], array sensors,[96,97] electrophoretic analysis[98] and the most commonly used method high-performance liquid chromatography.[99] These traditional approaches have several limitations. For example, existing amine assays are usually laborious, requiring expensive equipment, and are relatively slow and therefore unsuitable for rapid screening applications. As a result, a rapid and sensitive detection method for amines would be very promising to screen a large number of amines samples, especially those with similar structures and properties.

While many highly sensitive CPE-based sensors have been reported, most signal transduction mechanisms for these CPEs reply on the electron or energy transfer between the polymer and a quencher.[71,100,101] Other analytes such as amines cannot participate in these direct quenching processes due to their incompatible redox and spectral properties. In this situation, an alternative approach driven by analyte-induced aggregation has been employed, leading to self-quenching processes. This strategy takes advantage of the interchain conformational change of the polymer induced by electrostatic and/or hydrophobic interactions between these nonquenching analytes and polymers. Moreover, the assembly of polymers by different amines leads to different aggregative responses.

In this chapter, we utilize **P3** (an anionic PPE functionalized with carboxylate groups, Figure 3-1) to investigate the different aggregative responses by a group of three structurally similar amines: ethylenediamine (**C2N2**), cavaderine (**C5N2**) and tris(3-aminoethyl)amine (**N4**) (structures shown in Figure 3-1).Upon the addition of amines, only **N4** was found to effectively induce the formation of tightly associated aggregates between the polymer chains in solution, while **C2N2** and **C5N2** showed negligible effect on the polymer aggregate formation. The results are consistent with similar work reported by Swager.[57] Different fluorescence responses to different amines were also observed, indicating that the interaction between polymer chains and amines varied depending on the shape, valence and length of the amines. This work provides an

easy way to discriminate these similar amines and a better idea of how different analytes interact with polymers.

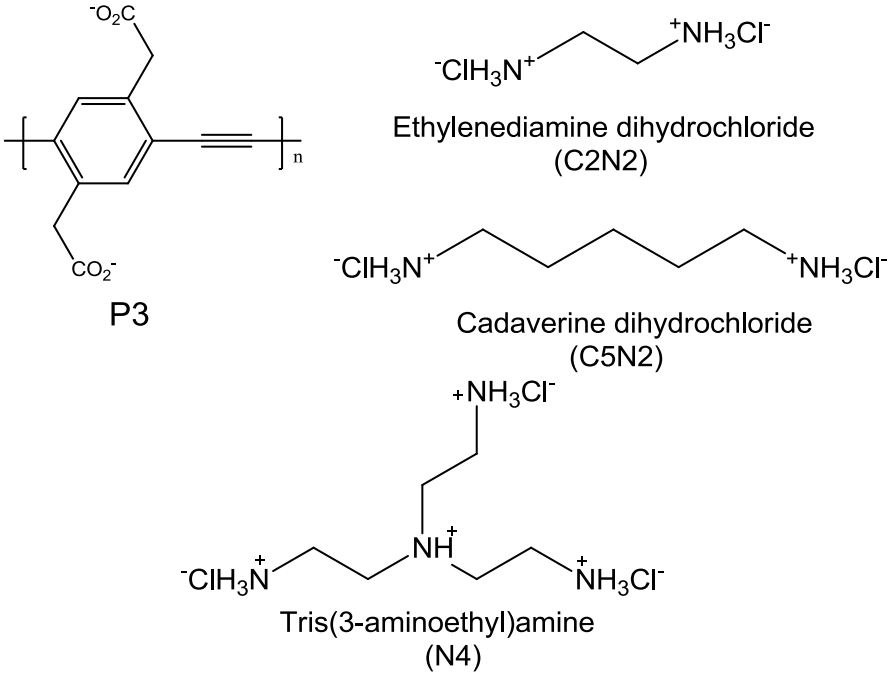

Figure 3-1. Chemical structures of **P3**, ethylenediamine dihydrochloride (**C2N2**), cadaverine dihydrochloride (**C5N2**) and tris(2-aminoethyl)amine (**N4**).

Results and Discussion

Photophysical Properties of P3

A conjugated polyelectrolyte substituted with carboxylate groups (**P3**) was designed and utilized in our experiments.[102] The normalized absorption and fluorescence spectra for **P3** in various solvents are shown in Figure 3-2. In methanol, **P3** exhibits an absorption wavelength maximum at 391 nm with a structured emission of 425 nm. In aqueous solutions, **P3** shows similar spectroscopic profiles with almost the same wavelength maxima or spectral band shape for the absorption and fluorescence spectra

(Table 3-1). This suggests **P3** is not aggregated in water, existing as molecularly dissolved chains.[103] It is likely the presence of the high negative charge density on each repeat unit of polymer minimizes the electrostatic interaction and interrupts the interchain aggregation, leading to enhancement in their fluorescence properties. For example, **P3** maintains a relatively high quantum yield in water (Φ_F = 0.42, using quinine sulfate in 0.1 M H_2SO_4 as standard), as it decreases only ~20 % compared with that in methanol (Φ_F = 0.52).

Table 3-1. Photophysical properties of **P3** in different solvents.

	MeOH			H_2O		
λ_{max}	λ_{max}^{abs}	λ_{max}^{em}	Φ_F	λ_{max}^{abs}	λ_{max}^{em}	Φ_F
P3	391	425	0.52	391	426	0.42

Quinine sulfate in 0.1 M H_2SO_4 is used as actinometer, Φ_F=0.545.

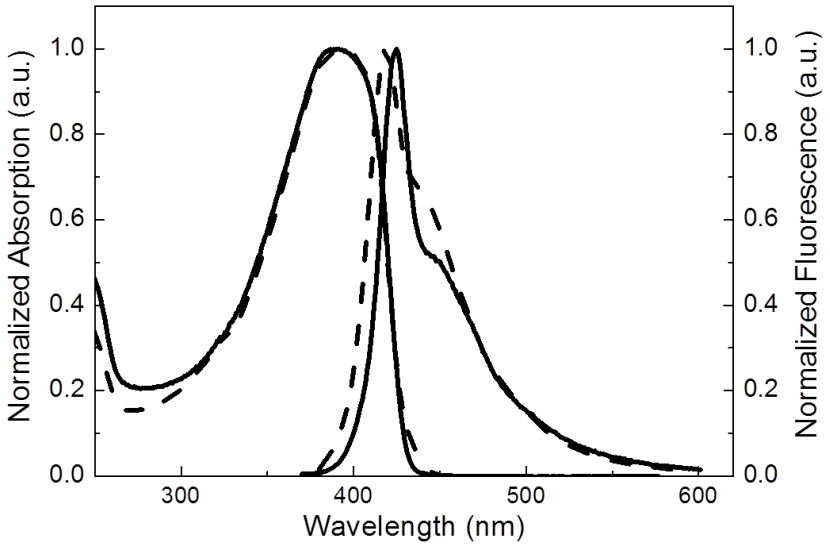

Figure 3-2. Normalized absorption and fluorescence spectra of **P3** in MeOH (solid line) and H_2O, pH = 6.5 (dashed line), λ_{ex} = 360 nm.

Fluorescence Quenching by Different Amines

Since anionic **P3** displayed "molecularly dissolved" property in aqueous solution, the aggregation behavior of this polymer to oppositely charged, small-molecule amines, was investigated. The aggregative responses of **P3** to different amines were carried out in water at a polymer concentration of 2.0 μM. In this experiment, three amines were chosen: ethylenediamine (**C2N2**), cadaverine (**C5N2**) and tris(2-aminopropyl)amine (**N4**) (see their chemical structures in Figure 3-1). Among these amines, the diamines vary by the number of methylene unit separating the diamino groups. The fluorescence titration spectrum for each amine at varying concentrations is displayed in Figure 3-3. As the concentration of **N4** increased, the fluorescence intensity significantly decreases and a red-shifted band shows up at ~530 nm, consistent with the aggregation-induced planarization of the polymer chains. In comparison, the addition of **C2N2** and **C5N2** were able to promote the planarization and a small degree of aggregation (possibly dimerization) between the polymer chains, resulting in fluorescence self-quenching. However, neither of them was capable of inducing the polymer aggregate formation. The degree of aggregation or possibly dimerization depended on the charge density and the structure of the amines.[104,105] Figure 3-3D shows the Stern-Volmer plot of the fluorescence spectra of **P3** with different amines. Overall, **N4** has the highest positive charge density (carrying three positive charges in pH 6.5 water based on pKa values[106]) and therefore features the most effective quenching ability compared to the other

diamines. Diamines were able to quench the polymer; however, they demonstrated different quenching efficiencies. The quenching efficiency decreases as the chain length of diamined increases, indicating that different structure of the diamines led to the π-π stacking of polymer chains to a different degree.[107] **C5N2** was the least effective quencher because its long and flexible structure that cannot bring two polymers in close distance to form tightly associated aggregates. Therefore, this CPE-based chemical sensor still exhibits some selectivity towards different amines.

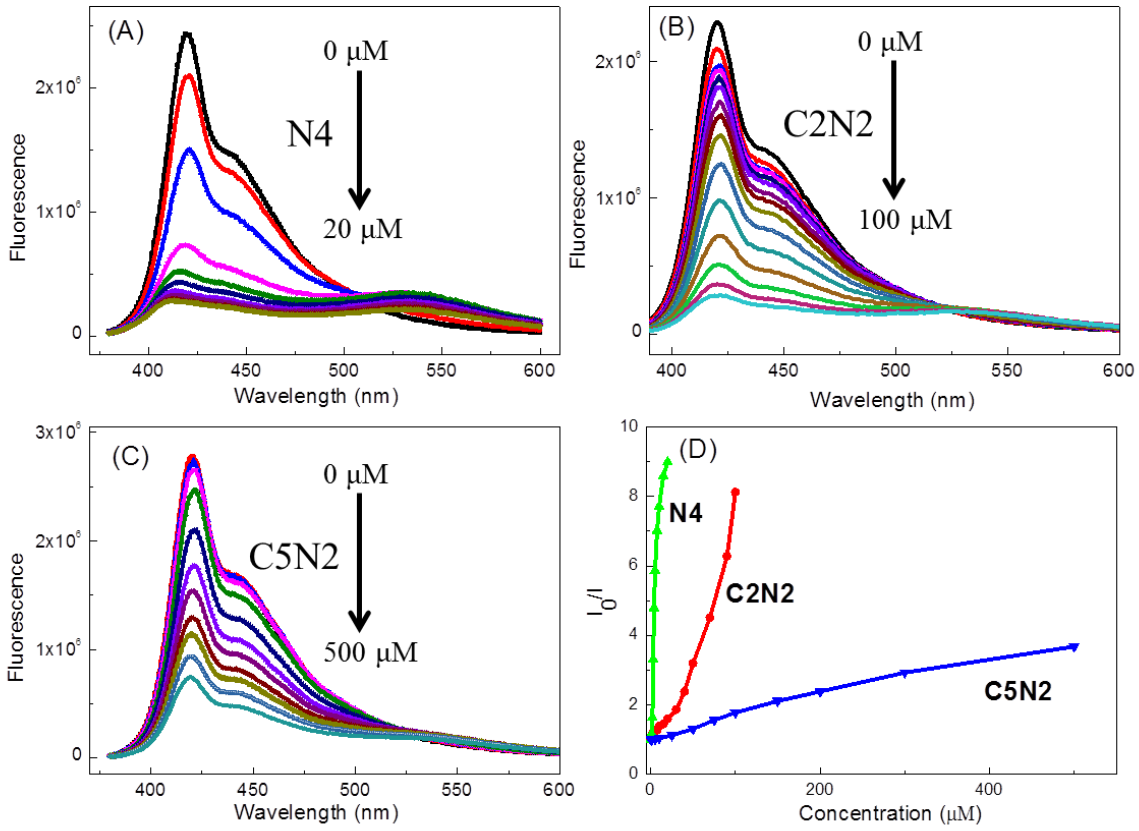

Figure 3-3. (A)-(C): Fluorescence spectroscopic changes of 2.0 μM **P3** solution observed upon titration of different amines in water: (A) **N4**, (B) **C2N2**, (C) **C5N2**; (D): Stern-Volmer plots of I_0/I as a function of amine concentration in water, pH = 6.5, λ_{ex} = 360 nm.

Effect on Amplified Quenching of P3 by MV^{2+}

Previously it is has been noted that aggregation has a significant effect on amplified quenching,[101] therefore we examined the effect of amine-induced aggregation on the amplified quenching of the polymer by methyl viologen (MV^{2+}, an electron transfer quencher). Figure 3-4A illustrates a series of Stern-Volmer plots for MV^{2+} quenching of **P3** fluorescence in the presence of various amines at a concentration of 25.0 μM in water (pH = 6.5). It is observed MV^{2+} quenches **P3** fluorescence with very different efficiency in different **P3**/amine systems. Interestingly, compared to the control experiment without amine, **N4** significantly enhances the quenching by MV^{2+}; whereas the other amines (**C2N2** and **C5N2**) decrease the amplified quenching effect. Overall, the quenching efficiency decreases in the order: **N4** > control (no amine) > **C2N2** > **C5N2**, corresponding to the decreasing positive charges and increasing chain length of the diamines. In the **P3**/**N4** complex, less than 200 nM MV^{2+} is required to quench 90% of the polymer fluorescence, while only ~65% of the fluorescence is quenched for the control experiment at the same level of [MV^{2+}]. More importantly, the Stern-Volmer plot in **P3**/**N4** system is superlinear even at low quencher concentrations. Superlinear quenching is observed immediately upon addition of a very small amount of MV^{2+} (less than 300 nM) in the presence of **P3** and **N4**, signaling the presence of aggregates. The enhanced quenching efficiency is ascribed from the increased exciton diffusion pathway in the PPE aggregates. In contrast, in the other two **P3**/diamine mixtures where the

polymer is much less effectively aggregated, the SV plot features a nearly linear plot and the slope (K_{sv} constant) is significantly less than that of the control at the same concentration level of MV^{2+}. We assume the reduced quenching efficiency is probably due to the fact that longer diamines like **C2N2** and **C5N2** are unable to induce efficient interchain aggregation at lower concentrations; therefore less quenching sites are available for MV^{2+} due to the excess presence of positively charged diamines. These diamines will preferably occupy one or two side groups within one polymer chain, which will screen the binding between **P3** and MV^{2+}. Therefore, it is suggested that the effect of adding amines on the amplified quenching is strongly dependent on the association constant between the polymer and diamine, which is related to the charge density as well as the rigidity of the amine structures. Only amines featuring high charge density lead to efficient aggregation of polymer. This finding illustrates the correlation between the quencher-induced aggregations of CPEs and amplified quenching effects.

To get a detailed perspective of how the presence of diamines affect amplified quenching, the amplified quenching effect of **P3** by MV^{2+} in the **P3**/**C2N2** complex solutions was investigated with varying [**C2N2**] from 0, 10, 25 to 50 μM. The Stern-Volmer results are illustrated in Figure 3-4B. The addition of **C2N2** decreases the amplified quenching efficiency and increasing [**C2N2**] will even lower the amplified quenching effect. For example, at the highest [MV^{2+}] level, the quenching efficiency is ~ 97 % for the control without addition of **C2N2**; but it decreases to ~ 90 %, ~85 % and

~78 % when [**C2N2**] is increased to 10, 25 and 50 μM. From the comparison, we can conclude the more and more binding sites on the polymer chain will become unavailable for MV^{2+} as [**C2N2**] is increased, leading to a higher competition and a decreased amplified quenching efficiency. The result is basically consistent with what we have discussed above.

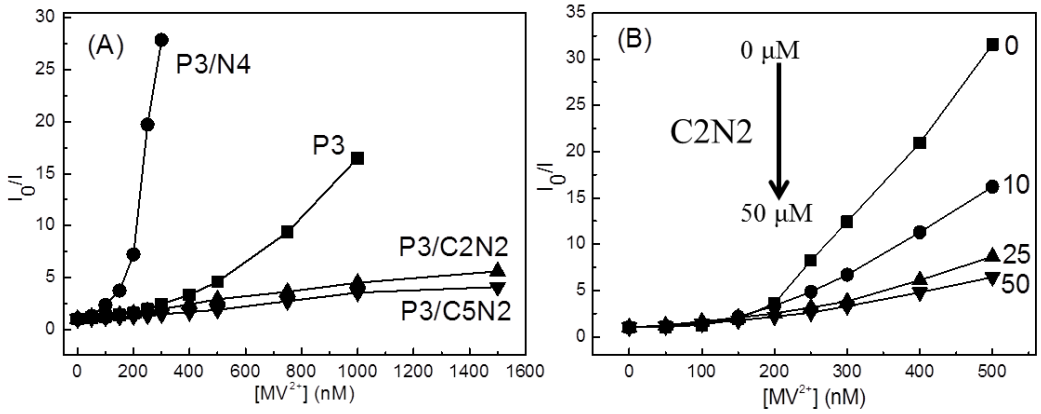

Figure 3-4. (A): Stern-Volmer plots of I_0/I as a function of MV^{2+} concentration for different **P3**/amine systems in water. [**P3**] = 2.0 μM, [amine] = 25.0 μM. (B): Stern-Volmer plots of I_0/I as a function of MV^{2+} concentration for **P3**/**C2N2** mixtures in w at different concentrations. ([**C2N2**] = 0, 10, 25 and 50 μM). [**P3**] = 2.0 μM. pH = 6.5, λ_{ex} = 360 nm.

Quantitation of Aggregation by Fluorescence Correlation Spectroscopy

Fluorescence correlation spectroscopy (FCS) was carried out to investigate the aggregation behavior of **P3** upon addition of different amines. Figure 3-5 summarizes the FCS experimental results for sample solutions containing 2.0 μM **P3** and 20 μM amine of **N4**, **C2N2** and **C2N5**, respectively. The result shows that **P3**/**N4** complex exhibits a significantly longer diffusion time (4.21 ms) compared with that of **P3** (0.0625 ms),

indicating the formation of large aggregates. In contrast, the correlation curve for **P3**/**C2N2** complex reveals a diffusion time of 0.0832 ms, which is only slightly larger than that of the free polymer, suggesting the size of the polymer increases a little but not too much. The increase is even less for **P3**/**C5N2** complex with a diffusion time 0.0741 ms, indicating longer amines are unable to induce effective aggregation of polymers. Therefore, it is expected both diamines were only able to promote a small degree of aggregation (most likely dimerization) between polymer chains. The FCS result demonstrated the quenching efficiency of amines decreases with decreasing positive charge and also decreases with increasing of chain length, which is consistent with the results from the fluorescence quenching studies.

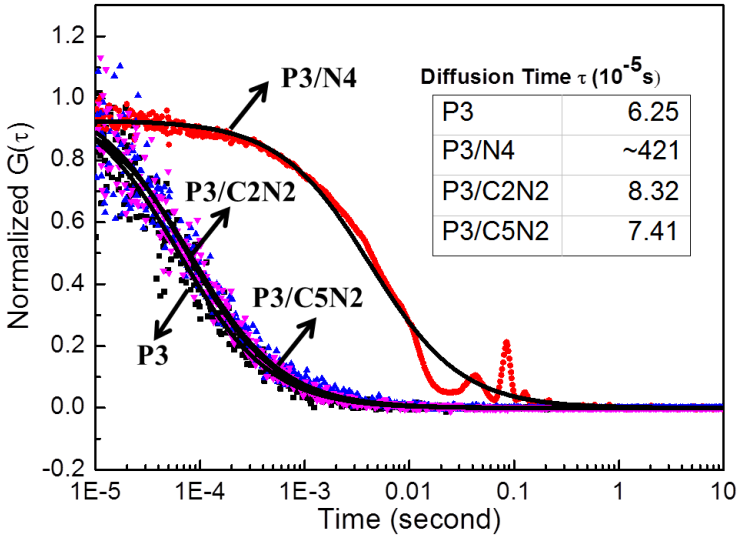

Figure 3-5. Normalized correlation curves for different systems in water. Black: [**P3**] = 2 μM; Red: [**P3**] = 2 μM, [**N4**] = 20 μM; Blue: [**P3**] = 2 μM, [**C2N2**] = 20 μM; Pink: [**P3**] = 2 μM, [**C5N2**] = 20 μM. The black solid lines are single specific fitting curves, pH = 6.5.

Proposed Mechanism

The quenching responses from **P3** towards structurally similar amines result from the multiple contacts between the carboxylate side chains on the polymer and the amino groups from amines through electrostatic and/or hydrophobic interactions. However, the quenching efficiency is highly dependent on the charge density as well as the shape of the amines. For example, tight and more packed interpolymer π-π stacking aggregates will form when adding a highly charged amine such as tetraamine.[35,108,109] In this situation, large PPE aggregates are observed and the polymer fluorescence is more quenched (Figure 3-6, path A). For diamines like **C2N2** and **C5N2**, they are unable to cross-link the polymer to form interpolymer stacking aggregates, due to their lower binding affinity (low positive charges). In addition, the chain length of these diamines is relatively long and therefore their structure is highly flexible and rotated, consequently, most of them will preferentially bind to one polymer chain instead multiple polymer chains (Figure 3-6, path B). In this situation, no large PPE aggregates formed. The quenching is resulted from the reduced electrostatic repulsion on the side chains, leading to the decrease of the fluorescence by increasing the free rotation of the polymer chains.

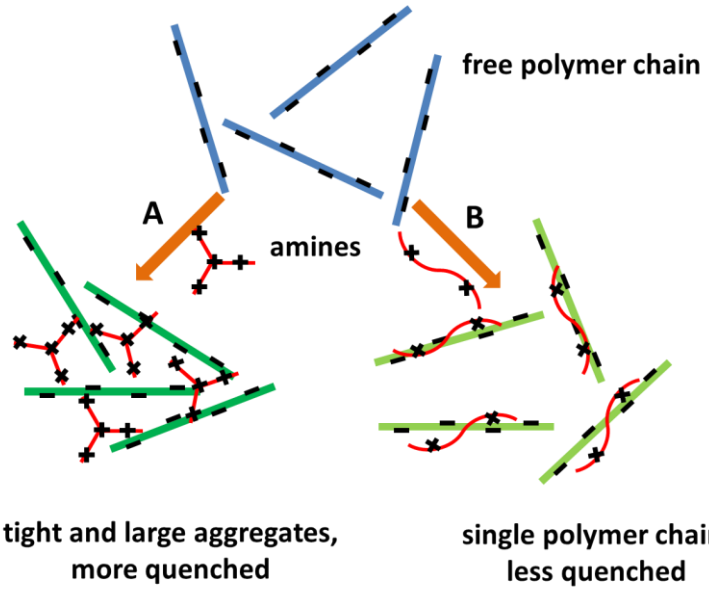

Figure 3-6. Schematic representation of analyte-induced aggregation between polymer and different amines.

Summary

In this chapter, we have investigated the interactions between a carboxylate-functionalized poly (phenylene ethynylene) (**P3**) and different amines. **P3** is "molecularly dissolved" and exhibits structured emission in aqueous solution. Both fluorescence quenching measurements and FCS measurements have been carried out. The results demonstrated that the positive charge density and the length of the amines have significant effects on the aggregated states of **P3** and also amplified quenching effect.

Based on the fluorescence quenching studies, it is suggested the quenching efficiency decreases in the order of: **N4** > **C2N2** > **C5N2**, which corresponds to the decreasing positive charge density and the increasing chain length of the diamines. The

effect of the presence of amines on amplified quenching has also been studied. It is found that different amines exhibit different effects on amplified quenching of **P3** by MV^{2+}. Significantly enhanced amplified quenching was observed in the presence of **N4,** resulting from its strong complexing ability with **P3** to form large and tight aggregates. The formation of aggregates increases the three-dimensional diffusion pathway for excitons . While for the diamines including **C2N2** and **C5N2**, they greatly weaken the amplified quenching effect. It is assumed that these diamines attach to the multiple binding sites of one polymer chain instead of adjacent polymer chains, due to the flexibility of their chemical structure as well as the low positive charge density. Therefore, they are not able to induce efficient interchain aggregation of the polymers. Instead, the occupancy of the diamines will reduce the available binding sites for the incoming MV^{2+}, leading to decreased quenching efficiency. The amplified quenching efficiency of MV^{2+} decreases with the increasing [**C2N2**]. At the same time, the FCS measurements demonstrate that only **N4** is capable of forming large aggregates with **P3** while the size changes for the other two **P3**/amines mixtures are negligible. Possible aggregation/quenching mechanisms for **P3** with different amines are carefully explained. Upon the addition of different amines, **P3** can be either cross-linked to form interpolymer aggregates or remain as free single chain or possibly dimers. The former case leads to the fluorescence quenching of **P3** while the latter also results in the fluorescence

quenching owing to the free rotation of the polymer chains after the side groups have been neutralized.

From previous reports by Lavigne et al.,[104] they showed that diamines form either tight or loose aggregates with polymers. While in our study, we proposed that longer diamines will preferably bind to one polymer chain instead of multiple polymer chains based on both amplified quenching studies and FCS measurements, which is consistent with the results reported by Swager.[57] However, direct evidence of how the aggregates look like is still insufficient. But our CPE-based sensor study provides a simple and rapid way to discriminate different amines.

Experimental

Materials

The synthesis of **P3** is described in the literature.[110] All sample solutions were prepared using water which is distilled and purified by using a Millipore purification system (Millipore Simplicity Ultrapure Water System). Methyl viologen dichloride hydrate, ethylenediamine dichloride, cavaderine dichloride and tris(3-aminoethyl)amine were purchased from Sigma-Aldrich. All chemicals were used as received, unless otherwise noted.

Instrumentation

UV-vis absorption spectra were recorded on a Shimadzu 1800 photospectrometer. Steady state emission spectra were measured and obtained from a spectrofluorometer

from Photon Technology International. All the spectra have been corrected by using correction factors generated with a primary standard lamp. FCS measurements are taken on a homemade setup using a 405 nm diode laser (Coherent, CUBE) as the excitation light. 30 nM fluorescein in 10 mM phosphate buffer (pH = 8) is used as the calibration standard for the system.

CHAPTER 4
PRINCIPAL COMPONENT ANALYSIS FOR PYROPHOSPHATE SENSORS USING CONJUGATED POLYELECTROLYTES

Background

Pyrophosphate ($P_2O_7^{4-}$, PPi and Figure 4-1) is a biologically significant anion that plays an essential role in bioenergetics and metabolic processes including energy transduction, extracellular signal mediations and protein synthesis.[111-114] In particular, PPi is known to be involved in several biochemical reactions, such as DNA and RNA polymerization,[115] hydrolysis of ATP,[116] cyclic AMP synthesis and many other enzymatic reactions.[61,117] It also has been reported that the abnormal level of PPi is related to various diseases including cancer,[118-120] arthritis,[121] and vascular calcification.[122] Therefore, the selective detection and sensing of PPi is important to understand its role in these biological processes. Among all the techniques, fluorescence detection methods received most attention due to their advantages such as superior sensitivity and selectivity, low cost, easy detection, versatility and wide dynamic range.[7]

In the past few years, the development of fluorescence sensors for PPi has become a major research focus and many PPi fluorescence probes have been reported, mostly based on small-molecule sensing methods.[123-125] In their approaches, small chromophores incorporated with metal cations, including zinc,[126] copper,[127] cadmium,[120] palladium, were employed as PPi receptors. PPi will coordinate with the metal ions to form host-guest complex, resulting in fluorometric (and/or colorimetric) signals changes.

The high binding affinity of PPi towards metal ions can be attributed to its good chelation and bridging capabilities. Even though PPi sensors based on small molecules have been broadly studied, there is increasing incentive to find alternative methods for PPi sensing owing to low PPi/Pi selectivity, considerable synthetic effort, involvement of heavy metal ions and limited applications in fabrication devices.[128-130]

Principal component analysis (PCA) is a standard mathematical method for data analysis that is generally applied to multivariate analytical system.[131-133] It was first established in 1901 by Karl Pearson and it has become one of the most used tools in exploratory data analysis and making predictive models since then.[134] Many sensory systems based on PCA methods have been reported,[135-138] and it has been proved that PCA provides a simple and robust way to reduce data dimensionality and reveal useful information behind the complex data set with minimal effort. However, only a few papers described the use of PCA for the analysis of spectroscopic data set,[139-141] which is probably due to the complication of the data set, interference of background spectra and problems regarding uncalibrated spectral features.

In this chapter, we report a sensitive and selective fluorescent “turn-on” sensor for PPi based on conjugated polyelectrolytes. The earlier discussions in Chapter 3 provide the basis for the study presented here, where we find the addition of tris(3-aminoethyl)amine (**N4**) is capable of inducing inter-chain aggregation of **P3** in aqueous solutions. The **N4**-quenched fluorescence of **P3** can be turned on selectively by

PPi. The fluorescence recovery is achieved by breaking the **P3**/**N4** complex, due to the strong association between PPi and **N4**. Particularly, the enhanced fluorescence of the CPE is blue-shifted upon complexation with PPi. PCA was used as the calibration method to quantitatively measure the concentration of PPi in the sensory system. The results demonstrated that the PCA calibration method provided a fast and convenient way for PPi concentration measurement with a high accuracy ~ 95% when PPi is within concentration range from 100 μM to 3 mM.

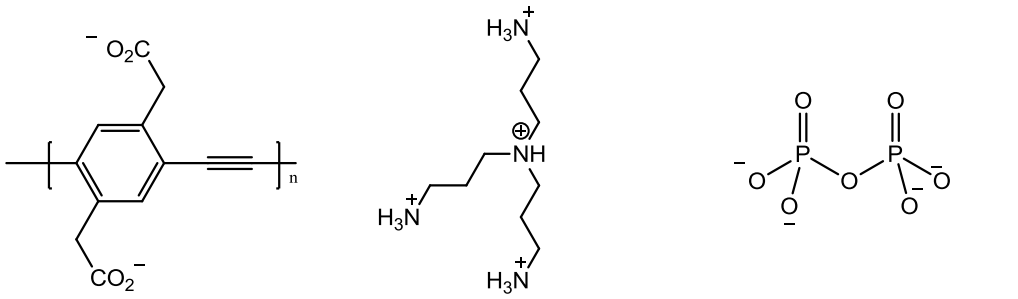

P3 Tris(3-aminoethyl)amine (N4) Pyrophosphate (PPi)

Figure 4-1. Structures of polymers and substrates.

Principal Component Analysis

Basic Methods and Procedures for PCA

Principal component analysis is an analytical technique to identify the similar patterns in data by reducing dimensions without loss of information, which in turn results in the predictions for some recognizable factors. In order to perform a principal component analysis, we need to first establish a data matrix $\mathbf{D_0}$ from the raw fluorescence data which are presented below as Equation 4-1,

$$\mathbf{D_0} = [X_{i,j}]_{i=1\ldots m;\ j=1\ \ldots\ n} \quad (4\text{-}1)$$

where $X_{i,j}$ is the jth factor associated with row i. In our study, we refer $X_{i,j}$ as the fluorescence intensity at wavelength i in the jth group from the raw data set. In order to avoid any inconsistency during experiment operation, each fluorescence spectrum is area normalized using Equation 4-2,

$$\mathbf{D} = \mathbf{D_0} \times 10^9 / A \tag{4-2}$$

where A is the integration area for the fluorescence spectrum of **P3** (2 μM) in HEPES buffer (10mM, pH 7.4), and 10^9 is an arbitrary number for the normalization. To make this data matrix to be factor analyzable, it can be written as a linear sum of product terms in the form of:

$$\mathbf{D} = \mathbf{RC} \tag{4-3}$$

Here, **R** and **C** are referred as scores and loading matrices for **D**, which can be used to reproduce the original matrix **D**. Consequently, the next step is to find out **R** and **C** matrices from a known matrix **D**. First, we need to find out the covariance matrix of **D**, which is inherently a square matrix:

$$\mathbf{Z} = \mathbf{D}^{\mathbf{T}}\mathbf{D} \tag{4-4}$$

This matrix is then diagonalized into Equation 4-5:

$$\mathbf{Q}^{-1}\mathbf{ZQ} = [\lambda_j \delta_{jk}] \tag{4-5}$$

Since the covariance matrix **Z** is square, we can calculate the eigenvectors and the corresponding eigenvalues for the matrix based on Equation 4-6,

$$\mathbf{Z}q_j = \lambda_j q_j \tag{4-6}$$

where q_j is the jth column of **Q**. Therefore matrix **Q** can be easily achieved by using the eigenvectors from **Z**. Since these columns (or eigenvectors) constitute a mutually orthonormal set, one can show that

$$\mathbf{Q^{-1}} = \mathbf{Q^{T}} \tag{4-7}$$

By exploiting Equation 4-7, two equations are easily obtained and **R** and **C** matrices are consequently calculated based on the relationship below,

$$\mathbf{R} = \mathbf{DQ} \tag{4-8}$$

$$\mathbf{C} = \mathbf{Q^{T}} \tag{4-9}$$

The procedure explained so far is a general scheme for abstract factor analysis.[141] In this approach, the eigenvectors are consecutively calculated in order to minimize the residual error in each step. As a result, each successive eigenvector accounts for the largest variation in the data. When all of the eigenvalues are calculated by using Equation 4-5, the variation corresponding to the largest eigenvalue and eigenvector is subtracted from the covariance matrix as shown in Equation 4-10:

$$\mathbf{R_1} = \mathbf{Z} - \lambda_1 q_1 {q_1}^T \tag{4-10}$$

From this residual matrix, the second principal eigenvector and its associated eigenvalue are calculated.

$$\mathbf{R_1} q_2 = \lambda_2 q_2 \tag{4-11}$$

To obtain the third eigenvector, we define $\mathbf{R_2}$ as

$$\mathbf{R_2} = \mathbf{Z} - \lambda_1 q_1 {q_1}^T - \lambda_2 q_2 {q_2}^T \tag{4-12}$$

When one continues in this fashion, the remaining eigenvectors and eigenvalues are extracted in succession.[141]

Target Transformation

As previously mentioned, the R and C matrices do not have any physical or chemical meanings as they constitute an abstract solution. Therefore a target transformation is necessary to change them into meaning factors, and this is achieved by applying a transformation matrix and combining with Equation 4-3,

$$\mathbf{D} = \mathbf{RC} = (\mathbf{RT})\,(\mathbf{T^{-1}C}) \tag{4-13}$$

In Equation 4-13, transformation matrix **T** is a square matrix of dimension n, where n is the number of significant factors determined by PCA. **T** has the following form for a data matrix that can be described with two principal factors:

$$\boldsymbol{T} = \begin{pmatrix} a\cos\,(\theta)\,;\, -b\sin\,(\theta) \\ c\sin\,(\theta)\,;\, d\,\cos\,(\theta) \end{pmatrix} \tag{4-14}$$

If the transformation is orthogonal (i.e., it preserves the angles between the factor axes), then *a*, *b*, *c*, and *d* are unity. However, if the transformation is nonorthogonal, then these constants should be determined by taking into account prior information about the real factors.[141]

Results and Discussion

Overview of PPi Turn-on Sensor

An anionic conjugated polyelectrolyte featuring carboxylate functional groups is used in our study (**P3**, Figure 4-1). The cartoon in Figure 4-2 illustrates the PPi turn-on

mechanism, which is based on an “unquench-quench-unquench” process. First, this polymer dissolves as free single chains in aqueous solution and it displays strong fluorescence emission with a maximum peak at ~434 nm. The high quantum yield (0.42 in water) also indicates this polymer does not aggregate in water. Then the fluorescence of **P3** is quenched by the addition of tris(3-aminoethyl)amine (**N4**, Figure 4-1), which is attributed to the inter-chain aggregation of **P3**. A blue-to-green emission change is observed and the red-shift is caused by the aggregated polymer.[22] At last, the quenched fluorescence is recovered after PPi is introduced to the **P3**/**N4** solution. Fluorescence recovery occurs because PPi chelates **N4** with a higher binding affinity, leading to breakup of the **P3**/**N4** cluster. Therefore, **N4** can no longer complex with the polymer and liberated the polymer from aggregated clusters. The addition of PPi is signaled by a blue-shift and enhancement in the polymer’s fluorescence intensity. This “on-off-on” process affords a convenient way to determine the presence of PPi.

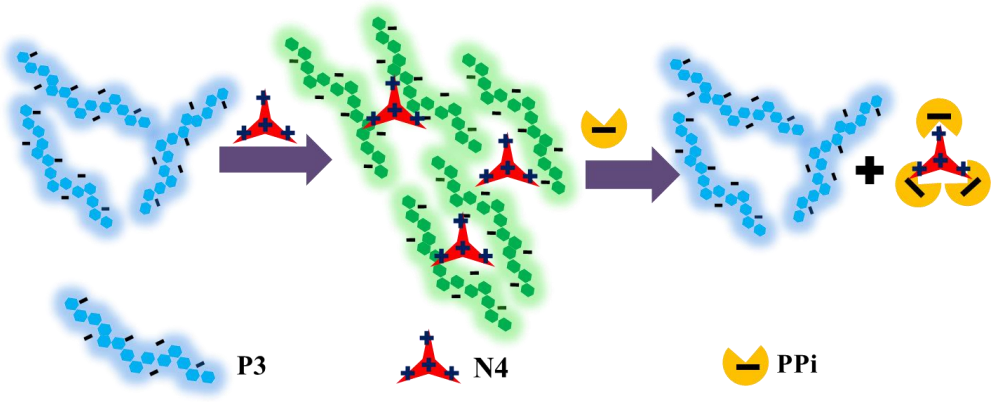

Figure 4-2. Mechanism of PPi “Turn-on” sensor.

Fluorescence quenching of P3 by N4

The interaction of **P3** with **N4** was investigated first. As discussed in Chapter 3, **P3** remains as single chains in water and it is probably due to the high negative charge density on the side groups. In HEPES buffer solutions (10 mM, pH = 7.4), **N4**, can induce efficient aggregation of **P3**, indicating that three positive side groups of **N4** bridge the single polymer chains to form aggregates, contributing to the most significant quenching effect. The detailed titration spectra have been represented in Figure 4-3. When **N4** (c = 0 - 10 μM) was titrated into 2 μM of **P3** in the HEPES buffer solution (10 mM, pH = 7.4), a strong peak at wavelength ~424 nm gradually decreases which is originally from the blue emission of single CPE chains. At the same time, another broad band shows up at longer wavelength ~540 nm and this is attributed to the green emission of the aggregated CPE. The Stern-Volmer constant (K_{SV}) was calculated to be ~3.5 × 10^4 M^{-1}.

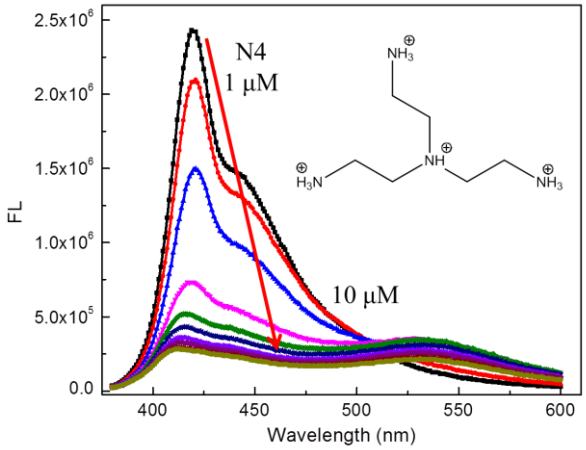

Figure 4-3. Fluorescence spectra changes upon titration of polyamine (0 - 10 μM) into 2 μM **P3** in HEPES buffer solution (10 mM, pH = 7.4).

Fluorescence recovery of P3/N4 by PPi

In earlier literatures, it was reported PPi could complex with polyamine or similar structures through coordination very effectively.[142,143] In order to investigate the interaction between PPi and **P3**/**N4** mixtures, a series of PPi titration with concentration from 10 μM to 3 mM was conducted in HEPES (10 mM, pH 7.4) buffer solutions containing 2 μM **P3** and 4 μM **N4**. As shown by Figure 4-4A, the fluorescence intensity of **P3** at 424 nm is quenched almost 90 % (red) relative to the initial fluorescence of pure **P3** (black) after 4 μM **N4** is introduced. Upon the addition of PPi, the fluorescence intensity at 424 nm increases while the green band at 540 nm decreases. After 3 mM PPi is titrated, the fluorescence at 424 nm is recovered to ~91% of the initial intensity for the pure polymer and meanwhile ~70% of the fluorescence intensity at 540 nm is decreased compared to mixture solution in the presence **N4**. The recovered fluorescence intensity can be explained by the reduced amount of aggregated polymer chains. Note that every spectrum was obtained after a complicated kinetic equilibrium has been reached, where PPi competed with the polymer to bind with **N4**.

In contrast, the effect of Pi on the fluorescence recovery of **P3**/**N4** complex was investigated (Figure 4-4B). Upon the titration of Pi ranging from 10 μM to 3 mM, Pi failed to induce any significant fluorescence recovery due to its lower binding affinity to **N4**, suggesting that this fluorescent sensor has a high selectivity towards PPi over Pi.

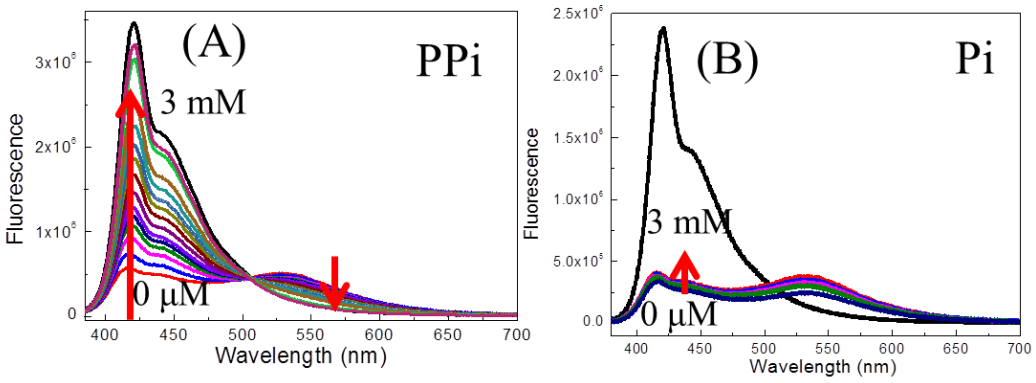

Figure 4-4. Fluorescence spectra changes upon titration of PPi and Pi (0 - 3 mM) into mixture of 2 μM **P3** and 4 μM **N4** in HEPES buffer solution (10 mM, pH = 7.4); (A). PPi; (B). Pi.

Fluorescence correlation spectroscopy measurement

To prove our hypothesis that this "on-off-on" process is indeed a conformational change of **P3** by adding different substrates, fluorescence correlation spectroscopy (FCS) technique was carried out to investigate the size changes of the polymer. The correlation curves as well as the nonlinear fittings for different systems are described in Figure 4-5, where [**P3**] is fixed at 2 μM. For **P3** alone, it has a diffusion time ~6.3 × 10^{-5} s, which is quite close to the normal value for a well dispersed conjugated polyelectrolyte in aqueous solution.[144] The correlation curve for the **P3**/**N4** complex ([**N4**] = 4 μM) greatly shifts to the right, with a more than 10-fold increase of the diffusion time (~65 × 10^{-5} s). This significant increase clearly indicated the addition of **N4** induces the aggregation of the polymer.[19] As expected, the correlation curve shifts back to a smaller diffusion time (~6.4 × 10^{-5} s) after 200 μM PPi was applied to the **P3**/**N4** mixture, where it almost

overlap with the original correlation curve for the polymer alone. Overall, the introduction of PPi successfully broke the polymer aggregates and released the free polymer chains, which has a small diffusion time and increased fluorescence intensity.

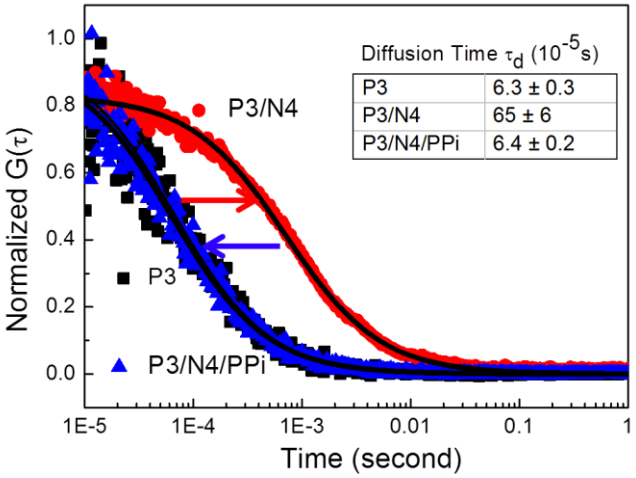

Figure 4-5. Normalized correlation curves and diffusion time for different systems. Black: [**P3**] = 2 μM; Red: [**P3**] = 2 μM, [**N4**] = 4 μM; Blue: [**P3**] = 2 μM, [**N4**] = 4 μM, [PPi] = 200 μM. The black solid lines are single specific fitting curves.

PCA Calibration Result for Spectroscopic Data Set

In order to apply PCA in our study, a titration experiment with PPi was initially carried out to obtain a calibration standard and the spectroscopic data set was collected and investigated by PCA method. The titration was performed in the **P3**/**N4** mixture solution ([**P3**] = 2 μM, [**N4**] = 4 μM) using HEPES buffer (10 mM, pH = 7.4) and the emission spectra were obtained by a fluorescence spectrometer at thirteen different PPi concentrations. This set of 13 emission data was normalized by adjusting the integration areas for the pure polymer emission data to 10^9 and displayed at Figure 4-6A. Then the

spectroscopic data was transformed into a 316×13 data matrix, $\mathbf{D}_{316\times13}$ (where 316 rows correspond to emission wavelength covering spectral range from 384 to 700 nm and 13 columns correspond to the PPi concentrations).

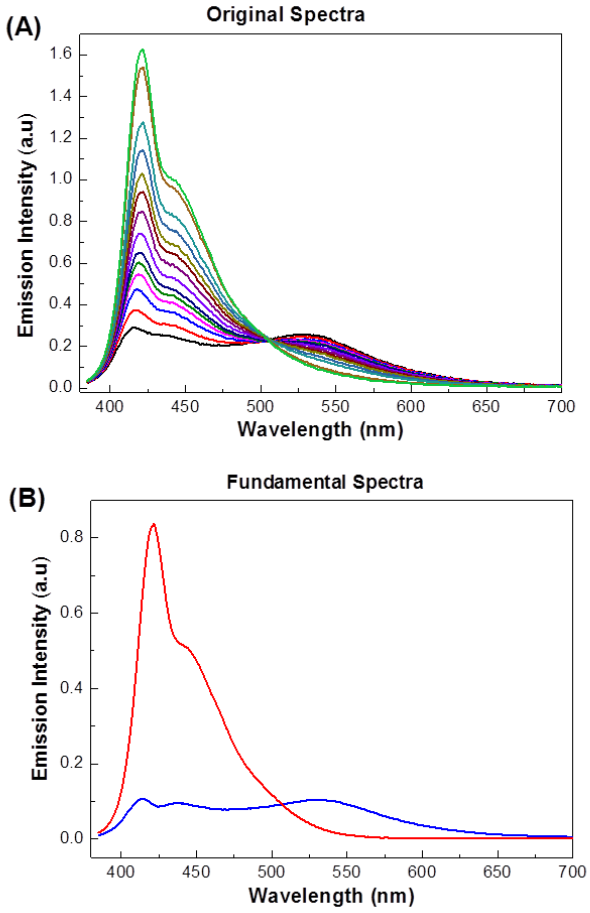

Figure 4-6. (A) Original emission spectra of changes upon titration of PPi (0 - 3 mM) into mixture of 2 μM **P3** and 4 μM **N4** in HEPES buffer solution (10 mM, pH = 7.4), (B) Fundamental spectra (matrices, **R**) for two largest eigenvalues.

Target transformation

This data matrix $\mathbf{D}_{316\times13}$ was applied and calculated by PCA algorithm. Two significant eigenvectors of covariance matrices **Z** (out of a total of 13) were obtained and

they account for 99.99 % of the total variation. As previously discussed, the initial eigenvectors generated by PCA do not have any physical meanings, for example, one of the eigenvectors features a negative amplitude (Figure 4-7). Hence, an appropriate target transformation is necessary to rotate these initial eigenvectors into physically meaningful factors. Two guidelines must be followed before the rotation:[141] (1) Negative emission intensity is not allowed; and (2) both eigenvectors should be related to the emission spectra that are attributed from either fluorescent state of the polymer. Consequently, a new transformation matrix was produced and shown as Equation 4-16:

$$\mathbf{T} = \begin{pmatrix} 1.1\cos\ (5.15)\,;\ -2.3\sin\ (5.15) \\ 2.1\sin\ (5.15)\,;\ 6.2\ \cos\ (5.15) \end{pmatrix} \quad (4\text{-}15)$$

where the coefficients and rotation angles were determined semiempirically. Followed by the multiplication of the initial **R** matrix by this transformation matrix **T**, two new eigenvectors were obtained and displayed in Figure 4-6B. Red line ($\mathbf{R_1}$) represents the fundamental spectrum for the first eigenvector, whereas blue line ($\mathbf{R_2}$) represents the fundamental spectrum for the second eigenvector. As displayed in Figure 4-6B, $\mathbf{R_1}$ exhibits a strong structured emission spectrum with a maximum peak ~430 nm, very similar to the fluorescence emission of **P3** at its single chain state. The results suggest that the first eigenvector is mostly single-polymer-dependent, representing the single-chain polymer emission. $\mathbf{R_2}$ shows a broad emission band at longer wavelength ~540 nm, which is dominated by the aggregated polymer state. Note that there are also two other small bands showing up at ~430 nm and ~450 nm which is still slightly affected

by the presence of single state polymer. Even though the separation is not perfect for $\mathbf{R_2}$, however, it accounts for the contribution mostly from aggregated polymer emission to the total emission spectrum. Hence, the PCA method successfully resolves most of the emission variations from single-chain state to aggregated state polymers by providing two eigenvectors after target transformation, leading to the improved accuracy and estimation for PPi concentrations.

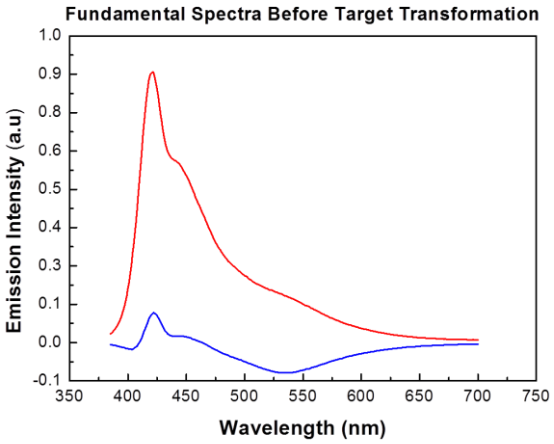

Figure 4-7. Fundamental spectra for abstract factors.

Loading data for each eigenvectors at different [PPi]

Based on Equation 4-9, the loading percentage for each eigenvector at different PPi conditions ([PPi] = 0 - 3 mM) can be calculated and therefore they can be replotted to get a reconstructed data matrix. Figure 4-8A and B illustrated the fractional contributions of both eigenvectors to the total reconstructed emission spectra at varying [PPi]. By combining them together, a reconstructed fluorescence emission spectrum is finally achieved shown in Figure 4-8C, which displays a similar pattern compared to the

original emission spectrum (Figure 4-6A). The result clear shows that PCA analysis successfully reduces a large set of data into two principal components that can explain most of the spectroscopic change at different conditions without loss of much information.

The plot in Figure 4-9 gives a detailed loading percentage graph for both eigenvectors at varying [PPi]. With increasing amount of PPi, the effect of the first eigenvector (red line) increases while the second eigenvector (black line) decreases. The blue line is actually the total amount loading of first and second component as a sum, which appears to be a horizontal line. As noted above, the first eigenvector is mainly single-polymer-dependent and the second one is primarily related to the effect of fluorescence from polymers at aggregated states; therefore the blue line should be expected to be a horizontal line if we assume the polymer can only stay as either state (single chain or aggregate). In addition, it is of note that the value of the blue line is close to a constant (in this case, it equals to 0.25) at the standard experimental condition, suggesting the total contribution from both eigenvectors at any [PPi] condition is a constant. This can be probably attributed to the fact that the amount of polymers and amine in the standard conditions are fixed. Since the total emission spectrum is the combination of fluorescence spectrum from single polymers as well as the aggregated polymers, the total effect of both eigenvectors under the same experimental condition should be constant as long as the concentrations of polymer and amine are fixed.

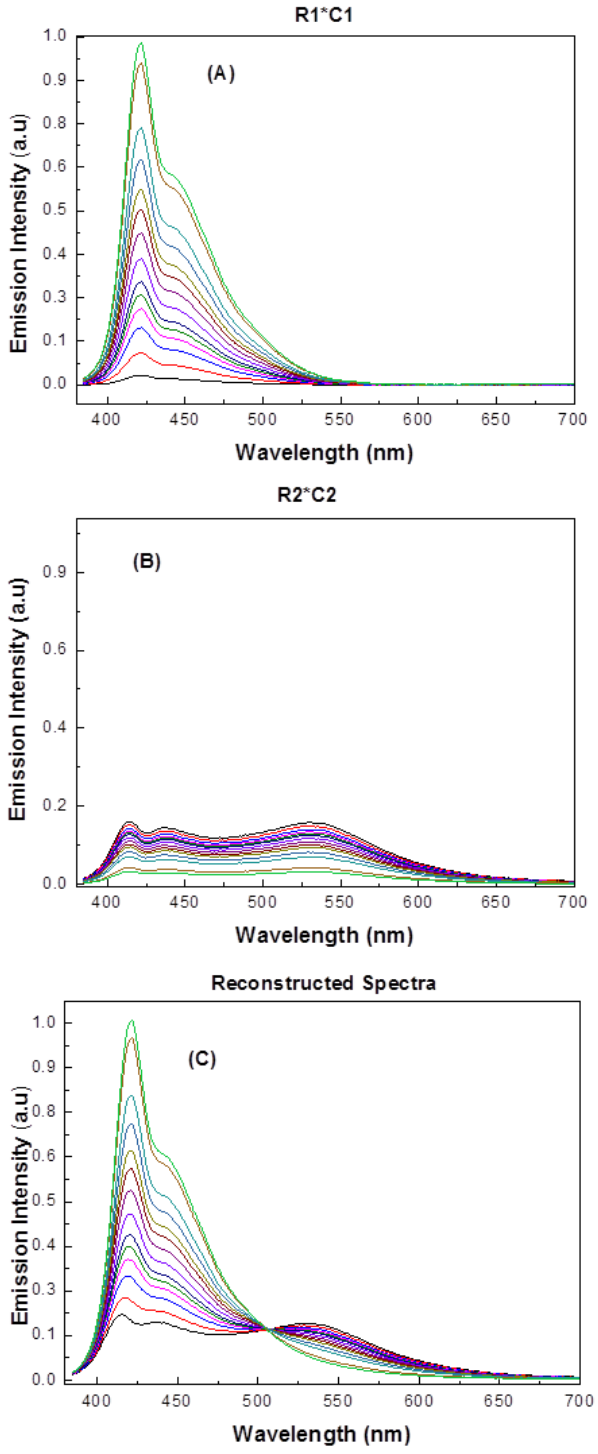

Figure 4-8. (A) Contribution of the first fundamental spectrum ($\mathbf{R_1}$) to total emission at various [PPi]. (B) Contribution of the second fundamental spectrum ($\mathbf{R_2}$) to total emission at various [PPi]. (C) Reconstructed spectra $\mathbf{D} = \mathbf{R_1C_1} + \mathbf{R_2C_2}$ obtained by combining the total contributions from the two largest eigenvalues.

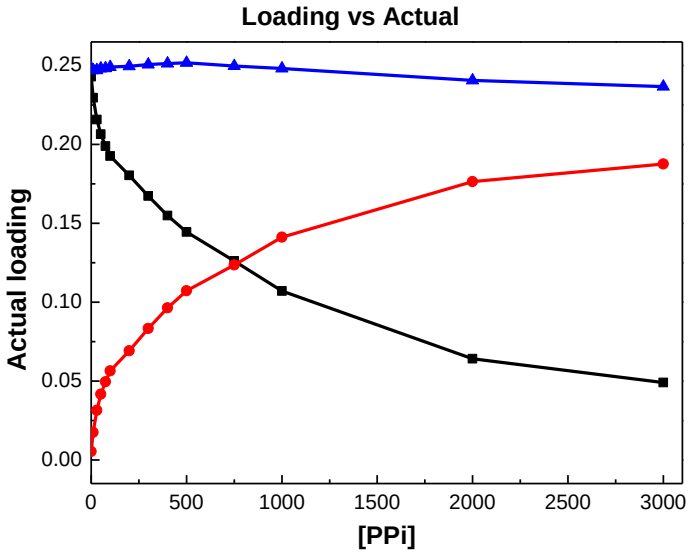

Figure 4-9. The contribution of two eigenvectors at different [PPi].

Regression analysis

One of the main objectives in our study is to allow the prediction of PPi concentration from an unknown sample by using PCA calibration method. In order to apply the data from standard experiment to other unknown system, regression analysis was carried out to determine the values of the coefficients for a model function that best fits the set of data from standard experiment.[145,146] For example, the $\mathbf{C_1}$ and $\mathbf{C_2}$ values obtained from PCA were fitted to the PPi concentrations using several nonlinear model functions. The best fit function is displayed as Equation 4-16 with confidence level of fits at 95%,

$$y = -3964870 - 3828670\frac{1}{2}x^2 - 2224950x^2 \pm 350448x^3 + 2767\left(\frac{1}{x}\right) - 343679x^4 - 2.06627\left[\frac{1}{(1-x)}\right] + 3940000\exp(x) \ \pm 13.9\ (\mu M) \quad (4\text{-}16)$$

where *y* is the PPi concentration and *x* is the contribution percentage of $\mathbf{C_1}$ ($\mathbf{C_1}$%). The correlation coefficients for the empirical fits were 0.999 or better. Note that earlier we have explained that the sum of $\mathbf{C_1}$% and $\mathbf{C_2}$% equals to 1 since the total of $\mathbf{C_1}$ and $\mathbf{C_2}$ is a constant when the experimental condition is fixed; therefore in this situation we use $\mathbf{C_1}$% and "1- $\mathbf{C_1}$%" (equals to $\mathbf{C_2}$%) instead of using $\mathbf{C_1}$ and $\mathbf{C_2}$ directly for the regression analysis. By reducing the variables from 2 to 1, the complexity of the system and the order of the polynomial equations are reduced.

Applications to unknowns

Figure 4-10 provides the calibration plot for the standard data that can be used to predict the concentration of PPi from unknown sample. In this two dimensional graph, the black points represent the values of $\mathbf{C_1}$% calculated from PCA analysis for the standard data set, whereas the red nonlinear plot represents the function in Equation 4-16. The regression function provides the fundamentals for the unknown prediction. In our system, the largest two eigenvectors from PCA are corresponding to the two states of the polymer, and there is only variable (PPi concentration) that would affect the fluorescence emission spectrum of the polymer as long as the standard experimental conditions are fixed. Most importantly, the variance of [PPi] will only balance the equilibrium between single state polymer and aggregated state polymer. Therefore they will not change the eigenvectors as well as their fundamental matrices ($\mathbf{R_1}$ and $\mathbf{R_2}$) for the sample system but only their loading percentage ($\mathbf{C_1}$% and $\mathbf{C_2}$%); therefore, the

eigenvectors obtained from standard sample should be able to be directly applied to the unknown samples under the same experimental condition. To calculate the $\mathbf{C_1}$ and $\mathbf{C_2}$ values for an unknown sample, the fluorescence data matrix for the unknown should be firstly obtained after normalization, which is to avoid any inconsistency during experimental operation. Then we apply the fundamental matrices ($\mathbf{R_1}$, $\mathbf{R_2}$) for the eigenvectors from standard data matrix into our unknown matrix according to Equation 4-3, the loading value ($\mathbf{C_{u,1}}$ and $\mathbf{C_{u,2}}$) for each eigenvector can be easily achieved. There are 17 groups of unknown samples that have been tested and their loading percentage for $\mathbf{C_{u,1}}$ is calculated. All the values from unknown samples are put into the calibration plot in Figure 4-10, shown as blue triangles. From the comparison it suggested most of the data from unknown samples locate very close to the calibration plot and consequently the concentration of PPi for each unknown sample can be estimated.

Table 4-1 summaries the predicted average [PPi] as well as standard errors for 17 groups of unknown samples by using Equation 4-16. From the results it reveals that the estimated [PPi] stays close to the real concentrations that most of the errors are ~5%. It is believed some of the errors are system errors, which are resulted from solution preparation, instrument errors and operation errors. Regarding to so many possible interferences, in overall, PCA analysis provides good precision and accuracy when predicting the concentrations of PPi.

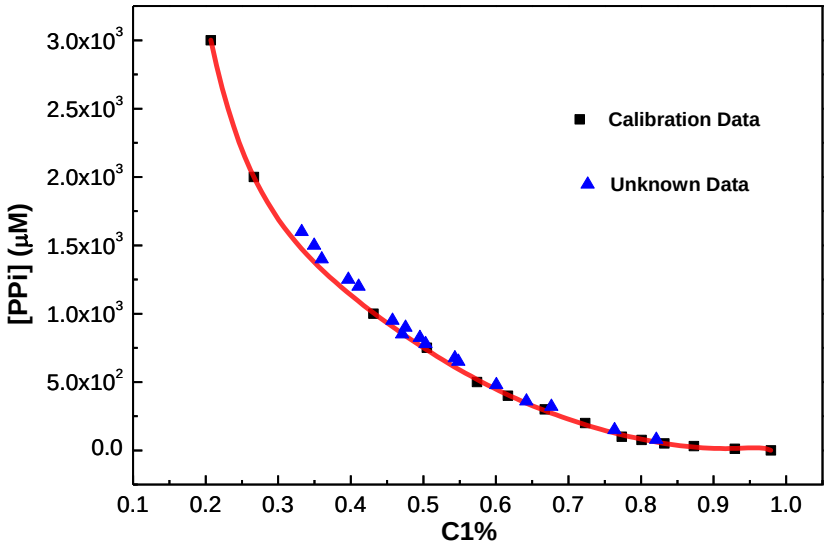

Figure 4-10. [PPi] calibration curve obtained according to Equation 4-16. Standard calibration points from raw data are respented as black squares. Unknown points are resprented as blue triangles.

Table 4-1. Accuracy of average [PPi] obtained with PCA calibration method.

$[PPi]_{real}$ (μM)	$[PPi]_{est}$ (μM)	% error in [PPi]
80	85	6.25
150	149	-0.67
320	291	-9.06
360	363	0.83
480	462	-3.75
650	609	-6.31
675	624	-7.56
780	754	-3.33
825	780	-5.45
850	866	1.88
900	849	-5.67
950	916	-3.58
1200	1101	-8.25
1250	1162	-7.04
1400	1333	-4.79
1500	1388	-7.47
1600	1484	-7.25

Summary

A CPE-based “turn-on” sensor for PPi was designed and developed. The sensory system is composed of a highly fluorescent conjugated polyelectrolyte (**P3**) featuring carboxylate side chains and a positively charged polyamine (**N4**), and the recovery of **N4**-quenched fluorescence of **P3** is highly selective for PPi over other inorganic anions such as Pi. The presence of **N4** can effectively cross-link the “molecularly dissolved” polymers to form large aggregates, leading to fluorescence decrease. Followed by the addition of PPi which exhibits a higher binding affinity to **N4**, the fluorescence will be recovered eventually after **N4** is released from the polymer aggregates. The size change is also monitored by FCS technique, indicating this is an analyte-induced aggregation/deaggregation mechanism. The green-to-blue fluorescence change is readily visible to the naked eye. This approach avoids the use of heavy metal ions which are typically involved in traditional PPi sensing methods, significantly eliminating any risks or pollutions to the environment.

Principal component analysis (PCA) has been used to the analysis of fluorescence spectroscopic data of the sensory system as a calibration method to measure the concentration of PPi. Two principal components were obtained by PCA analysis and they have been applied to find out their relationship with [PPi] by establishing a nonlinear equation via regression analysis. The unknown investigation reveals that PCA calibration affords high accuracy and precision (~5% error) in the predication of [PPi] from unknown

samples. Additionally, PCA calibration method can be applied for unknown [PPi] predication across a wide concentration range from lower micromolar to up to several millimolar (10 μM - 3 mM), significantly broadening its application in different areas with various needs. Most importantly, expertise is less required for the quantitative measurement of PPi with the help of computational calculation via Matlab. In overall, this method provides an easy and fast way for PPi detection without requirement of any controls.

Even this work shows a lot of advantages as an efficient qualitative and quantitative tool for PPi detection, it has some limitations. First of all, the PCA analysis is computationally demanding and it is relative time-consuming when there is a large set of data involved. Second, the regression equation obtain in our study is only working properly under a specific experimental condition and any changes to the experimental parameters (including substrate concentration, buffers, temperature, etc.) is subject to a consequently change to the regression equation. Last, more efforts are needed to improve the detection limit of the system.

Experimental

Materials

All sample solutions were prepared using water which is distilled and purified by using a Millipore purification system (Millipore Simplicity Ultrapure Water System). HEPES buffer solution (10 mM, pH = 7.4) was provided with

4-(2-hydroxyethyl)-1-piperazineethanesulfonic acid and sodium hydroxide. Tris (3-aminoethyl)amine and potassium pyrophosphate were purchased from Sigma-Aldrich. All chemicals were used as received, unless otherwise noted.

Instrumentation

Fluorescence spectra were measured and obtained from a spectrofluorometer from Photon Technology International. All the spectra have been corrected by using correction factors generated with a primary standard lamp. FCS measurements are taken on a homemade setup using a 405 nm diode laser (Coherent, CUBE) as the excitation light. 30 nM fluorescein in 10 mM phosphate buffer (pH = 8) is used as the calibration standard for the system.

CHAPTER 5
ACETATE KINASE ASSAY USING POLY (PHENYLENE ETHYNYLENE) WITH POLYAMINE SIDE CHAINS

Background

Since its discovery by Lipmann in 1944 and isolation from *Escherichia coli* by Ochoa in 1954,[147,148] acetate kinase (ACK, EC 2.7.2.1) has been considered as an important enzyme for energy production and one of the earliest phosphoryl transfer enzymes.[149-151] In nature, acetate kinase is widely distributed in both anaerobic and aerobic microbes of the *Bacteria* and *Archaea* domains.[152] The enzyme plays an essential role in carbon metabolism as it is able to decompose complex organic materials in anaerobic conditions to methane by microbial food chains.[153,154] Early reports demonstrated that acetate kinase can catalyze the reversible transfer of a phosphate group from acetyl phosphate to ADP and then produce acetate and ATP.[155,156] Other substrates including phosphates (Pi) can also function as phosphoryl acceptors to form pyrophosphate (PPi), which is a biologically significant anion involved in many cellular processes. Note that the acetate kinase which particularly uses Pi and acetyl phosphate as substrates are recognized as acetate kinase (diphosphate) (EC 2.7.2.12) in enzymology since ADP or other common nucleoside diphosphates cannot replace Pi as phosphoryl acceptor in the direction of acetate formation.[157] It is well known that acetyl phosphate serves not only as a precursor for many important intermediates in metabolism, including acetyl coenzyme A,[149,158] but also

as a potential response regulator in bacterial signal-transduction pathways.[159,160] As a result, the phosphorylation reactions by ACK contribute to the regulation of central reactions in metabolism via acetyl phosphate. Moreover, acetate kinase is reported to be involved in the process of glycolysis in *Aerobacter aerogenes*.[161,162] These bacteria can use acetate as their sole source of carbon and also excrete acetate when growing on glucose. The growth of the bacterial mutant lacking acetate kinase is confirmed to be inhibited by glucose, indicating that the nature enzyme is able to excrete the excess carbohydrate.[163-165] The amphibolic role of acetate kinase in acetate excretion and activation makes this enzyme significantly necessary in microorganisms.

Several ACK assays that use different substrates in the direction of acetate formation based on bioluminescent and enzyme-coupled methods have been developed.[166-168] For the ACK-catalyzed system involved with acetyl phosphate and ADP, the most commonly used assay is to couple ATP formation to the reduction of NADH through hexokinase and glucose-6-phosphate dehydrogenase.[168] The reaction is monitored by measuring the changes of NADH emission at 340 nm by exciting at 290 nm. However, few papers have reported assays for the other ACK system that generates acetate and PPi from acetyl phosphate and Pi. Although PPi-sensing methods have been widely studied, there is only one paper published by Reeves and Guthrie in 1975 that discusses the kinetic investigation for ACK (diphosphate) activity.[157] The authors used four standard methods for different substrates coupled with several other kinases

and substrates. Due to the complexity of the system, this assay suffers several disadvantages, including interference and contamination from other substrates, as well as issues concerned with sensitivity and selectivity. Additionally, it is not possible to perform a real-time measurement for ACK using either ADP or Pi as substrates on all the methods discussed above, and they are both laborious and time-consuming.

We have recently developed a fluorescent “turn-off” sensor for PPi based on a cationic conjugated polyelectrolyte (CPE) having bulky branched side chains.[31] This CPE (PPE-$^{d}NH_3$, Figure 5-1A) features six ammonium functional groups on each repeat unit, and it is “molecularly dissolved” in aqueous solution due to the strong interchain electrostatic repulsion.[30] The fluorescence intensity of this unaggregated CPE can be efficiently quenched by the addition of PPi, due to the aggregate formation induced by PPi. The blue-to-green fluorescence change is readily observed by naked eye and the fluorescence-based sensing strategy offers good sensitivity and real-time measurement. In addition, the effects of other inorganic anions, including Pi, on this polymer were also investigated, only negligible changes were observed. This high selectivity for PPi over Pi indicates that this CPE can be used in biological assays involving these two anions. This chapter described the development of the CPE-based fluorescent “turn-off” assay for ACK (diphosphate) that requires acetyl phosphate and Pi as substrates. With the introduction of ACK to a solution containing PPE, acetyl phosphate, Pi and Mg^{2+}, ACK catalyzes the phosphate transfer from acetyl phosphate to Pi, producing PPi and acetate.

The decrease of fluorescence intensity is quantitatively related to the production of PPi concentration as a function of incubation time. The real-time measurement allows the determination of kinetic parameters for ACK and the assay exhibits high sensitivity and selectivity comparable to that of other enzyme assays. The assay is conducted at physiological pH and offers a straightforward and rapid detection method for ACK activity with the enzyme present in the nanomolar concentration range.

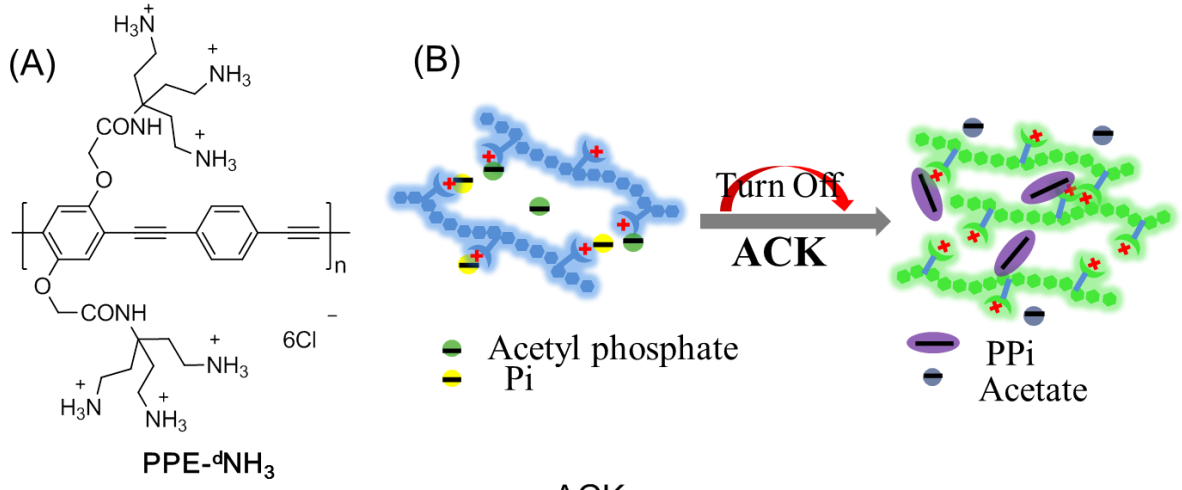

Figure 5-1. (A). Structure of PPE-$^{d}NH_3$ and reaction scheme for acetate kinase. (B). Mechanism of ACK turn-off assay.

Results and Discussion

Overview of ACK Turn-off Assay

A cationic conjugated polyelectrolyte carrying dendritic ammonium side groups, PPE-$^{d}NH_3$, is the signaling element for ACK activity. As described previously, the introduction of the bulky, charged side groups significantly increases electrostatic repulsion between adjacent polymer chains; thereby circumventing the aggregation of

PPE-$^{d}NH_3$ in aqueous solution.[31] The cartoon shown in Figure 5-1B illustrates the "turn-off" mechanism for the ACK turnoff assay, which is based on aggregation of the polymer. In 25 mM 2-(N-morpholino) ethanesulfonic acid (MES) buffer solution (pH 6.5), PPE-$^{d}NH_3$ exhibits a strong and sharp fluorescence peak at 434 nm with a quantum yield of ~0.23.[31] After substrates acetyl-phosphate (AP) and Pi are added, the fluorescence intensity decreases only slightly, although the cationic side groups on the polymer are partially neutralized by the anionic substrates. Therefore at this time PPE-$^{d}NH_3$ remains "molecularly dissolved" in the presence of Pi and Acetyl-Pi. In a turn-off approach, ACK is added to the polymer/substrate solution, and initiates phosphate transfer from acetyl-Pi to Pi and produces PPi and acetate.[157,169] The product PPi is capable of efficiently binding and cross-linking adjacent polymers, leading to formation of inter-chain polymer aggregates. As a result, the structured emission of the polymer decreases and shifts to longer wavelength. As the reaction proceeds, the amount of PPi available to cross-link the polymer increases, and the fluorescence is further quenched ("off" state of the polymer). Another product, acetate, similar to Pi and acetyle-Pi, having only one negative charge, is unable to induce interpolymer interactions, and the production of PPi is the only reason for the quenched fluorescence. Therefore, the catalytic activity of ACK is signaled by the fluorescence of PPE-$^{d}NH_3$ switching from the "on" state to the "off" state. The decreased fluorescence intensity is associated with the product concentration, [PPi], which increases as a function of time in the enzymatic reaction, thereby allowing

quantitative investigation of ACK activity. A divalent metal ion, Mg^{2+}, is required for the ACK activity, because it is reported to be an important cofactor for ACK.[170-172]

Fluorescence Quenching of PPE-$^{d}NH_3$ by Pyrophosphate (PPi)

The fluorescence response of PPE-$^{d}NH_3$ to Pi, AP, PPi and acetate provides the basis for development of an ACK assay. A series of titrations were carried out using Pi, acetyl-Pi, PPi or acetate, respectively, over a concentration range from 0 to 10 μM into a MES buffer (25 mM, pH = 6.5) solution containing 2 μM PPE-$^{d}NH_3$. Figure 5-2 is the Stern-Volmer plot I_0/I_q of PPE-$^{d}NH_3$, where I_0 and I_q are the fluorescence intensities of PPE-$^{d}NH_3$ before and after the addition of each component, as a function of the concentration of Pi, AP, PPi and acetate, giving a clear demonstration of the fluorescence quenching efficiency of each species. From Figure 5-2 we can see that the quenching efficiency decreases in the order of PPi >> AP > Pi = acetate at the same concentration level, consistent with the decreasing negative charge density on these species. PPi has the largest negative charge density, and thus features the strongest electrostatic interaction with the dendritic ammonium groups on the polymer. The rigid structure of PPi enables it to cross-link two polymer chains, leading to the formation of inter-chain aggregates. Both characteristics contribute to the greatest quenching efficiency of PPi. The Stern-Volmer constant (K_{sv}) for PPi is calculated to be ~1.3×10^{5} M^{-1}. The aggregation mechanism was also proved by fluorescence correlation spectroscopy (FCS).[173] As described above, AP, Pi and acetate exhibit very weak

quenching effects on PPE-$^{d}NH_3$ even though the negative charges can partially neutralize the positive charges on the polymer, they are unable to induce efficient interpolymer interactions. Therefore, the fluorescence decrease of the experiment is associated with the production of PPi. By observing the fluorescence change, we can monitor the enzyme activity in the presence of low substrate concentrations. Note this assay is not appropriate for high substrate concentrations (>1 mM), since the large concentration of negatively charged substrates will have a considerable effect on the aggregation of PPE-$^{d}NH_3$.

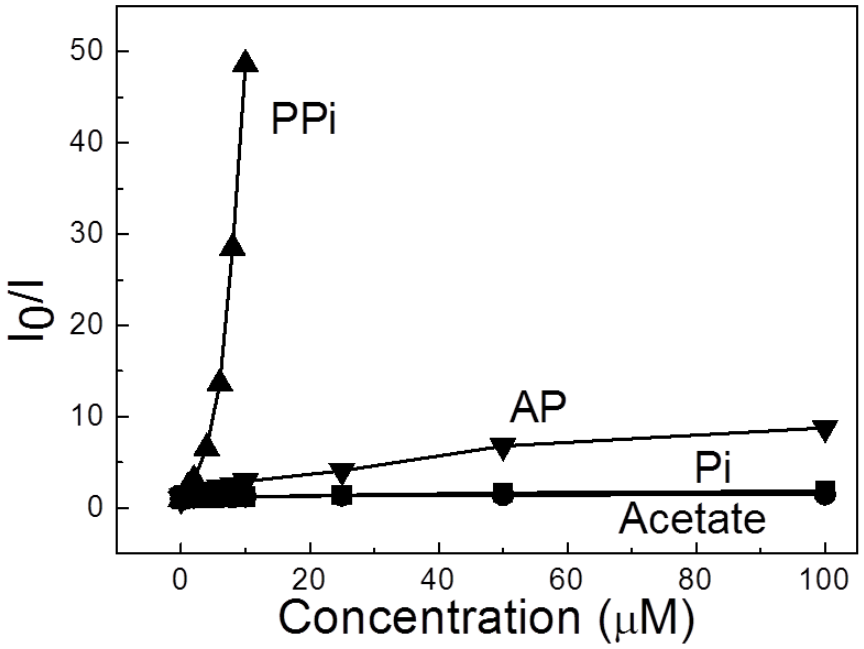

Figure 5-2. Stern-Volmer plot for PPE-$^{d}NH_3$ upon titration with Pi, acetate, PPi and AP, respectively. Solution conditions: 2 μM PPE-$^{d}NH_3$ and 1 mM $MgCl_2$ in 25 mM MES (pH = 6.5) buffer, λ_{ex} = 404 nm.

ACK Turn-off Assay

In order to eliminate possible interferences, the effect of addition of ACK on the fluorescence of PPE-$^{d}NH_3$ was examined. Figure 5-3 demonstrates that there is negligible change in polymer fluorescence intensity with the addition of [ACK] up to 20 µg/mL, thereby ruling out the possibility that the fluorescence change of the assay is caused by the added enzyme.

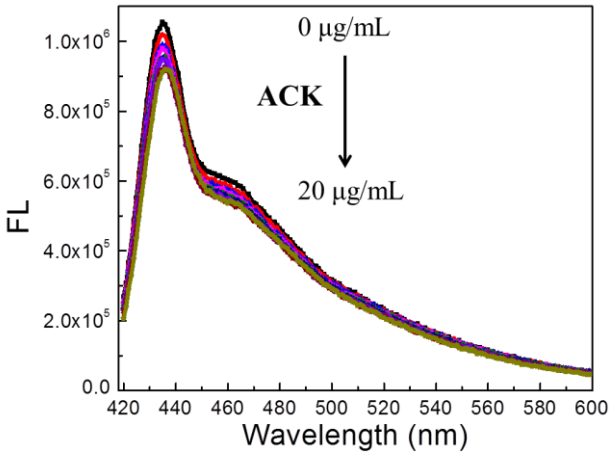

Figure 5-3. Fluorescence spectroscopic change upon the addition of ACK enzyme over a concentration range from 0 to 20 µg/mL. Solution conditions: 2 µM PPE-$^{d}NH_3$ and 1 mM $MgCl_2$ in 25 mM MES (pH = 6.5) buffer, λ_{ex} = 404 nm.

In a mixture solution containing PPE-$^{d}NH_3$, AP, Pi and the cofactor $MgCl_2$, the introduction of ACK initiates phosphate transfer from AP to Pi to generate PPi and acetate as the products (see chemical reaction in Figure 5-1A). The enzymatic activity is monitored by the continuous decrease of the polymer fluorescence intensity. Figure 5-4A presents the fluorescence spectroscopic changes observed for the standard assay

solution at 30 °C every 1 min for 10 min. The initial polymer fluorescence spectrum is well-shaped with a strong structured emission at ~434 nm. Following addition of 5 µg/mL ACK, the enzymatic reaction is activated and the product PPi acts as a cross-linker to form inter-chain aggregates. Therefore, as the incubation time increases, the structured band decreases significantly, as the broad and structureless band at longer wavelength (~520 nm) becomes more prominent, consistent with PPi-induced aggregation.[22,71,33]

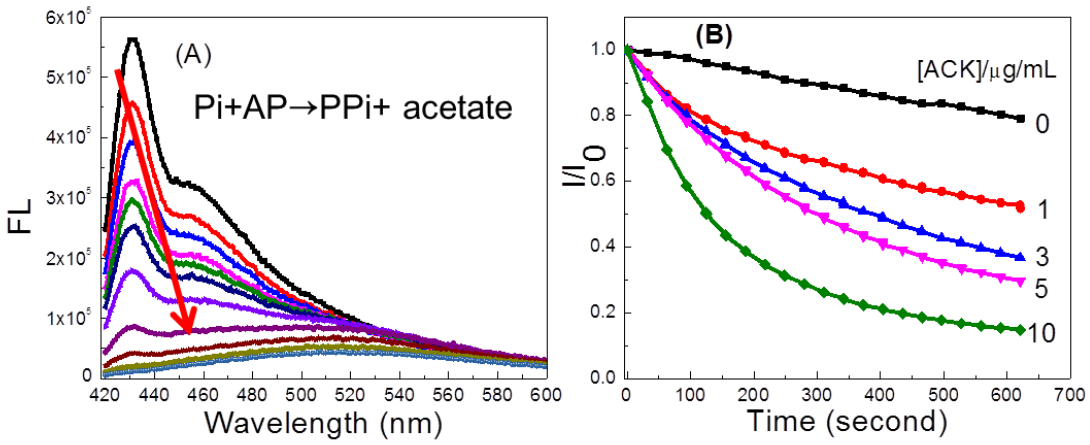

Figure 5-4. (A) Fluorescence spectroscopic changes as a function of time after addition of 5 µg/mL ACK in a 10 min period. (B) Change of fluorescence intensity at 434 nm recorded every 30 s during the real-time ACK turn-off assay with various ACK concentrations (0 – 10 µg/mL). Solution conditions: 2 µM PPE-$^{d}NH_3$, 1 mM $MgCl_2$, 100 µM Pi and 10 µM AP in 25 mM MES (pH = 6.5) buffer at 30 °C, λ_{ex} = 404 nm.

In order to test the feasibility of using this PPE-$^{d}NH_3$/AP/Pi system as a real-time turn-off assay for ACK activity, a series of ACK-catalyzed assays was carried out as a function of time at varying ACK concentrations at standard assay conditions (10 µM AP, 100 µM Pi and 1 mM Mg^{2+} at 30 °C). Figure 5-4B shows plots of the continuous

decrease of fluorescence intensity at 434 nm for solutions with five different concentrations of ACK from 0 to 10 μg/mL, where the fluorescence intensity was measured at 30 s intervals. In a 10-min measurement period, it is clearly noted that the initial reaction rate increases with [ACK]. The fluorescence intensity decreases linearly during the initial period (first 2 min) and then it slows down as the reaction continues. This effect is more significant at higher [ACK] and is believed to be caused by the reaction's coming to equilibrium. Note that the fluorescence decrease of the control experiment (black curve) is caused by photobleaching. Under standard experimental conditions, the reaction favors the forward reaction which produces PPi, but formation of PPi also initializes the reverse reaction and slows the rate of PPi production.

In a series of investigations, we examined the effect of substrate concentration (AP and Pi) on the reaction rate. Figure 5-5 demonstrates the fluorescence decrease at varying substrate concentrations with Pi from 50 μM to 300 μM and AP from 5 μM to 30 μM. The reaction rate increases with increasing [substrate]. At higher substrate concentration (Figure 5-6, C&D), the reaction reached equilibrium in less than 2 min, and more than 90% of the initial fluorescence intensity was quenched, indicating that more PPi was produced at higher substrate concentrations. Figure 5-6 illustrates a plot of initial reaction rate (υ_0) as a function of ACK concentrations. Within 1 min after the reaction begins, υ_0 is directly proportional to [ACK] in the range of 0 - 0.8 μg/mL, suggesting that the enzymatic reaction is kinetically controlled by ACK in the initial stage

of reaction. It is expected from the plot that the detection limit of this assay is ~ 0.05 μg/mL.

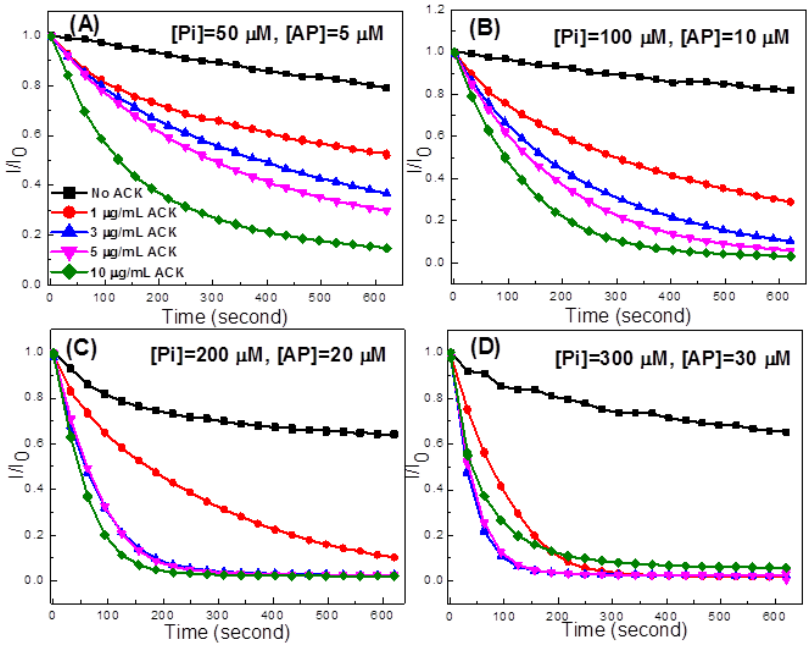

Figure 5-5. Time-based fluorescence intensity recorded every 30 s during the real-time measurement of ACK turn-off assay in a 10-min period at various [ACK] with different substrate concentrations; (A). [Pi] = 50 μM, [AP] = 5 μM, (B). [Pi] = 100 μM, [AP] = 10 μM, (C). [Pi] = 200 μM, [AP] = 20 μM, (D). [Pi] = 300 μM, [AP] = 30 μM. Different colors indicate different [ACK], 0 (black), 1 (red), 3 (blue), 5 (pink) and 10 (green) μg/mL.

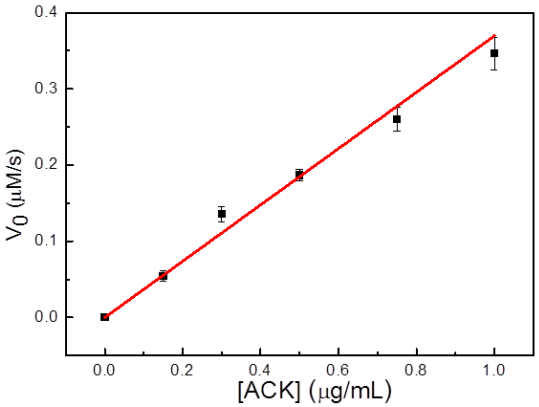

Figure 5-6. Dependence of initial rate of reaction (υ_0) on ACK concentrations. Solution conditions: 2 μM PPE-$^{d}NH_3$, 1 mM $MgCl_2$, 100 μM Pi and 10 μM AP in 25 mM MES (pH = 6.5) buffer at 30 ° C, λ_{ex} = 404 nm, λ_{em} = 434 nm.

Determination of ACK-catalyzed kinetic parameters

The kinetic parameters (K_m and V_{max}) for the ACK-catalyzed reaction can be obtained from the CPE-based fluorescence turn-off assay. As described in the experimental section, in a bisubstrate enzymatic reaction, the standard approach to study the kinetic behavior is to measure the rate of product formation while varying the concentrations of both substrates. For example, we first varied the AP concentration from 2.5 to 25 μM at different level of Pi (100, 150, 200 and 250 μM, respectively) and all the assays were conducted with 0.2 μg/mL ACK in 25 mM MES (pH 6.5) at 30 °C. The initial rate (υ_0) for each experiment was calculated. Next, a plot of $1/\upsilon_0$ vs 1/[Pi] was prepared and fitted to the modified Michaelis-Menten equation (see Equation 5-5 in the experimental section) as illustrated in Figure 5-7A. The derived intercepts for each linear fitting were plotted vs 1/[Pi] and another linear plot was obtained, as shown in Figure 5-7B. According to Equation 5-6 (see experimental section), K_m for AP were calculated with values of 135 μM. In a similar way, Figure 5-7C&D are used to calculate the K_m for Pi with values of 625 μM. And V_{max} was calculated to be 0.617 ± 0.089 μM/sec. Compared to reported apparent K_m values for AP (~60 μM) and Pi (~2.2 mM),[157] the values obtained from our approach are in good agreement with the reported data.

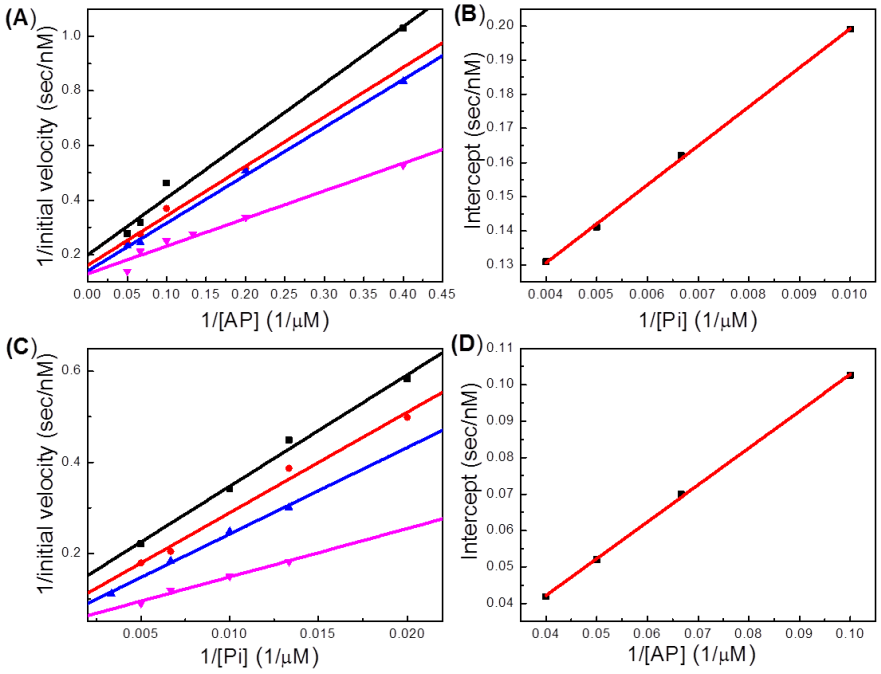

Figure 5-7. Enzyme kinetics parameters measurement by using ACK turn-off assay. (A): Double-reciprocal plot of 1/initial rate vs. 1/[AP] at several different concentrations of Pi. The [AP] is varied from 2.5 to 25 μM. (B): Secondary replot of intercept vs.1/[Pi]. (C): Double-reciprocal plot of 1/initial rate vs. 1/[Pi] at several different concentrations of AP. The [Pi] is varied from 25 to 200 μM. (D): Secondary replot of intercept vs.1/[AP].

Effect of Mg^{2+} on ACK activity in turn-off assay

It has been reported that Mg^{2+} is an important cofactor in the catalyzed ACK transfer of a phosphate group from AP to Pi in the acetate kinase assay.[172,174] Therefore the enzyme activities in both presence and absence of Mg^{2+} are presented in Figure 5-8. The red curve is the control experiment without adding kinase. It clearly shows that there is almost no change of the polymer fluorescence for the control experiment. The slight decrease of the fluorescence in the time period is probably caused by photobleaching of

PPE under constant illumination.[175,176] The blue curve illustrates the fluorescence change in a complete assay system with both [Mg^{2+}] at 1 mM and [ACK] at 5 μg/mL. As previously described, the addition of ACK activates the phosphate transfer from AP to produce PPi, resulting in a decrease in fluorescence intensity, with nearly 90% of the fluorescence quenched in 10 min. In comparison, the black curve shows how the PPE-$^{d}NH_3$ fluorescence behaves without adding Mg^{2+}. Even in the presence of 5 μg/mL ACK, no efficient quenching process happens, with results quite similar to the control experiment (<25% decrease of the fluorescence in 10 minutes). From these results, we can conclude that the presence of Mg^{2+} plays an essential role in the acetate kinase assay.

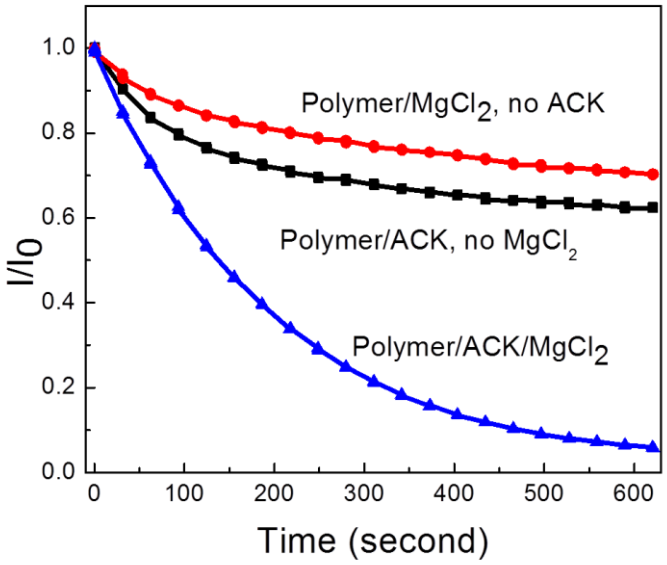

Figure 5-8. Effect of confactor $MgCl_2$ on the enzymatic activity of ACK. [Polymer] = 2 μM. Red curve: [$MgCl_2$] = 1 mM, No ACK added. Black curve: [ACK] = 5 μg/mL, no $MgCl_2$ added. Blue curve: [ACK] = 5 μg/mL and [$MgCl_2$] = 1 mM.

Specificity of ACK turn-off assay

The specificity of the ACK turn-off assay was also tested in order to prove that it is an effective and selective biosensor for the target enzyme, and a number of experiments were conducted using other proteins, including peptidase from porcine intestinal mucosa (PTD), hexokinase from *saccharomyces cerevisiae* (HOK), phospholipase D from peanut (PLD), glucose oxidase from *Aspergillus niger* (GOX) and peroxidase from horseradish (POD) as controls. None of these proteins has any specific interactions with PPi. ACK along with these control proteins were incubated with PPE-$^{d}NH_3$ under the same standard conditions (100 μM Pi and 10 μM AP in the 25 mM MES buffer at 30 ^{o}C). In each assay, the protein concentration was controlled at 0.2 μg/mL. In a 60-min period of incubation, the fluorescence intensity was recorded every 30 second at 434 nm and the final fluorescence change is illustrated and compared in Figure 5-9A. Overall, the assay containing ACK showed a ~90% decrease in fluorescence intensity in one hour, while all the control proteins showed no significant change, with fluorescence decrease in the range between 13% and 25%. Figure 5-9B provides the detailed information of how the fluorescence intensity varied with time. Over the 1 hour period, the fluorescence intensity decreased very rapidly after ACK was added. In contrast, the addition of other proteins induced an initial decrease in the first 5 min, followed by a very slow decrease in the fluorescence intensity. We attribute this phenomenon to non-specific binding between proteins and any species in the solution.[177] It is believed that the introduction of

these proteins disturb the electrostatic balance which may affect the fluorescence intensity. The fluorescence decrease in the initial 5 min caused by non-specific interactions for the control proteins accounted for most of the overall fluorescence change. Regardless of the slight fluorescence decrease by non-specific binding, it is clear that the fluorescence change for the other proteins is negligible when compared to that for ACK. As a result, we are confident to conclude that this turn-off assay is specific for ACK and most of the fluorescence decrease is due to the ACK enzyme activity with only a small portion arising from non-specific interactions.

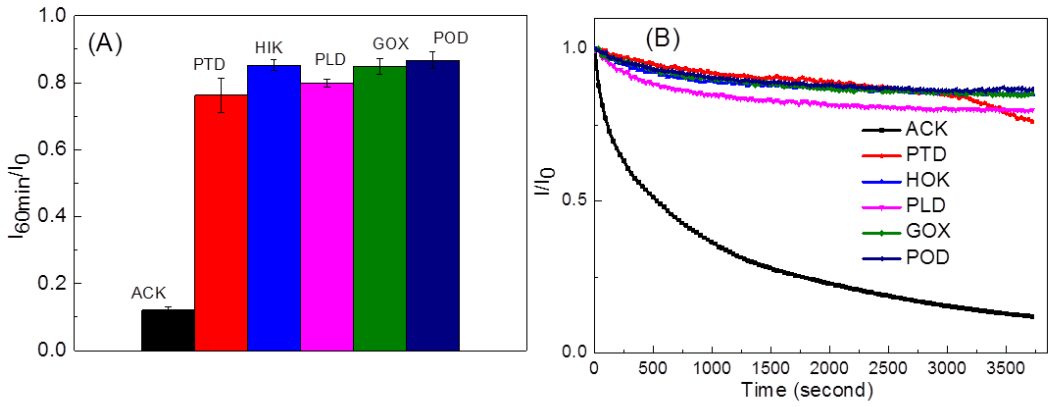

Figure 5-9. Specificity of ACK turn-off assay. (A) Changes in fluorescence intensity at 434 nm after 60 min of incubation with six different proteins (ACK, PTD, HOK, PLD, GOX and POD) at 30 ^{o}C. (B) Time-based fluorescence measurements for these proteins. All protein concentrations are set at 0.2 μg/mL. Standard assay condition: 2 μM PPE, 1 mM $MgCl_2$, 200 μM Pi and 20 μM AP in 25 mM MES (pH = 6.5) buffer, λ_{ex} = 404 nm.

Discussion

This chapter described a novel CPE-based fluorescence “turn-off” assay to monitor ACK-catalyzed enzymatic activity in the direction of PPi production. To the best of our

knowledge, this is the first report of using conjugated polyelectrolytes for ACK real-time measurements. Compared to the traditional enzyme-coupled sensing methods, the CPE method eliminates the need for additional enzymes, and therefore reduces the possibility of contamination and complexity. Mostly importantly, the assay can be carried out with substrate concentrations as low as micromolar range, which are much lower than those of other reported ACK assay conditions, and the K_m values obtained for both substrates are close to the reported values. In addition, the CPE method offers superior sensitivity in terms of enzyme concentrations and exhibits selectivity over other enzymes. Finally, this fluorescence-based assay can be easily adapted to a high-throughput screening format. Overall, this real-time CPEs-based sensing system affords an easy and rapid method for ACK detection.

While this CPE-based “turn-off” approach provides many advantages, it also presents some challenges. First, photobleaching of the CPEs and non-specific interactions between the polymer and other proteins may cause systematic errors. Second, the assay is not ideal at high substrate concentrations. Even though low substrate concentrations have little effect on fluorescence of the polymer; the presence of high concentrations of negatively charged substrates will quench the fluorescence intensity, leading to systematic errors. Last, the inhibition study is still inefficient and more inhibition studies needed to be tested in the future.

Summary

This chapter described the design and development of a novel fluorescence turn-off assay for ACK enzyme activity which offers easy, rapid and real-time measurements with high sensitivity and selectivity. Based on the interchain aggregation of PPE induced by the product PPi, the CPE-based system is utilized as a “turn off” sensor for ACK. The assay allows for determination of kinetic parameters for both substrates and it operates with substrates in the micromolar range with relatively good selectivity. Since this work demonstrates high specificity for PPi over Pi, this method can be extended to other substrate/enzyme systems that involve the discrimination of PPi and Pi. For example, in a recent work published by our group, an anionic PPE-CO_2 coupled with Cu^{2+} using PPi as the substrates was applied to study the enzymatic activity of alkaline phosphatase (ALP). However, our PPE system does not require addition of a heavy metal ion (Cu^{2+}), and affords similar speed, sensitivity and selectivity. We believe this system will be promising and useful as a signal transducer for other enzymatic reactions.

Experimental

Materials

The synthesis of PPE- $^{d}NH_3$ is described in the literature.[31] The aqueous stock solution of PPE- $^{d}NH_3$ was diluted with MES buffer to a final concentration of 2 μM. All aqueous solutions were prepared with water that was pre-distilled and then purified by

using a Millipore purification system. MES buffer solution (25 mM, pH 6.5) was prepared with 2-(N-morpholino)ethanesulfonic acid and sodium hydroxide. Lithium potassium acetyl phosphate was obtained from Sigma-Aldrich. Magnesium chloride, sodium phosphate tribasic and sodium acetate were purchased from Fisher Chemical. Sodium pyrophosphate was purchased from J.T.Baker Chemical Co. Acetate kinase was prepared and provided by Dr. Cheryl Ingram-Smith at Clemson University. The enzyme stock solution was prepared immediately before use in the fluorescence assays.

General Methods

Fluorescence turn-off assay procedure

The enzyme assays were conducted in 25 mM MES buffer (pH 6.5) at 30 ^{o}C. For real-time assays, the fluorescence intensity was recorded with excitation and emission wavelengths of 404 and 434 nm, respectively. A standard assay procedure was carried out as follows: a 2.0 mL aliquot of a solution containing PPE-$^{d}NH_3$, AP, Pi, and Mg^{2+} was mixed and allowed to reach equilibrium at 30 ^{o}C, and the initial polymer fluorescence intensity (I_{b0}) at 434 nm was recorded. In order to avoid interference caused by polymer photobleaching, the solution was placed in the spectrometer and the fluorescence intensity change as a function (I_{bt}) of time was measured every 10 s as a blank control. At the same time, a second 2.0 mL aliquot of fresh PPE/AP/Pi/ Mg^{2+} solution was prepared and incubated at 30 ^{o}C. Then ACK was quickly added via a microliter pipet, and the fluorescence intensity (I_t) of the solution was measured at 10 s increments. The

fluorescence intensity for both blank and sample solutions was recorded under the same conditions. The sample fluorescence intensity was corrected to I_{tc} using blank solution according to Equation 5-1:[178]

$$I_{tc} = I_t \times \frac{I_{b0}}{I_{bt}} \quad (5\text{-}1)$$

To monitor the assay in an end-point format, the fluorescence intensity versus wavelength spectra were recorded with the excitation wavelength at 404 nm.

Calculation of initial reaction rate (υ_0)

To obtain the relationship between fluorescence change and product PPi concentration, the corrected fluorescence intensity was converted into [PPi] as function of time using Equation 5-2, which is derived from a calibration plot obtained from a standard sample solution with known concentration of PPi:

$$[\mathrm{PPi}]_t = [\mathrm{PPi}]_0 \frac{\frac{I_{tc}}{I_p} - 1}{\frac{I_{0c}}{I_p} - 1} \quad (5\text{-}2)$$

where $[PPi]_0$ is the known PPi concentration of the standard sample, $[PPi]_t$ is the product concentration at time t, I_p is the fluorescence intensity of PPE-^{d}NH_3 before addition of substrate, I_{0c} is the initial corrected fluorescence intensity at t = 0, that is, the fluorescence intensity after addition of substrate but before the addition of enzyme and I_{tc} is the corrected fluorescence intensity at time t after enzyme addition. A plot of $[PPi]_t$ vs t was then derived and υ_0 was calculated from the slope by using the data where [PPi] is a linear function of time.

Calculation of kinetic parameters

The Michaelis–Menten equation is generally applied to calculate the kinetic parameters and is expressed as,

$$v_0 = \frac{v_{max}[S]_0}{K_m + [S]_0} \quad (5\text{-}3)$$

where $[S]_0$ is the initial substrate concentration, V_{max} is the maximum rate of the enzyme-catalyzed reaction at saturation substrate concentration, and K_m is the Michaelis constant.

However, our enzyme system involves two substrates, Pi and AP, and is more complicated than a single-substrate system. Therefore, a modified approach based on the Michaelis-Menten equation for a bisubstrate enzyme reaction was used,[179]

$$v_0 = \frac{v_{max}[A][B]}{K_{ia}K_b + K_a[B] + K_b[A] + [A][B]} \quad (5\text{-}4)$$

In Equation 5-4, K_{ia} is the intrinsic dissociation constant for substrate *A*, and K_a and K_b are the Michaelis constants for substrate *A* and *B*, respectively.

In double-reciprocal form, the rate equation becomes Equation 5-5, which can be analyzed via suitable linear plots,

$$\frac{1}{v_0} = \frac{K_{ia}K_b}{v_{max}[A][B]} + \frac{K_b}{v_{max}[A]} + \frac{K_a}{v_{max}[B]} + \frac{1}{v_{max}} \quad (5\text{-}5)$$

For example, when [*A*]is varied at constant [*B*], the equation becomes

$$\frac{1}{v_0} = \frac{1}{[A]}\left(\frac{K_{ia}K_b}{v_{max}[B]} + \frac{K_b}{v_{max}}\right) + \frac{K_a}{v_{max}[B]} + \frac{1}{v_{max}} \quad (5\text{-}6)$$

where a double-reciprocal plot of $1/v_0$ vs 1/[*A*] has the form of y = *m*x + *b*, in which the slope term [($K_{ia}K_b/V_{max}[B]+K_b/V_{max}$] and intercept term [$K_a/V_{max}$[B]+$1/V_{max}$] show a

dependency on the concentration of substrate *B*. The slope and intercept values are both in the form of linear equations and can thus be plotted to give values corresponding to V_{max} and Michaelis constants. To evaluate K_a and V_{max}, a series of Equations 2-5 plots are prepared for different constant [*B*], and this intercept, *b*, follow Equation 5-7,

$$y = \frac{1}{[B]}\left(\frac{K_a}{V_{max}}\right) + \frac{1}{V_{max}} \tag{5-7}$$

Thus, by plotting *b* vs. 1/[*B*], we can obtain a secondary plot with intercept equals to $1/V_{max}$ and slope corresponding to to K_a/V_{max}. Thus, two kinetic parameters of interest, V_{max} and K_a, can be evaluated by implementing this approach. Defining *A* as Pi and *B* as AP, first vary Pi at different constant levels of AP to obtain a series of plots based on Equation 5-6. Then, the intercepts are plotted vs 1/[*B*] to obtain V_{max} and K_a for Pi. Then the same procedure is preformed varying AP for different constant levels of Pi to obtain V_{max} and K_b for AP.

CHAPTER 6
CONCLUSION

In conclusion, the design and development of optical biosensors using functionalized water-soluble conjugated polyelectrolytes (CPEs) have been presented and discussed. By taking advantage of analyte-induced aggregation mechanism, all three CPE-based sensory systems exhibited good sensitivity and selectivity. Both fluorescence spectroscopy and fluorescence correlation spectroscopy (FCS) were involved to investigate the aggregation behaviors of CPEs in the presences of different target molecules. These sensory systems provided rapid and convenient ways for detection of metal ions, pyrophosphate ions (PPi) and enzyme activity.

Ion-Induced Aggregation of Conjugated Polyelectrolytes Studied by Fluorescence Correlation Spectroscopy

While the mechanisms for fluorescence quenching of CPEs are widely studied and elucidated in the literatures, detailed information of how different types of quenchers interact with CPEs is still insufficient. Therefore fluorescence correlation spectroscopy (FCS) was introduced to study the physical state changes of CPEs upon the addition of different ions. Two examples were described. First, the interaction of an anionic CPE PPE-$^{d}CO_2$ with a variety of metal ions including Na^+, K^+, Ca^{2+}, Cu^{2+}, Fe^{2+} and Fe^{3+} was investigated. Correlation curves for each CPE/metal ion mixtures at different [metal ion] were depicted and compared. It was found that the diffusion time increased in the order

of $K^+ \approx Na^+ < Ca^{2+} < Cu^{2+} < Fe^{2+} < Fe^{3+}$; and large diffusion times usually indicate large CPE aggregates. The results suggested that monovalent metal ions bonded to the CPE chain but cannot induce aggregation and divalent metal ions (Ca^{2+}, Cu^{2+}) were able to bind and induce the formation of small aggregates; while for iron catioins (Fe^{2+} and Fe^{3+}), they can bind strongly and induce the formation of large CPE aggregates. The outstanding abilities of iron to induce aggregation was attributed to the propensity of these metals to bind to six ligands, and thus bridge two of the tri-acid units on two PPE-$^dCO_2^-$ chains. Then the diffusion time ratio plot from FCS was compared with Stern-Volmer plot from fluorescence spectroscopy, and the slow response of FCS plot explained the effects of amplified quenching in a new aspect. We also investigated the interaction of PPE-$^dNH_3$ with PPi and the solid evident supported large aggregates formed when PPi was titrated into PPE-$^dNH_3$ solution.

Principal Component Analysis for Pyrophosphate Sensors Using Conjugated Polyelectrolytes

In this chapter, a novel CPE-based “turn-on” sensor for PPi was designed and applied to detect pyrophosphate concentration with the help of principal component analysis. Polymer **P3** exists as single chains in both methanol and water because of the novel carboxylate methylene side groups. Upon the addition of tris(3-aminoethyl)amine, very strong and large aggregates of **P3** were formed, driven by both electrostatic interaction and hydrophobic interaction. Then the addition of PPi will take the tetraamine

away and release the polymer chains because of the highly bind affinity between PPi and tetraamine, resulting in a fluorescence recovery. Since the system was involved with several different substrates and the fluorescence spectroscopic spectrums were also relatively complex with one peak going up and the other band go down, principle component analysis (PCA) method was used to analyze this system. Two principle components were obtained as well as their loading percentage at each [PPi] concentration. The established equation obtained from regression analysis can be applied to calculate the unknown [PPi] in such a system without a reference. And it has been proved that the sensor together with PCA method is able to predict the unknown concentration for PPi with a ~95% accuracy when PPi is within concentration range from 100 μM to 3 mM.

Acetate Kinase Assay Using Poly (phenylene ethynylene) with Polyamine Side Chains

As previous described in Chapter 2, the fluorescence of a cationic poly(phenylene ethynylene) polymer (PPE-$^{d}NH_3$) with branched side chains can be quenched very efficiently by pyrophosphate (PPi). The quenching occurs because PPi can effectively cross-link PPE to form large aggregates. Other substrates including Pi, Acetyl-phosphate and acetate fail to induce any significant fluorescence change. Therefore, a real-time fluorescence turn-off assay for the enzyme acetate kinase (ACK) using PPE-$^{d}NH_3$ as the signal transducer was developed. ACK will initiate the phosphate

transfer from acetyl-Pi to Pi and produce PPi and acetate. The fluorescence of the polymer PPE-$^{d}NH_3$ will decrease gradually after ACK is introduced into the Acetyl-Pi/Pi system. The assay operates with substrates in the micromolar range, and it offers a straightforward and rapid detection of ACK activity with the enzyme present in the nanomolar concentration range. The effect of Mg^{2+} on the ACK catalytic activity was also investigated and it was proved that Mg^{2+} was an important activator for the ACK dephosphorylation. A modified approach based on Michaelis-Menten equation was used to study the kinetic parameters for this bisubstrate system, from which the equilibrium constants K_m for Pi and Acetyl-Pi were obtained. Besides, the highly selectivity of this system was proved by the comparison with other enzymes.

APPENDIX

MATLAB CODING FOR PCA

```
load CheerSpectraAmineAll.txt;
D1=CheerSpectraAmineAll(2:317,11:37);
Concentration=CheerSpectraAmineAll(1,11:37);
Wavelength=CheerSpectraAmineAll(2:317,1);
[m,n]=size(D1);
  O=zeros(1,n);
O=sum(D1);
  for g=1:n
      N(g)=(1/O(g)*O(g));
end
for a=1:n
      for l=1:m
            D(l,a)=D1(l,a)*N(a);
      end
end
D;
  Lambda1=0;
RR=zeros(n,n);
  Z=D'*D;
  CC=zeros(m,n); Rc=zeros(m,n); HH=zeros(m,n); e=1; Vec=0;
p=1;
while e > 0
      if p > 1
            Z=RR;
      end
          RR=Z-Lambda1*Vec*Vec';
      [Q,Lambda]=eig(RR);
      Lambda1=max(max(Lambda));
      if p ==1
            maxii=Lambda1;
      end

      for y=1:n
            for t=1:y
                  if Lambda1 == Lambda(t,y);
                        x=y;
```

```
                end
            end
        end
        Vec=Q(:,x);
            if Lambda1 > maxii*0.001
            HH=D*Q;
            Rc(:,p)=HH(:,x);
            CC(p,:)=Vec';
        else
            e=0;
        end
        p=p+1;
end
R=zeros(m,p-2);
C=zeros(p-2,n);
for aa=1:p-2
        R(:,aa)=Rc(:,aa);
        C(aa,:)=CC(aa,:);
end
R;
C;
U=0; O=0; N=zeros(1,n);
U=D.*D;
O=sum(U);
for g=1:n
        N(g)=sqrt(1/O(g)*O(g));
end
for a=1:n
        for l=1:m
            Dn(l,a)=D(l,a)*N(a);
        end
end
Dn;
  R1=R;
C1=C;
for phii=295:295
        phi=phii*pi/180;
T=[1.1*cos(phi) -1.8*sin(phi); 1.9*sin(phi) 6.5*cos(phi)];
        R=R1*T;
```

```
C=inv(T)*C1;
  figure(1)
plot(Wavelength,D)
title('Original Spectra')
xlabel('Wavelength (nm)')
ylabel('Intensity (a.u.)')
figure(2)
clf
plot(Wavelength,R*C)
title('Reconstructed Spectra')
xlabel('Wavelength (nm)')
ylabel('Intensity (a.u.)')
figure(3)
plot(Wavelength,R)
title('Fundamental Spectra')
xlabel('Wavelength (nm)')
ylabel('Intensity (a.u.)')
grid on
figure(4)
plot(Concentration,C(1,:),'bo-',Concentration,C(2,:),'g+-',Concentration,C(1,:)+C(2,:),'rx-')
title('Loadings vs. actual')
xlabel('Concentration')
ylabel('Actual Loadings');
  F=C';
if abs(F(1,1))-abs(F(2,1)) < 0.002
      a=1;
      b=2;
else
      a=2;
      b=1;
end
  phii;
pause(0.5)
end
```

LIST OF REFERENCES

(1) Gunes, S.; Neugebauer, H.; Sariciftci, N. S. *Chem Rev* **2007**, *107*, 1324.

(2) Kraft, A.; Grimsdale, A. C.; Holmes, A. B. *Angew Chem Int Edit* **1998**, *37*, 402.

(3) Montali, A.; Smith, P.; Weder, C. *Synthetic Met* **1998**, *97*, 123.

(4) Torsi, L.; Dodabalapur, A.; Rothberg, L. J.; Fung, A. W. P.; Katz, H. E. *Science* **1996**, *272*, 1462.

(5) Sirringhaus, H. *Adv Mater* **2005**, *17*, 2411.

(6) McQuade, D. T.; Pullen, A. E.; Swager, T. M. *Chem Rev* **2000**, *100*, 2537.

(7) Thomas, S. W.; Joly, G. D.; Swager, T. M. *Chem Rev* **2007**, *107*, 1339.

(8) Gierschner, J.; Cornil, J.; Egelhaaf, H. J. *Adv Mater* **2007**, *19*, 173.

(9) Nguyen, T. Q.; Wu, J. J.; Doan, V.; Schwartz, B. J.; Tolbert, S. H. *Science* **2000**, *288*, 652.

(10) Pinto, M. R.; Schanze, K. S. *Synthesis-Stuttgart* **2002**, 1293.

(11) Moroni, M.; Lemoigne, J.; Luzzati, S. *Macromolecules* **1994**, *27*, 562.

(12) Yang, J. S.; Swager, T. M. *J Am Chem Soc* **1998**, *120*, 11864.

(13) Yang, J. S.; Swager, T. M. *J Am Chem Soc* **1998**, *120*, 5321.

(14) Schanze, K. S.; DiCesare, N.; Pinto, M. R.; Lakowicz, J. R. *Langmuir* **2002**, *18*, 7785.

(15) Wilson, J. S.; Frampton, M. J.; Michels, J. J.; Sardone, L.; Marletta, G.; Friend, R. H.; Samori, P.; Anderson, H. L.; Cacialli, F. *Adv Mater* **2005**, *17*, 2659.

(16) Barata, P. D.; Costa, A. I.; Ferreira, L. F. V.; Prata, J. V. *J Polym Sci Pol Chem* **2010**, *48*, 5040.

(17) Tour, J. M. *Chem Rev* **1996**, *96*, 537.

(18) Bunz, U. H. F.; Kim, I. B.; Dunkhorst, A.; Gilbert, J. *Macromolecules* **2005**, *38*, 4560.

(19) Wu, D. L.; Feng, F. D.; Xie, D. P.; Chen, Y.; Tan, W. H.; Schanze, K. S. *J Phys Chem Lett* **2012**, *3*, 1711.

(20) Nelson, J. C.; Saven, J. G.; Moore, J. S.; Wolynes, P. G. *Science* **1997**, *277*, 1793.

(21) Prince, R. B.; Saven, J. G.; Wolynes, P. G.; Moore, J. S. *J Am Chem Soc* **1999**, *121*, 3114.

(22) Tan, C. Y.; Pinto, M. R.; Schanze, K. S. *Chem Commun* **2002**, 446.

(23) Tan, C. Y.; Alas, E.; Muller, J. G.; Pinto, M. R.; Kleiman, V. D.; Schanze, K. S. *J Am Chem Soc* **2004**, *126*, 13685.

(24) Halkyard, C. E.; Rampey, M. E.; Kloppenburg, L.; Studer-Martinez, S. L.; Bunz, U. H. F. *Macromolecules* **1998**, *31*, 8655.

(25) Kim, J.; Swager, M. *Nature* **2001**, *413*, 548.

(26) Levitus, M.; Zepeda, G.; Dang, H.; Godinez, C.; Khuong, T. A. V.; Schmieder, K.; Garcia-Garibay, M. A. *J Org Chem* **2001**, *66*, 3188.

(27) Walters, K. A.; Ley, K. D.; Schanze, K. S. *Langmuir* **1999**, *15*, 5676.

(28) Rothberg, L. J.; Yan, M.; Papadimitrakopoulos, F.; Galvin, M. E.; Kwock, E. W.; Miller, T. M. *Synthetic Met* **1996**, *80*, 41.

(29) Schanze, K. S.; Tan, C. Y.; Pinto, M. R. *Chem Commun* **2002**, 446.

(30) Lee, S. H.; Komurlu, S.; Zhao, X. Y.; Jiang, H.; Moriena, G.; Kleiman, V. D.; Schanze, K. S. *Macromolecules* **2011**, *44*, 4742.

(31) Zhao, X. Y.; Schanze, K. S. *Chem Commun* **2010**, *46*, 6075.

(32) Muller, J. G.; Atas, E.; Tan, C.; Schanze, K. S.; Kleiman, V. D. *J Am Chem Soc* **2006**, *128*, 4007.

(33) Jiang, H.; Zhao, X. Y.; Schanze, K. S. *Langmuir* **2006**, *22*, 5541.

(34) Reinert, S.; Mohr, G. J. *Chem Commun* **2008**, 2272.

(35) Sun, H.; Feng, F.; Yu, M. H.; Wang, S. *Macromol Rapid Comm* **2007**, *28*, 1905.

(36) MacKnight, W. J.; Ponomarenko, E. A.; Tirrell, D. A. *Accounts Chem Res* **1998**, *31*, 781.

(37) Kabanov, A. V.; Bronich, T. K.; Kabanov, V. A.; Yu, K.; Eisenberg, A. *J Am Chem Soc* **1998**, *120*, 9941.

(38) Chen, L. H.; McBranch, D.; Wang, R.; Whitten, D. *Chem Phys Lett* **2000**, *330*, 27.

(39) Zhou, Q.; Swager, T. M. *J Am Chem Soc* **1995**, *117*, 12593.

(40) Whitten, D. G.; Chen, L. H.; McBranch, D. W.; Wang, H. L.; Helgeson, R.; Wudl, F. *P Natl Acad Sci USA* **1999**, *96*, 12287.

(41) Gaylord, B. S.; Wang, S. J.; Heeger, A. J.; Bazan, G. C. *J Am Chem Soc* **2001**, *123*, 6417.

(42) Zhao, X. Y.; Pinto, M. R.; Hardison, L. M.; Mwaura, J.; Muller, J.; Jiang, H.; Witker, D.; Kleiman, V. D.; Reynolds, J. R.; Schanze, K. S. *Macromolecules* **2006**, *39*, 6355.

(43) Fan, C. H.; Hirasa, T.; Plaxco, K. W.; Heeger, A. J. *Langmuir* **2003**, *19*, 3554.

(44) Jiang, H.; Zhao, X. Y.; Schanze, K. S. *Langmuir* **2007**, *23*, 9481.

(45) Magde, D.; Webb, W. W.; Elson, E. *Phys Rev Lett* **1972**, *29*, 705.

(46) Krichevsky, O.; Bonnet, G. *Reports on Progress in Physics* **2002**, *65*, 251.

(47) Yin, Y. D.; Yuan, R. F.; Zhao, X. S. *J Phys Chem Lett* **2013**, *4*, 304.

(48) Shin, H. S.; Okamoto, A.; Sako, Y.; Kim, S. W.; Kim, S. Y.; Pack, C. G. *J Phys Chem A* **2013**, *117*, 27.

(49) Zettl, U.; Hoffmann, S. T.; Koberling, F.; Krausch, G.; Enderlein, J.; Harnau, L.; Ballauff, M. *Macromolecules* **2009**, *42*, 9537.

(50) Fogarty, K.; Van Orden, A. *Methods* **2009**, *47*, 151.

(51) Waldeck, D. H.; Kaur, P.; Yue, H. J.; Wu, M. Y.; Liu, M.; Treece, J.; Xue, C. H.; Liu, H. Y. *J Phys Chem B* **2007**, *111*, 8589.

(52) Haustein, E.; Schwille, P. *Annu Rev Bioph Biom* **2007**, *36*, 151.

(53) Waldeck, D. H.; Yue, H. J.; Wu, M. Y.; Xue, C. H.; Velayudham, S.; Liu, H. Y. *J Phys Chem B* **2008**, *112*, 8218.

(54) Chen, Y.; Munteanu, A. C.; Huang, Y. F.; Phillips, J.; Zhu, Z.; Mavros, M.; Tan, W. H. *Chem-Eur J* **2009**, *15*, 5327.

(55) Humpolickova, J.; Benda, A.; Beranova, L.; Hof, M. *Chem Listy* **2009**, *103*, 911.

(56) Pal, N.; Verma, S. D.; Singh, M. K.; Sen, S. *Anal Chem* **2011**, *83*, 7736.

(57) Satrijo, A.; Swager, T. M. *J Am Chem Soc* **2007**, *129*, 16020.

(58) Selkoe, D. J. *Nature* **2003**, *426*, 900.

(59) Aebersold, R.; Mann, M. *Nature* **2003**, *422*, 198.

(60) Lee, J. H.; Kim, D. G.; Kwon, N. Y.; Jang, G. S.; Son, J. H.; Lee, M.; Cho, H. J.; Kweon, H. S.; Lee, T. S. *J Polym Sci Pol Chem* **2011**, *49*, 138.

(61) Nyren, P. *Anal Biochem* **1987**, *167*, 235.

(62) Blagbrough, I. S.; Adjimatera, N.; Kral, T.; Hof, M. *Pharm Res* **2006**, *23*, 1564.

(63) Bazan, G. C.; Li, H.; Yang, R. *Macromolecules* **2008**, *41*, 1531.

(64) Gaylord, B. S.; Heeger, A. J.; Liu, B.; Wang, S.; Fan, C. H.; Bazan, G. C. *Abstr Pap Am Chem S* **2003**, *225*, U985.

(65) Jin, Y.; Yang, R.; Suh, H.; Woo, H. Y. *Macromol Rapid Comm* **2008**, *29*, 1398.

(66) Andrew, T. L.; Swager, T. M. *Macromolecules* **2008**, *41*, 8306.

(67) Wang, D. L.; Gong, X.; Heeger, P. S.; Rininsland, F.; Bazan, G. C.; Heeger, A. J. *P Natl Acad Sci USA* **2002**, *99*, 49.

(68) Kim, I. B.; Dunkhorst, A.; Bunz, U. H. F. *Langmuir* **2005**, *21*, 7985.

(69) Swager, T. M.; Thomas, S. W.; Joly, G. D. *Chem Rev* **2007**, *107*, 1339.

(70) Kim, I. B.; Bunz, U. H. F. *J Am Chem Soc* **2006**, *128*, 2818.

(71) Schanze, K. S.; Liu, Y.; Ogawa, K. *J Photoch Photobio C* **2009**, *10*, 173.

(72) Holdcroft, S. *J Polym Sci Pol Phys* **1991**, *29*, 1585.

(73) Balgi, G.; Leckband, D. E.; Nitsche, J. M. *Biophys J* **1995**, *68*, 2251.

(74) Chiantia, S.; Kahya, N.; Schwille, P. *Langmuir* **2007**, *23*, 7659.

(75) Sasmal, D. K.; Mondal, T.; Sen Mojumdar, S.; Choudhury, A.; Banerjee, R.; Bhattacharyya, K. *J Phys Chem B* **2011**, *115*, 13075.

(76) Chen, L. H.; McBranch, D. W.; Wang, H. L.; Helgeson, R.; Wudl, F.; Whitten, D. G. *Proceedings of the National Academy of Sciences of the United States of America* **1999**, *96*, 12287.

(77) Zhao, X. Y.; Jiang, H.; Schanze, K. S. *Abstr Pap Am Chem S* **2007**, *233*.

(78) Smith, T. A.; Ramachandran, G.; Gomez, D.; Ghiggino, K. P. *Synthetic Metals* **2005**, *152*, 17.

(79) Wang, D. L.; Wang, J.; Moses, D.; Bazan, G. C.; Heeger, A. J. *Langmuir* **2001**, *17*, 1262.

(80) Wang, J.; Wang, D. L.; Miller, E. K.; Moses, D.; Bazan, G. C.; Heeger, A. J. *Macromolecules* **2000**, *33*, 5153.

(81) Shalaby, A. R. *Food Res Int* **1996**, *29*, 675.

(82) Bibillo, A.; Figlerowicz, M.; Kierzek, R. *Nucleic Acids Res* **1999**, *27*, 3931.

(83) Kusano, T.; Yamaguchi, K.; Berberich, T.; Takahashi, Y. *J Plant Res* **2007**, *120*, 345.

(84) Larque, E.; Sabater-Molina, M.; Zamora, S. *Nutrition* **2007**, *23*, 87.

(85) Groppa, M. D.; Benavides, M. P. *Amino Acids* **2008**, *34*, 35.

(86) Onal, A. *Food Chem* **2007**, *103*, 1475.

(87) Fujita, K.; Nagatsu, T.; Shinpo, K.; Maruta, K.; Teradaira, R.; Nakamura, M. *Clin Chem* **1980**, *26*, 1577.

(88) Ma, Y. F.; Liu, G. S.; Du, M.; Stayton, I. *Electrophoresis* **2004**, *25*, 1473.

(89) Casero, R. A.; Marton, L. J. *Nat Rev Drug Discov* **2007**, *6*, 373.

(90) Yeh, C. Y.; Lin, S. J.; Hwang, D. F. *J Food Drug Anal* **2004**, *12*, 128.

(91) Mertz, E.; Zimmerman, S. C. *J Am Chem Soc* **2003**, *125*, 3424.

(92) Greene, N. T.; Shimizu, K. D. *J Am Chem Soc* **2005**, *127*, 5695.

(93) S. G. G. Cheng and Z. M. Merchant, Biosensors in Food Analysis,in Characterization of Foods: Emerging Methods, ed. A. G.Gaonkar, Elsevier Science, New York, 1995, ch. 14

(94) Jung, J. H.; Lee, S. J.; Kim, J. S.; Lee, W. S.; Sakata, Y.; Kaneda, T. *Org Lett* **2006**, *8*, 3009.

(95) Secor, K.; Plante, J.; Avetta, C.; Glass, T. *J Mater Chem* **2005**, *15*, 4073.

(96) Rakow, N. A.; Sen, A.; Janzen, M. C.; Ponder, J. B.; Suslick, K. S. *Angew Chem Int Edit* **2005**, *44*, 4528.

(97) Zhou, H. C.; Baldini, L.; Hong, J.; Wilson, A. J.; Hamilton, A. D. *J Am Chem Soc* **2006**, *128*, 2421.

(98) Teradaira, R.; Fujita, K.; Nagatsu, T.; Shinpo, K.; Maruta, K.; Nakamura, M. *J Clin Chem Clin Bio* **1980**, *18*, 698.

(99) Rossi, S.; Lee, C.; Ellis, P. C.; Pivarnik, L. F. *J Food Sci* **2002**, *67*, 2056.

(100) Liu, M.; Kaur, P.; Waldeck, D. H.; Xue, C. H.; Liu, H. Y. *Langmuir* **2005**, *21*, 1687.

(101) Liu, Y.; Schanze, K. S. *Anal Chem* **2009**, *81*, 231.

(102) Fude Feng, Kirk S. Schanze, paper in preparation

(103) Tan, C. Y.; Pinto, M. R.; Schanze, K. S. *Abstr Pap Am Chem S* **2002**, *223*, D43.

(104) Nelson, T. L.; O'Sullivan, C.; Greene, N. T.; Maynor, M. S.; Lavigne, J. J. *J Am Chem Soc* **2006**, *128*, 5640.

(105) Maynor, M. S.; Nelson, T. L.; O'Sullivan, C.; Lavigne, J. J. *Org Lett* **2007**, *9*, 3217.

(106) Blackman, A. G. *Polyhedron* **2005**, *24*, 1.

(107) Schanze, K. S.; Zhao, X. Y.; Jiang, H. *Macromolecules* **2008**, *41*, 3422.

(108) Bao, B. Q.; Yuwen, L. H.; Zheng, X. N.; Weng, L. X.; Zhu, X. R.; Zhan, X. W.; Wang, L. H. *J Mater Chem* **2010**, *20*, 9628.

(109) Nelson, T. L.; Tran, I.; Ingallinera, T. G.; Maynor, M. S.; Lavigne, J. J. *Analyst* **2007**, *132*, 1024.

(110) Feng, F. D.; Yang, J.; Xie, D. P.; McCarley, T. D.; Schanze, K. S. J Phys Chem Lett 2013, submitted.

(111) Chakrabarti, P. *J Mol Biol* **1993**, *234*, 463.

(112) Bodin, P.; Burnstock, G. *Neurochem Res* **2001**, *26*, 959.

(113) Zyryanov, A. B.; Tammenkoski, M.; Salminen, A.; Kolomiytseva, G. Y.; Fabrichniy, I. P.; Goldman, A.; Lahti, R.; Baykov, A. A. *Biochemistry-Us* **2004**, *43*, 14395.

(114) Pathak, R. K.; Tabbasum, K.; Rai, A.; Panda, D.; Rao, C. P. *Anal Chem* **2012**, *84*, 5117.

(115) Lipscomb, W. N.; Strater, N. *Chem Rev* **1996**, *96*, 2375.

(116) Mathews, C. K.; van Holde, K. E. Biochemistry; The Benjamin/ Cummings Publishing Company, Inc.: Redwood City, CA, 1990

(117) Tabary, T.; Ju, L. Y.; Cohen, J. H. M. *J Immunol Methods* **1992**, *156*, 55.

(118) Satarug, S.; Baker, J. R.; Urbenjapol, S.; Haswell-Elkins, M.; Reilly, P. E. B.; Williams, D. J.; Moore, M. R. *Toxicol Lett* **2003**, *137*, 65.

(119) Jiang, G. F.; Xu, L.; Song, S. Z.; Zhu, C. C.; Wu, Q.; Zhang, L. *Toxicology* **2008**, *244*, 49.

(120) Goyer, R. A.; Liu, J.; Waalkes, M. P. *Biometals* **2004**, *17*, 555.

(121) Timms, A. E.; Zhang, Y.; Russell, R. G. G.; Brown, M. A. *Rheumatology* **2002**, *41*, 725.

(122) Lomashvili, K. A.; Cobbs, S.; Hennigar, R. A.; Hardcastle, K. I.; O'Neill, W. C. *J Am Soc Nephrol* **2004**, *15*, 1392.

(123) Gao, J.; Riis-Johannessen, T.; Scopelliti, R.; Qian, X. H.; Severin, K. *Dalton T* **2010**, *39*, 7114.

(124) Huang, X. M.; Guo, Z. Q.; Zhu, W. H.; Xie, Y. S.; Tian, H. *Chem Commun* **2008**, 5143.

(125) Wu, C. Y.; Chen, M. S.; Lin, C. A.; Lin, S. C.; Sun, S. S. *Chem-Eur J* **2006**, *12*, 2263.

(126) Su, G. Y.; Liu, Z. P.; Xie, Z. J.; Qian, F.; He, W. J.; Guo, Z. J. *Dalton T* **2009**, 7888.

(127) Schanze, K. S.; Zhao, X. Y.; Liu, Y. *Chem Commun* **2007**, 2914.

(128) Cheng, T. Y.; Wang, T.; Zhu, W. P.; Chen, X. L.; Yang, Y. J.; Xu, Y. F.; Qin, X. H. *Org Lett* **2011**, *13*, 3656.

(129) Park, C.; Hong, J. I. *Tetrahedron Lett* **2010**, *51*, 1960.

(130) Lee, H. N.; Swamy, K. M. K.; Kim, S. K.; Kwon, J. Y.; Kim, Y.; Kim, S. J.; Yoon, Y. J.; Yoon, J. *Org Lett* **2007**, *9*, 243.

(131) Lau, Y. T. R.; Weng, L. T.; Ng, K. M.; Chan, C. M. *Anal Chem* **2010**, *82*, 2661.

(132) Zhang, Z. F.; Liu, Y.; Zhang, H. *Spectrosc Spect Anal* **2009**, *29*, 3263.

(133) Farcomeni, A. *Computation Stat* **2009**, *24*, 583.

(134) Pearson, K. *Philos Mag* **1901**, *2*, 559.

(135) Tan, Z. J. *Opt Eng* **2009**, *48*.

(136) Chen, C. C.; Shih, J. S. *J Chin Chem Soc-Taip* **2008**, *55*, 979.

(137) Lu, Y. J.; Partridge, C.; Meyyappan, M.; Li, J. *J Electroanal Chem* **2006**, *593*, 105.

(138) Sasaki, I.; Tsuchiya, H.; Nishioka, M.; Sadakata, M.; Okubo, T. *Sensor Actuat B-Chem* **2002**, *86*, 26.

(139) Vogt, F.; Mizaikoff, B. *Anal Chem* **2003**, *75*, 3050.

(140) Cui, F. X.; Fang, Y. H.; Lan, T. G.; Xiong, W.; Yuan, Y. M. *Spectrosc Spect Anal* **2011**, *31*, 2794.

(141) Kose, M. E.; Omar, A.; Virgin, C. A.; Carroll, B. F.; Schanze, K. S. *Langmuir* **2005**, *21*, 9110.

(142) Watchasit, S.; Kaowliew, A.; Suksai, C.; Tuntulani, T.; Ngeontae, W.; Pakawatchai, C. *Tetrahedron Lett* **2010**, *51*, 3398.

(143) Avaeva, S. M.; Sklyanki.Va; Botvinik, M. M. *J Gen Chem Ussr* **1969**, *39*, 559.

(144) ang, J. Wu, D.L.; Xie, D.P.; Schanze, K.S. Ion-induced aggregation of CPEs studied by Fluorescence Correlation Spectroscopy. Submitted.

(145) Keithley, R. B.; Heien, M. L.; Wightman, R. M. *Trac-Trend Anal Chem* **2009**, *28*, 1127.

(146) Leng, C. L.; Wang, H. S. *J Comput Graph Stat* **2009**, *18*, 201.

(147) Lipmann, F. *J Biol Chem* **1944**, *155*, 55.

(148) Rose, I. A.; Grunbergmanago, M.; Korey, S. R.; Ochoa, S. *J Biol Chem* **1954**, *211*, 737.

(149) Schonheit, P. *Hyperthermophilic Enzymes, Pt B* **2001**, *331*, 168.

(150) Spector, L. B. *P Natl Acad Sci-Biol* **1980**, *77*, 2626.

(151) Bowman, C. M.; Valdez, R. O.; Nishimura, J. S. *J Biol Chem* **1976**, *251*, 3117.

(152) Ren, N. Q.; Lin, H. L.; Zhang, K.; Zheng, G. X.; Duan, Z. J.; Lin, M. *Curr Microbiol* **2007**, *55*, 167.

(153) Mukhopadhyay, S.; Hasson, M. S.; Sanders, D. A. *Bioorg Chem* **2008**, *36*, 65.

(154) Thauer, R. K.; Mollerzinkhan, D.; Spormann, A. M. *Annu Rev Microbiol* **1989**, *43*, 43.

(155) Kahane, I.; Razin, S.; Muhlrad, A. *Israel J Med Sci* **1978**, *14*, 807.

(156) Kahane, I.; Razin, S.; Muhlrad, A. *Fems Microbiol Lett* **1978**, *3*, 143.

(157) Reeves, R. E.; Guthrie, J. D. *Biochem Bioph Res Co* **1975**, *66*, 1389.

(158) Schafer, T.; Selig, M.; Schonheit, P. *Arch Microbiol* **1993**, *159*, 72.

(159) Perraud, A. L.; Weiss, V.; Gross, R. *Trends Microbiol* **1999**, *7*, 115.

(160) Buss, K. A.; Cooper, D. R.; Ingram-Smith, C.; Ferry, J. G.; Sanders, D. A.; Hasson, M. S. *J Bacteriol* **2001**, *183*, 3536.

(161) Brown, T. D. K.; Stormer, F. C.; Pereira, C. R. S. *J Bacteriol* **1972**, *112*, 1106.

(162) Sanwal, B. D. *Bacteriol Rev* **1970**, *34*, 20.

(163) Elmansi, E. M. T.; Holms, W. H. *J Gen Microbiol* **1989**, *135*, 2875.

(164) Fox, D. K.; Meadow, N. D.; Roseman, S. *J Biol Chem* **1986**, *261*, 3498.

(165) Koplove, H. M.; Cooney, C. L. *J Bacteriol* **1978**, *134*, 992.

(166) Lipmann, F.; Tuttle, L. C. *J Biol Chem* **1945**, *159*, 21.

(167) Rose, I. A. *Methods in Enzymology* **1955**, *1*, 591.

(168) Gorrell, A.; Lawrence, S. H.; Ferry, J. G. *J Biol Chem* **2005**, *280*, 10731.

(169) Fowler, M. L.; Ingram-Smith, C.; Smith, K. S. *Eukaryot Cell* **2012**, *11*, 1249.

(170) Ingram-Smith, C.; Gorrell, A.; Lawrence, S. H.; Iyer, P.; Smith, K.; Ferry, J. G. *J Bacteriol* **2005**, *187*, 2386.

(171) Miles, R. D.; Gorrell, A.; Ferry, J. G. *J Biol Chem* **2002**, *277*, 22547.

(172) Oultram, J. D.; Burr, I. D.; Elmore, M. J.; Minton, N. P. *Gene* **1993**, *131*, 107.

(173) Jie Yang, Kirk S. Schanze, paper in preparation.

(174) Grundy, F. J.; Waters, D. A.; Allen, S. H. G.; Henkin, T. M. *J Bacteriol* **1993**, *175*, 7348.

(175) De Jong, M. J. M.; Vissenberg, M. C. J. M. *Philips J Res* **1998**, *51*, 495.

(176) Shibata, T.; Hattori, T.; Onodera, S.; Kaino, T. *Nippon Kagaku Kaishi* **1998**, 831.

(177) Dwight, S. J.; Gaylord, B. S.; Hong, J. W.; Bazan, G. C. *J Am Chem Soc* **2004**, *126*, 16850.

(178) Liu, Y.; Ogawa, K.; Schanze, K. S. *Anal Chem* **2008**, *80*, 150.

(179) Smith, J. H., Simons, C., Enzymes and Their Inhibition: Drug Development; CRC Press 2004

BIOGRAPHICAL SKETCH

Jie (Cheer) Yang was born in Hubei Province, China. Jie started her undergraduate studies at Wuhan University in 2004. Four years later, she received her bachelor degree in chemistry. During that same year, she went to United States to continue her graduate studies in Department of Chemistry at University of Florida, where she joined Dr. Schanze's group. In the past five years, she focused her research on the design and development of analytical methods based on fluorescent conjugated polyelectrolytes for sensing applications. She received her Ph.D from the University of Florida in the spring of 2013.